Spring 2013

Processing and properties of ZrB_2-$ZrSi_2$ matrix composites reinforced with continuous SiC fiber

Benjamin John Bowin Lai

Recommended Citation

PROCESSING AND PROPERTIES OF ZrB$_2$-ZrSi$_2$ MATRIX COMPOSITES

REINFORCED WITH CONTINUOUS SiC FIBER

by

BENJAMIN JOHN BOWIN LAI

A THESIS

Presented to the Graduate Faculty of the

MISSOURI UNIVERSITY OF SCIENCE AND TECHNOLOGY

In Partial Fulfillment of the Requirements for the Degree

MASTER OF SCIENCE IN CERAMIC ENGINEERING

2013

Approved by

Dr. Gregory E. Hilmas, Advisor
Dr. William G. Fahrenholtz
Dr. K. Chandrashekhara

PUBLICATION THESIS OPTION

This thesis has been prepared in the style such that the individual sections may be submitted for journal publications in the materials science and engineering fields. Pages 27 through 64 entitled "Densification, Microstructure, and Properties of Hot-Pressed ZrB_2-$ZrSi_2$ Ceramics" were submitted to the *Journal of the European Ceramic Society* on April 6, 2013. Pages 65 through 93 entitled "ZrB_2-$ZrSi_2$ Matrix Composites Reinforced with Continuous SiC Fiber" will be submitted to the *International Journal of Applied Ceramic Technology* pending further revision.

ABSTRACT

The research presented in this thesis focuses on the processing, microstructure, and mechanical properties of ZrB_2-based composites. The main goal was to develop a process that incorporates high strength continuous SiC fiber in a ZrB_2-based matrix. In order to achieve this, the densification, microstructure, and mechanical properties of ZrB_2-$ZrSi_2$ monolithic ceramics were characterized along with various SiC fiber reinforced ceramic matrix composites (CMCs) utilizing the same matrix.

There were two main areas of study in this thesis. The initial study demonstrated that additions of $ZrSi_2$ into a ZrB_2 ceramic increases densification at significantly reduced processing temperatures ($\leq 1600°C$). This study revealed that low concentrations of $ZrSi_2$ (7.5 vol%) yield near fully dense (>96% relative density) ZrB_2-based ceramics with strengths >700 MPa. The microstructures exhibited well-dispersed second phases, with the exception of ZrB_2 containing 20 vol% $ZrSi_2$ that contained larger second phase regions (~40 μm). The second study demonstrated the ability to incorporate various grades of commercially available SiC fibers into a matrix based on the ZrB_2-$ZrSi_2$ ceramics developed in the initial study. Composites consisted of dense ZrB_2-$ZrSi_2$ matrices with SiC fiber loading ranging from 15 to 20 vol%. Apparent peak flexure strengths were reduced for ZrB_2-based CMCs incorporating continuous SiC fiber (<500 MPa), but strain to failure was increased up to 3%.

Together these studies demonstrate the viability of using a ZrB_2-based matrix in a continuous SiC fiber reinforced CMC. Several key challenges were investigated to enable compatibility. The impact of SiC fiber reinforcement in ZrB_2-based CMC mechanical behavior was determined.

ACKNOWLEDGEMENTS

I would like to extend my sincerest gratitude to my advisors Drs. Gregory Hilmas and William Fahrenholtz for all of their assistance through my time as a Masters student. I value their guidance above all others and I extend my deepest gratitude for allowing me to study and work under their tutelage.

Dr. KC for taking the time to be on my committee and support of my thesis.

I would also like to thank Dr. Jeremy Watts for his constant support and banter as well as continually destroying me both physically and mentally. I have come much further than I ever imagined in regard to both.

Next, I would like to thank all of my friends and colleagues in the UHTC group - past and present. Thanks to Dr. Harlan Brown-Shaklee, Dr. Matt Thompson, Greg Harrington, Derek King, Jason Lonergan, Maryam Kazemzadeh Dehdashti, Eric Neuman, Andrea Els, Devon McClane, and Ryan Grohsmeyer.

Finally, I must thank my girlfriend, Lauren Svoboda, for her constant support and love. I would be a completely different man without her.

TABLE OF CONTENTS

LIST OF ILLUSTRATIONS

LIST OF TABLES

1. INTRODUCTION

Zirconium diboride (ZrB_2) is one of a class of materials known as ultra-high temperature ceramics (UHTCs) that have both strong covalent and metallic bonding character, resulting in melting temperatures above 3000°C, high hardness (>20 GPa), and high modulus (>500 GPa).[1,2] Thus, ZrB_2 has been considered for a number of ultra-high temperature applications including molten metal crucibles, high temperature electrodes, and cutting tools.[3-7] Owing to the high degree of metallic bonds, the relatively high thermal conductivity (60-125 $W \cdot (m \cdot K)^{-1}$) and low electrical resistivity (7.8-22 $\mu\Omega \cdot cm$) of borides set them apart from other potential UHTC materials, specifically carbides and nitrides.[8-11] ZrB_2 based composites have extremely high melting temperatures (3250°C), high strength (>500 MPa), resistance to chemical attack, as well as high thermal conductivity (60-145 $W \cdot (m \cdot K)^{-1}$) making them attractive candidates for ultra-high temperature aerospace applications such as thermal protection systems on hypersonic vehicles.[2,9-13]

However, in such applications a material is not only subjected to extreme temperatures due to aerothermal heating, but also is subjected to high stress due to nonuniform loading as well as thermal shock conditions caused by near instantaneous heating. Due to their inherently brittle nature, monolithic ceramics fall short of ideal behavior, where catastrophic failure is common. For example, ZrB_2 based monolithic ceramics are prone to thermal shock with relatively low instantaneous temperature changes (~400°C).[14] To potentially overcome these types of limitations, continuous fiber reinforcement has been proposed for several systems, such as carbon fiber in a silicon

carbide matrix (C/SiC), SiC fiber in a SiC matrix (SiC/SiC), SiC fiber in a silicon nitride matrix (SiC/Si_3N_4), but is limited with regard to ZrB_2 based systems.[15-19]

Ceramic matrix composites (CMCs) or continuous fiber reinforced ceramic composites (CFCCs) have been studied by a number of researchers due to their ability to overcome conventional monolithic ceramic limitations. C/SiC and SiC/SiC composites have been of interest recently for their higher temperature capabilities (i.e. ~1600°C) and improved damage tolerance under mechanical loads.[20-26] However, application of C/SiC and SiC/SiC composite systems to ultra-high temperature regimes (i.e. >2000°C typically seen in hypersonic flight conditions) is limited due to significant ablation, oxygen ingress (i.e. active oxidation dominates above 1600°C, where passive oxidation provided protection at lower temperatures), and embrittlement.[27-32] Use of CFCCs under these severe conditions necessitates a compatible ultra-high temperature matrix to resist ablation arising from thermomechanical, thermochemical, and thermophysical influences. In recent years, ZrB_2 based systems have seen significant improvements to oxidation resistance.[33] Additionally, significant advancements have been made regarding characterization of oxidation/ablation behavior (i.e. mechanisms operating in defined temperature regimes) in ZrB_2 based systems.[34-36] CFCCs utilizing an ultra-high temperature matrix and high-strength continuous fibers should offer a beneficial combination of a higher use temperature while maintaining an oxidation/ablation resistant matrix along with a graceful failing/damage-tolerant reinforcing phase.

Typical processing of ZrB_2 based materials requires very high temperatures (>2000°C), which is a regime unsuitable for processes incorporating SiC fiber reinforcements. Commercially available SiC fibers have reported maximum processing

and use temperatures in the range of 1000°C to 1600°C, depending on the manufacturer and grade where decreasing relative oxygen content results in a higher grade fiber.[37-41] Due to this discrepancy, the high temperatures utilized in densifying pure ZrB_2 materials limit the applicability of SiC fiber reinforcement in these materials. Utilizing additives and second phases, the processing temperatures required to achieve full density in a ZrB_2 based system are effectively reduced, increasing the viability of a continuous SiC fiber reinforcement phase. It has been shown that ZrB_2 incorporating combinations of boron carbide (B_4C), carbon (C), as well as fine SiC particulate effectively reduce processing temperatures, often bringing peak densification temperatures below 2000°C.[42-45] In light of maximum use temperatures of commercially available SiC fibers and their limited ultra-high temperature capabilities, further reductions in processing temperature are required. Silicon nitride (Si_3N_4) has been shown to reduce hot-pressing temperatures to ~1700°C to achieve near full density in ZrB_2.[46-48] It has been shown that disilicides form an in-situ liquid phase during processing, allowing for increased densification at significantly reduced processing temperatures (i.e. 1400 to 1800°C). Of particular interest are the transition metal disilicides, specifically, $HfSi_2$, $MoSi_2$, and $ZrSi_2$.[49,50] This increased sinterability allows for ZrB_2 to form a compatible matrix material to various grades of commercially available SiC fibers.

Previous studies have tended to focus on the mechanical properties of monolithic compositions of ZrB_2 with $ZrSi_2$ additions[51] or a ZrB_2 based matrix reinforced with second phase particulate, whiskers, or short-chopped fibers.[45,46,52,53] In contrast, the research reported in this thesis examines development of a suitable ZrB_2-$ZrSi_2$ matrix, green processing techniques utilizing continuous SiC fiber tow, and necessarily

investigates the microstructural evolution and mechanical properties of both. The

research answered a number of technical questions including:

1. How does $ZrSi_2$ affect the densification and mechanical properties of
   monolithic ZrB_2 with varying processing temperatures?

2. How does continuous SiC fiber reinforcement affect the mechanical
   properties of ZrB_2 based composites?

3. What is the effect of different commercially available SiC fiber types, as
   well as interface coatings, on mechanical performance?

To answer these questions, mechanical performance was evaluated by measuring

strength, hardness, toughness, as well as work of fracture for SiC fiber reinforced ZrB_2

based composites. Using flexural testing, mechanical performance was evaluated for

different ZrB_2-$ZrSi_2$ monolithic materials as well as several types of SiC fiber

reinforcement. Microstructural analysis was also conducted using optical and scanning

electron microscopy techniques.

2. LITERATURE REVIEW

The purpose of this section is to introduce the published research that is related to the work presented in this thesis. This section will first discuss the densification and mechanical properties of monolithic ZrB_2. Then, the later portion will discuss structure and properties influential in state-of-the-art ceramic fiber reinforced ceramic matrix composites, as well as their recent innovations.

2.1 ULTRA HIGH TEMPERATURE MATERIALS AND ZrB_2

The pursuit of hypersonic capable vehicles has led to increasing interest in ultra-high temperature ceramics (UHTCs). These materials are suitable for thermal protection systems (TPS) as well as structural materials due to their extremely high melting points (>3000°C) and high strength (>500 MPa). Current generation carbon/carbon (C/C) composites, as well as silicon carbide based composites (i.e. C/SiC and SiC/SiC), are useful at temperatures up to ~1600°C. Above 1600°C rapid oxidation and significant reductions to strength are observed.[54] An investigation of potential ultra-high temperature materials has shown that carbides and refractory metals have poor oxidation characteristics.[33] Zirconium diboride (ZrB_2) has been studied by a number of researchers due to its unique combination of thermal and mechanical properties. ZrB_2-based composites have high thermal conductivity (60-145 $W \cdot (m \cdot K)^{-1}$)[9,10,13] as well as high strength (>500 MPa),[2,55] making them attractive candidates for ultra-high temperature aerospace applications. Continued use of UHTCs under hypersonic flight conditions will repeatedly expose these materials to extreme environments (e.g. temperatures above 2000°C, high stresses and nonuniform loading due to aerothermal heating, as well as thermal shock and oxidative conditions). Next generation, hypersonic capable vehicles

will require materials capable of retaining high strength and thermal conductivity, as well environmental stability beyond current limitations.

2.2 FORMATION OF ZrB$_2$ CERAMICS

There exists a wide range of processing and densification methods for ZrB$_2$ based ceramics. The following sections focus on studies that are relevant to the research presented in this thesis. Typical green processing involves conventional ceramic powder processing methods, but recent advancements have been made to incorporate organic additives to ease processing (i.e. tape casting). Several methods of densification are employed for ZrB$_2$ based ceramics, including: hot isostatic pressing (HIP), spark plasma sintering (SPS), reactive hot pressing (RHP), hot pressing (HP), and pressureless sintering (PS). The following sections focus on the more widely used pressureless sintering and hot pressing.

2.2.1 Ceramic Slurry and Tape Casting.
Recent work has focused on the fabrication of green specimens of ZrB$_2$-based ceramics via tape casting and lamination methods traditionally employed for electronic ceramics (i.e. thin film capacitors).[56-58] Flexible, homogenous green specimens are formed by combining ceramic powders, organic additives, and aqueous or organic solvents. Colloidal processing to form suitable ceramic slurries traditionally involves a number of key steps: (i) ball milling ceramic powders with a solvent and an organic dispersant, (ii) addition of organic binder, (iii) incorporation of plasticizers, (iv) filtration to remove undissolved binder or plasticizer, as well as large particle agglomerates, and (v) de-airing of the slurry by vacuum evacuation and slow-rolling. Stabilization of a ZrB$_2$ ceramic slurry is achieved by either modification of the particle surface by a low molecular weight organic additive (i.e. those

employed in organic solvent based systems) or adjustment of pH in aqueous systems to control interparticle pair potentials.[58] Organic binders are typically high molecular weight polymers (M_w = 40,000-90,000 g·mol^{-1}) with softening points (T_g) between 60-90°C. The binder acts as a bridge between ceramic particles and adds strength to the green product. Plasticizers are added to maintain flexibility in the dried slurry. Slurries are then cast via a doctor blade and dried to fabricate thin (200 to 700 µm), homogenous, and flexible green tapes. Most often these tapes are then laminated by uniaxial load at temperatures slightly above the T_g of the binder to form green components. Recent work by Lu *et al*. showed that ZrB_2-SiC ceramics prepared by tape casting methods, followed by hot pressing, resembled microstructures similar to those prepared by conventional powder processing and hot pressing.[56] Additionally, work by Medri *et al*. showed that ZrB_2 and ZrB_2-SiC green tapes could be utilized to form complex shapes in the green state (e.g. tubes, rings).[57] Further, these specimens were densified to >95% relative density by pressureless sintering at 2150°C.

  2.2.2 Pressureless Sintering. Densification of ZrB_2 typically requires very high temperatures (>2000°C). Specimens are densified without the aid of a uniaxial load to assist in particle rearrangement during the initial stages of pressureless sintering. Use of this technique has gained interest due to its ability to yield larger, near net-shape parts with complex geometries. Early work concerning pressureless sintering of ZrB_2 typically required the addition of second phase additives to enhance densification, due to its high activation energy for sintering.[6] It has been shown that ZrB_2 can be fully densified at temperatures below 2000°C by a combination of particle size reduction (i.e. increasing surface area of starting powders, thus increasing surface free energy and driving force for

densification) and addition of second phases.[42,43,59] Specifically, additives such as C, B_4C, and $MoSi_2$ have been used to remove or modify surface oxides (i.e. ZrO_2 and B_2O_3) present on ZrB_2 powders (Reactions 1-3).[43,60] These oxides inhibit densification by enhancing surface diffusion and vapor transport, which are known to be nondensifying, grain coarsening mechanisms in solid-state sintering.[61]

$$7ZrO_2 + 5B_4C \rightarrow 7ZrB_2 + 3B_2O_3 + 5CO(g) \tag{1}$$

$$ZrO_2 + 5C + B_2O_3 \rightarrow ZrB_2 + 5CO(g) \tag{2}$$

$$2ZrO_2 + B_4C + 4C \rightarrow 2ZrB_2 + 4CO(g) \tag{3}$$
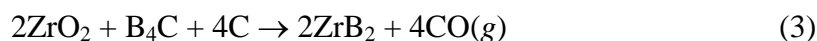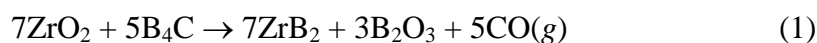
Additionally, transition metal disilicide additives ($MeSi_2$), such as $MoSi_2$, $TaSi_2$, or $ZrSi_2$, are thought to form an in-situ liquid phase at elevated temperature by reaction of SiO_2 and B_2O_3 to form borosilicate glassy phase.[62] This allows for increased particle rearrangement during the initial stages of sintering. The liquid phase exerts a psuedo-hydrostatic pressure (~3 MPa) on a powder compact due to capillary forces present in the porous particle network.[61] Silvestroni and Sciti showed that 15-20 vol% $MoSi_2$ in ZrB_2 achieved >98% relative density by pressureless sintering at 1800°C for one hour.[60] Further, work by Guo *et al*. showed that ZrB_2 with 20 vol% $ZrSi_2$ can be fully densified by pressureless sintering at 1650°C for one hour.[50]

    2.2.3 Hot Pressing. Densification of ZrB_2 is typically accomplished by hot pressing, due to its strong covalent bonding and low diffusion rates.[63] Applying pressure during high temperature densification typically allows for faster densification rates and finer grain sizes. For example, ZrB_2 has been shown to reach full density at temperatures

as low as 1900°C by hot pressing without additives.[12] In contrast, pressureless sintering requires temperatures that are a few hundred degrees higher.[42] However, in both methods, the peak densification temperatures and times required to reach full density can be reduced by incorporation of second phase additives. Similar to the studies of pressureless sintering, C, B_4C, and transition metal disilicides may be used to promote densification in hot pressed ZrB_2. With the aid of an externally applied load, densification is facilitated by different means. Removal of surface oxides using additives such as C and B_4C are still readily employed in hot pressing (peak densification temperature <2000°C), but further reductions in processing temperatures are required. For example, $MoSi_2$, $TaSi_2$, and $ZrSi_2$ additions have been shown to yield >95% relative density by hot pressing in the range of 1350°C to 1900°C.[64-66] The addition of $MeSi_2$ is generally considered to improve densification by two mechanisms: (i) reaction of SiO_2 surface impurities present on $MeSi_2$ powders with B_2O_3 surface impurities on ZrB_2, resulting in the formation of a low melting temperature liquid that lubricates and permits increased rearrangement of ZrB_2 particles; and (ii) ductility of the $MeSi_2$ at elevated temperature which allows it to deform and fill void space between the hard ZrB_2 particles. Work by Sciti et al. in a study of 15 vol% $TaSi_2$ additions in HfB_2 and ZrB_2 demonstrated a microstructural morphology consistent with the latter behavior after hot pressing at 1850°C (i.e. T_m of $TaSi_2$ = 2200°C), and similarly for $MoSi_2$ in ZrB_2 (i.e. T_m of $MoSi_2$ = 2030°C).[66] Guo et al. described this process for $ZrSi_2$ in ZrB_2 (Figure 2.1).[64]
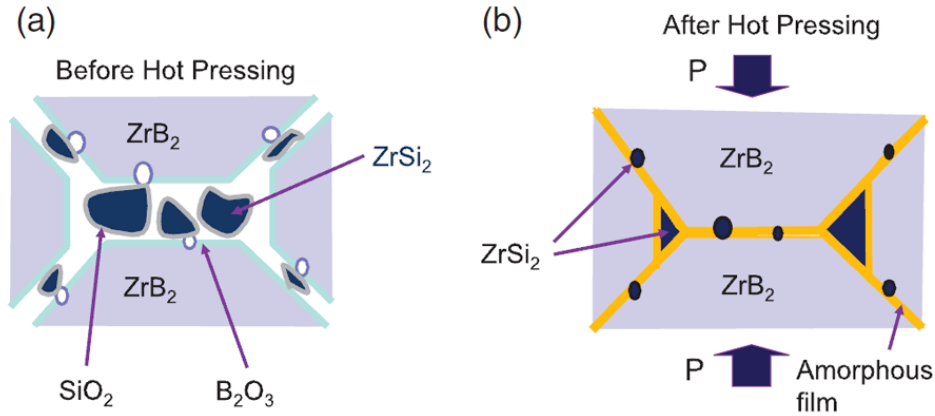
Figure 2.1. Schematic representation of the densification mechanism in ZrB$_2$-ZrSi$_2$ ceramics during hot pressing.[64]

2.3 MECHANICAL PROPERTIES

A number of testing procedures are used to evaluate how a ceramic will perform in its intended application. Most often, for high temperature structural ceramics, these include measuring properties such as strength, modulus, hardness, toughness, and creep. The following sections focus on flexure strength measurement and related microstructural effects pertaining to work presented in this thesis.

2.3.1 Flexure Strength. Determination of strength in brittle materials is typically obtained by flexure testing due to its ease of use and simple specimen geometry. ASTM C1161-02c describes the guidelines for flexure testing of advanced ceramics at ambient temperature. Strength is determined by measuring the load required for failure, defined in Equation 2.1

$$\sigma = \frac{My}{I} \tag{2.1}$$

where σ is flexural strength, M is the bending moment, y is the distance from the neutral axis, and I is the moment of inertia. Figure 2.2 depicts the shear and bending moment

forces generated during three-point and four-point flexure testing. Four-point flexure is favored for the vast majority of cases due to several reasons including: (i) a significantly greater volume of material is under load, so strength values obtained offer a more accurate representation of a material's characteristic strength; and (ii) elimination of shear forces in the region of highest bending moment, which removes Mode II and III (in-plane and out-of-plane shear) and makes failure dependent on only Mode I tension.[67] It should be noted that strength calculated using Equation 2.1 assumes a constant cross sectional area during a failure event. In the event of noncatastrophic failure (i.e. load decreases gradually over a period of time rather than instantaneously), Equation 2.1 underestimates the true characteristic strength. Tensile testing still provides the truest measure of strength,[67] but efforts have been made to infer tensile strength from observed flexure behavior in fiber-reinforced CMCs.[68]
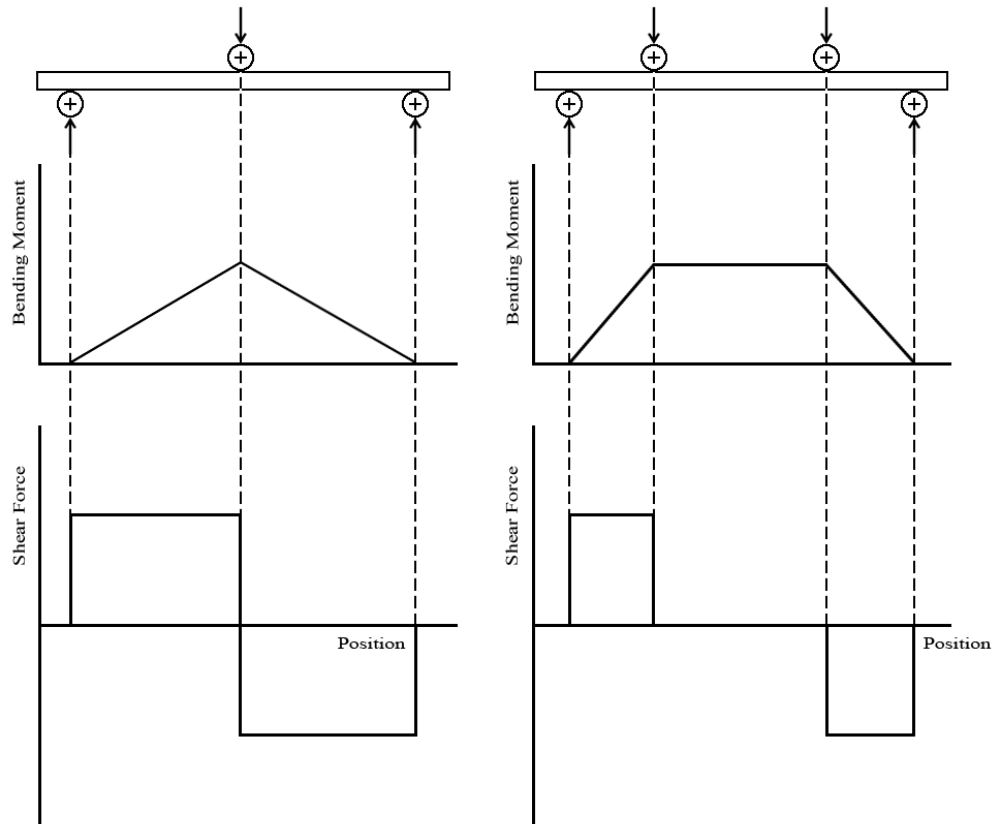
Figure 2.2. Three-point (left) and four-point (right) flexure testing setups with accompanying shear force and bending moment diagrams.[69]

2.3.2   Additive Effects. The addition of second phases improves densification, but also has significant effects upon mechanical properties including: hardness, elastic modulus, fracture toughness, and strength. The key to designing ceramics with the intended mechanical performance lies in control of the microstructure. Properties such as grain size, relative porosity, and composition of second phases are influential when discussing microstructural effects on mechanical properties. For example, hardness has been shown to decrease with increasing grain size in non-cubic crystalline materials.[70,71] The addition of second phases influences grain growth. For example, a dispersed SiC

particulate phase in ZrB_2 has been shown to inhibit grain growth, effectively pinning

small grains.[72] In contrast, in-situ liquid phases have been shown to enhance grain

growth in ZrB_2 due to enhanced diffusion through the liquid phase during high

temperature treatment.[52,60] In brittle ceramics that are free of other, larger defects, large

grains act as strength limiting flaws to determine the strength. Therefore, a

microstructure consisting of fine grains with no larger critical flaws exhibits a relatively

higher characteristic strength.[67] Additionally, porosity influences strength and modulus

by acting as stress risers (i.e., flaws) in the ceramic. Due to the significant effect of

microstructure on mechanical performance, design and interpretation of mechanical

performance must be necessarily accompanied by evaluation of the microstructure.

2.4   CERAMIC MATRIX COMPOSITES

Ceramic matrix composites (CMCs) or ceramic fiber reinforced ceramic matrix

composites (CFCCs) have been studied by a number of researchers due to their ability to

overcome conventional monolithic ceramic limitations. In addition to providing a useful

combination of increased toughness and graceful failure, continuous fiber reinforcement

provides resistance to thermal shock. These are essential considerations for future CMC

reliability. Current generation state-of-the-art CMCs are reinforced with either carbon or

SiC fiber inside a wide variety of matrix materials. Most often the matrix materials are

carbon or SiC, with some work into other high temperature refractory fillers. SiC fibers

have gained popularity due to their increased oxidation resistance compared to carbon

fibers. A small body of work has been performed concerning ZrB_2 reinforced with

continuous SiC fiber. The following sections discuss relevant information pertaining to

commercial SiC fibers, fiber-matrix interface structure and properties, and a brief overview of current generation CMCs.

        2.4.1   Commercial SiC Fiber. There exists a wide range of commercially available SiC fiber, with properties dependent on composition, processing conditions, and heat treatments. A number of commercial SiC fibers and their properties are summarized in Table 2.1. Historically, larger diameter (80 to 140 µm) fibers were formed by a series of alternating carbon and SiC chemical vapor deposition (CVD) steps on pitch-based carbon monofilament substrates, such as SCS-6 and SCS-9a fibers.[73,74] These fibers were developed mainly for use in metal matrix composites, such as a Ti-6Al-4V reinforced with SCS-6.[75] The SCS series of C/SiC fibers show good strength (4 to 6 GPa) and high temperature capability, but are narrow in application due to insufficient flexibility (i.e. ability to be woven into plies). In order to overcome such a limitation, smaller diameter fibers were required to increase workability. A polycarbosilane polymer precursor is used to form the vast majority of current generation small diameter fibers (7.5 to 15 µm). One method of forming SiC fibers utilizes polymer precursors where they are formed by melt spinning through a spinneret and crosslinked/heat treated at elevated temperature to form partially crystallized or fully crystallized SiC fiber.[76,77] Ceramic Grade (CG) Nicalon, produced by Nippon Carbon, is heat treated under oxygen atmospheres to form silicon oxycarbide fibers with as much as 12 wt% oxygen present in final fiber composition.[32] In these fibers, the matrix consists of ultra-fine β-SiC crystallites (<2 nm) and a Si-C-O amorphous phase. An average tensile strength of 3 GPa is typically observed for Nicalon fibers. Heat treatment under an inert atmosphere leads to excess turbostratic carbon present in the microstructure (i.e. ~1.4 C/Si ratio), represented by Hi-

Nicalon variants in industry. Relative oxygen impurity in Hi-Nicalon fibers is ~0.5 wt%.

Tensile strengths are slightly reduced at ~2.8 GPa in Hi-Nicalon fibers, presumably due

to increased grain growth resulting from excess carbon. Further refinement consists of a

high temperature treatment in H_2, forming Hi-Nicalon Type S fiber, where relative

oxygen content is reduced to ~0.2 wt%. Hi-Nicalon Type S fibers consist predominantly

of nearly stoichiometric SiC (i.e. C/Si ratio 1.05) with very little excess carbon.[78] The

Type S fibers have exhibited increased high temperature creep resistance due to its

increased crystallite size (i.e. 20 to 50 nm).[79] A similar small diameter fiber is produced

by Dow Corning using a polycarbosilane precursor doped with boron and titanium

containing precursors, known in industry as Sylramic fiber.[80] The final product of this

fiber composition is fine β-SiC crystallites ranging in size from 100 to 500 nm along with

small amounts (<3 wt%) of TiB_2 of size ~50 nm existing at β-SiC triple points.

Additionally, Sylramic fiber can undergo a high temperature treatment under N_2

atmosphere to form a thin (50 to 100 nm) in-situ boron nitride (BN) coating (Sylramic

iBN) that aids in protection by serving as a diffusion barrier at elevated temperatures.

Table 2.1. Commercially Available SiC Fiber Composition and Properties

Fiber	Density	Crystallite Size	Composition Si:C:O	C/Si	Filament Diameter	Tensile Strength	Tensile Modulus
	(g/cm^3)	(nm)	(wt%)	(at. ratio)	(μm)	(GPa)	(GPa)
SCS-6[73,75,81]	3.08	-	-	-	142	3.9	380
SCS-9a[82]	3.08	-	-	-	80	5.9	415
CG Nicalon[83]	2.55	< 2	57:32:12	1.31	14	3.0	210
Hi-Nicalon[80,83]	2.74	5-10	62:37:0.5	1.39	12-14	2.8	270
Hi-Nicalon Type S[83,84]	3.10	20-50	69:31:0.2	1.05	12	2.6	420
Sylramic[80,83,84]	3.10	100-500	66.6:28.5:0.8*	1.0	10	2.6	420
Tyranno Lox-M[85,86]	2.48	amorphous	55.4:32.4:10.2**	1.37	11	3.4	187
Tyranno-S[87]	2.68	2	50.4:29.7:17.9**	1.65	8.5	3.3	170
Tyranno-ZMI[88]	2.48	amorphous	56.1:34.2:8.7†	1.44	11	3.4	200
Tyranno-SA[84,89,90]	3.10	> 200	67.8:31.3:0.3††	1.08	7.5, 10	2.8	420

*Contains ~2 wt% B and Ti, and ~0.4 wt% N †Contains ~1 wt% Zr

**Contains ~2 wt% Ti ††Contains ≤ 2 wt% Al

A number of commercial SiC fibers, known as the Tyranno series, are also produced by Ube Industries using modified polytitanocarbosilane precursors. These modified precursors are typically formed from a polycarbosilane precursor and titanium tetrabutoxide. As a result of the precursor composition, the "low oxygen" Tyranno Lox-M and Tyranno-S fiber grades contain ~2 wt% titanium. This small amount of titanium has significant effects on the high temperature creep of the fiber, hence different modifications to the precursor composition were explored.[88] The Tyranno-ZMI fiber uses a zirconium precursor addition, and thus the final fiber composition contains ~1 wt% zirconium. These fibers consist of an amorphous Si-(Ti,Zr)-C-O phase. The oxidation rates of these fibers has been observed to be greater than that of bulk SiC.[88] Hence, investigation and formation of stoichiometric crystalline SiC fibers was necessitated. A nearly stoichiometric, and highly crystalline (i.e. crystallites >200 nm) Si-Al-C Tyranno fiber (Tyranno-SA) was developed containing ≤2 wt% aluminum. The tensile strength of the Tyranno fibers has been shown to decrease after treatment at 1300°C, falling below 0.5 GPa after treatment at 1600°C.[88] The Tyranno-SA fiber has improved high temperature capabilities, especially concerning creep resistance, due to its highly crystalline β-SiC structure. Additionally, the Tyranno-SA fiber has also been shown to have a slight increase in strength (i.e. 0.5 to 2 GPa) after heat treatment at 1700°C under argon, this is presumably due to partial sintering of the fiber originating from the residual Al content.

The literature concerning SiC fibers leads to a number of considerations when implementing different commercial SiC fiber types. To achieve reliable workability and adequate flexibility, the fiber must be of sufficiently small diameter (< 15 μm).

Additionally, to provide high strength, the structure must be amorphous or nanograined as well as contain defect free surfaces. The former is achieved by utilizing polymer precursors and successive pyrolysis stages to achieve desired crystallite sizes, while the latter is limited by the aperture through which precursor fibers are melt spun.[77] Fine grains (2-100 nm) offer increased strength at room and elevated temperatures, but lead to increased high temperature creep.[79] Hence, the development of Sylramic and Tyranno-SA fibers that show increased resistance to high temperature creep, with only small reductions to ultimate tensile strength.

    2.4.2 Fiber-Matrix Interface. Interphase coatings applied to ceramic fibers in ceramic matrix composites serve several vital purposes. The strength and long-term durability of CMCs are influenced by rupture of fibers in a matrix, but also environmental degradation of constituent fibers. The interface between the fiber and matrix must possess a lower surface energy so the matrix cracks will deflect at the interface, providing non catastrophic failure and damage tolerance (Figure 2.3). The debond energy and sliding resistance along the debond region are critical parameters in CMCs.[91-96] Cracks formed during failure are deflected along the interface, which enables energy dissipation through friction, giving rise to a pseudo-ductile macroscopic fracture behavior.[91,97] Composites that exhibit a high degree of interdiffusion between fiber and matrix have strong bonding at the fiber-matrix interface, which typically results in brittle fracture due to the inability of the interface to serve as a crack arrester. Thermochemical and thermomechanical considerations dictate that an interface consist of one or more inert, thin coatings (i.e. <2 μm) between fiber and matrix. As a crack propagates through the weak interphase, a suitably thin coating will confine the crack path compared to a

thicker coating (also included in Figure 2.3). In a thicker interphase coating, a crack will have a greater probability of meandering during propagation, thereby extending crack lengths and decreasing toughness.[98] The interphase also acts to protect fibers from damage during fabrication or environmental attack during use.[31]
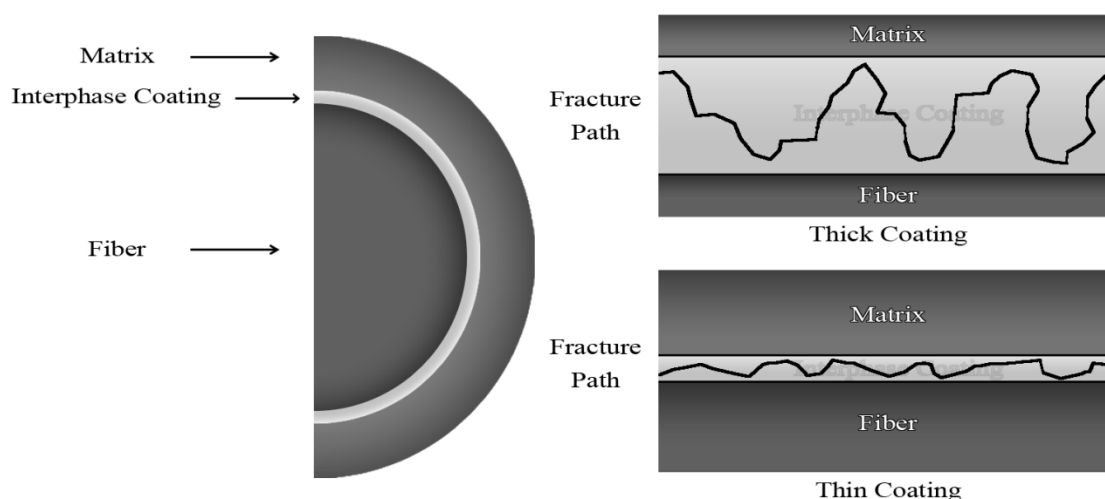
Figure 2.3. Representative CMC structure with accompanying representation of crack paths along weak interphase.

A number of interphases have been explored in C/C, C/SiC, and SiC/SiC CMCs. Pyrolytic carbon interphases have been shown to improve composite behavior in SiC/SiC CMCs.[89,90,99] For example, previous work by Shimoda *et al.*, pyrolytic carbon applied by CVD process with thicknesses greater than 0.5 μm in a SiC/SiC CMC showed significant crack deflection and fiber pullout during flexure testing.[99] Further, they showed that increasing pyrolytic carbon thicknesses had an inverse relationship with maximum flexure strength, where a thickness of ~1 μm reduced the maximum flexure strength from over 1 GPa to less than 400 MPa.

The use of BN coatings has gained prevalence over pyrolytic carbon recently due its increased oxidation resistance.[31] Typically, deposition of BN on ceramic fibers is

performed by CVD where the structure and performance are subject to processing conditions and composition. BN coatings deposited at low temperatures are amorphous or turbostratic BN, while those deposited at high temperatures (above ~1500°C) are hexagonal BN. One major concern concerning use of BN coatings is the intermediate temperature range oxidation and gasification of oxide species, specifically a hydrated borate species. Previous work by Tressler *et al.* showed that nominally pure CVD-BN deposited at 1800°C is oxidized and volatilized in relatively low partial pressures of H_2O (i.e. 1 to 10%) at 700 and 800°C.[31] One method to overcome this limitation is utilizing doping species in BN deposited by CVD, for example, Si. Utilizing a CVD-BN doped with ~22 wt% Si, oxidation and volatilization rates are effectively reduced in BN interphase coatings applied to ceramic fibers.[100] It is generally considered that formation of an in-situ amorphous SiO_2 phase effectively seals surface flaws and prevents further oxygen ingress to protect the fibers.[101]

Additionally, the fiber-matrix interface acts as a buffer zone to accommodate misfit stresses that arise from fiber movement in a matrix and thermal residual stresses. Work by Kerans, as well as Singh and Reddy, in studies of oxide coatings on SiC fibers, suggested that an interphase material must be of sufficiently low strength, but also adequately compliant.[98,102] They showed that increased elastic modulus in a fiber coating resulted in increased radial stresses. Further, it was shown that oxide coatings of thickness 0.5 to 1 μm were required to effectively reduce thermal expansion mismatch between bulk SiC and Nicalon fiber (4.5×10^{-6} K^{-1} and 3.1×10^{-6} K^{-1} respectively at room temperature). Conversely, work by Miller *et al.* showed that even pyrolytic carbon coatings with thicknesses of < 0.1 μm displayed fiber pull-out and considerably high

strain-to-failure (~0.5%, tensile).[103] Further, they showed that increasing the single

component pyrolytic carbon coating to thicknesses >0.13 µm rapidly reduced ultimate

flexure strength (i.e. 330 MPa at 0.27 µm thickness and 275 MPa at 0.58 µm thickness).

Additionally, BN interphases with thicknesses greater than 0.15 µm have been shown to

improve noncatastrophic mechanical failure in SiC/SiC composites. Work by Prouhet *et

al*. showed that BN interphase coatings of thickness 0.15 to 2.7 µm displayed increased

strain-to-rupture and increased fiber pull-out length.[104] However, ultimate strength and

elastic modulus were expectantly reduced. These studies leave uncertain as to what is the

ideal combination of interphase thickness and composition to achieve sufficient

mechanical performance in the form of damage tolerance and/or noncatastrophic failure.

A composite with sufficient strength, environmental stability, and noncatastrophic failure

will necessarily consider all these factors.

2.4.3 Carbon/Carbon. Carbon/carbon composites have been explored for

ultra-high temperature applications for a number of reasons. C/C composites have

excellent retention of strength and modulus at high temperatures, as well as high damage

tolerance.[105] However, significant oxidative degradation occurs when exposed to oxygen

containing environments above 500°C. Gasification and volatilization of carbon species

proceeds by the following reactions:

$$C + O_2 \,(g) \rightarrow CO_2 \,(g) \tag{4}$$

$$C + {}^1\!/_2 \, O_2 \,(g) \rightarrow CO \,(g) \tag{5}$$

Advancements have been made to C/C composites by utilizing coating materials to

prevent oxidation and form an in-situ oxide during high temperature testing. For

example, SiC applied to C/C to form a protective SiO_2 glassy phase, which also prevents

further ingress of oxygen due to its low oxygen permeability.[101,106,107] However, any

flaws that penetrate through the coating thickness have a "drilling" effect into the

underlying C/C composite (Figure 2.4). In this way, the carbon fibers and carbon matrix

are rapidly decomposed by Reactions 4 and 5 through a pinhole flaw in the protective

coating. Attempts were made to incorporate ZrB_2 to C/C composites in the form of

particulate, but without an exterior, impermeable coating oxidation protection was not

markedly improved.[108] Considering that a number of high temperature applications

include the potential for use in extreme environments that will contain some partial

pressure of O_2, advancements in the form of new materials systems were required. While

C/C composites have high strength and high temperature capability under inert

atmospheric conditions, they suffer from a highly restrictive drawback in the form of

their poor oxidation performance. Hence, transitions to material systems utilizing SiC

became widespread.
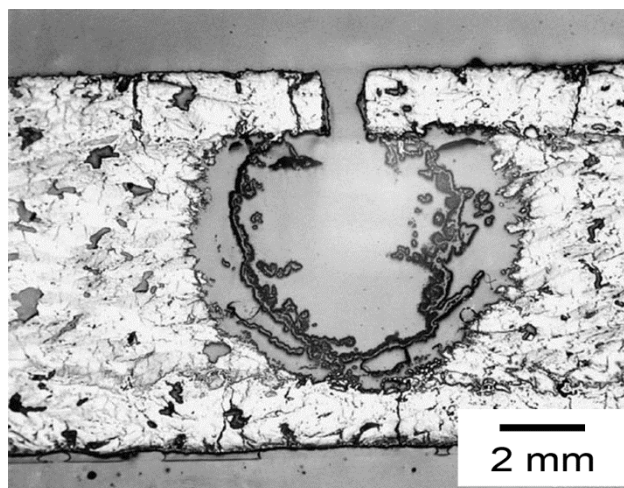
Figure 2.4. C/C Composite with SiC conversion coating oxidized by arc-jet for 3.5 hours
at ~1540°C.[106]

2.4.4   Carbon and SiC Fiber/SiC. A significant amount of work has been done investigating mechanical and oxidation performance of SiC fiber reinforced CMCs.[17,23,24,32,89,90,99,109,110] Several methods are common in preparation of SiC fiber reinforced composites including: polymer impregnation and pyrolysis (PIP), Si melt infiltration (MI), a combination of CVD and chemical vapor infiltration (CVI), as well as processes incorporating powder loaded slurries. It is common for these processes to be used in conjunction with one another, as well as utilizing traditional pressureless sintering and hot pressing techniques. For example, previous work by Dong *et al*. showed retained strengths of ~400 MPa in SiC/SiC composites after hot pressing at 1750°C. In contrast, the previously discussed processes are typically used to minimize thermal degradation of constituent fibers during processing. PIP processed composites are typically formed by infiltration of a polycarbosilane precursor into a woven fiber preform that undergoes successive pyrolysis stages to yield a final ceramic. In general, polymer impregnation and pyrolysis requires several cycles to achieve adequate final density. This is due to an ~80 wt% yield of polycarbosilane precursors, such as SMP-10, when converting to crystalline SiC. During pyrolysis, a shrinkage of ~72 vol% occurs due to the incomplete conversion and the difference in density between the polymer precursor and bulk SiC (0.98 g/cm^3 for SMP-10 and 3.21 g/cm^3 for SiC). As a result, voids, microdelaminations, and matrix cracking are observed. Despite repeated cycles to fill and eliminate cracks and voids developed during processing, these composites still contain ~10-15 vol% open porosity.[111] Hence, improvements to processing conditions were required.

CVI is an effective method of forming SiC matrix in SiC/SiC composites, but it has several drawbacks. SiC/SiC composites prepared by solely CVI, for instance, contain

large matrix pores (10-500 µm), have lower thermal conductivity (<15 W·(m·K)$^{-1}$), and permit access to the composite interior in oxidizing atmospheres (Figure 2.5).[23,112] Additionally, pores act as stress concentrators leading to low proportional limits at <200 MPa (i.e. transition from elastic to inelastic and pseudo-ductile fracture behavior).[113] In contrast, SiC/SiC composites prepared by silicon melt infiltration have lower matrix porosity (also in Figure 2.5), a relatively higher thermal conductivity (~60 W·(m·K)$^{-1}$), and higher proportional limits (i.e. first matrix cracking stresses) at ~500 MPa.[23] However, residual silicon in these materials can be anywhere from 10 to 30 vol%.[114] Typically, SiC/SiC composites have proven to be highly reliable, and offer a beneficial combination of high strength and environmental stability. For example, a SiC/SiC component formed by a combination of PIP and MI processing was shown to retain functionality during mechanical loading and oxidizing conditions for hundreds of hours at $\sim1400°$C.[115]
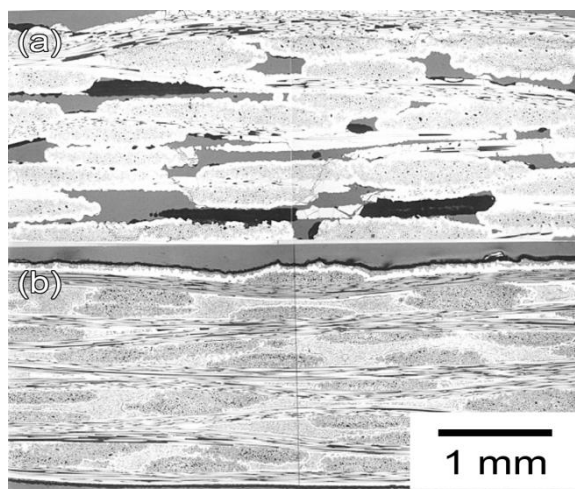
Figure 2.5. SiC/SiC composite microstructures formed by (a) CVI and (b) Si MI.[23]

The fundamental limitation to SiC/SiC composites is their performance at temperatures greater than 1400°C in oxidizing environments. It is well known that SiC

transitions from passive (Reaction 6) to active (Reaction 7) oxidation behavior at elevated temperatures.

$$SiC + {}^3\!/_2\, O_2\,(g) \rightarrow SiO_2 + CO\,(g) \tag{6}$$

$$SiC + O_2\,(g) \rightarrow SiO\,(g) + CO\,(g) \tag{7}$$

Vaughn and Maahs observed this transition to occur between ~1350°C and ~1550°C dependent on the total pressure.[116] Following this transition an adherent scale will rupture due to significant SiO gas formation below the viscous SiO_2 layer. In this way, oxidation performance is significantly reduced at temperatures exceeding ~1600°C. SiC/SiC composites have excellent mechanical performance and long lifetime reliability, but further advancements are required for applications that will experience more extreme environments.

2.4.5 Carbon and SiC Fiber/ZrB_2. Reinforcement of ZrB_2 has been traditionally limited to particles, whiskers, or short chopped fibers. A large body of work exists for ZrB_2 reinforced with SiC particulate, where strengths are vastly improved.[12,45,51,72,117] For example, ZrB_2 containing 30 vol% SiC particulate has been shown to have strengths of up to 1150 MPa at room temperature;[45] however, brittle fracture still dominates during failure due to insufficient toughening mechanisms. Recent attempts have been made to introduce short carbon fibers in ZrB_2 to increase toughness.[118,119] For example, Yang *et al*. used short, chopped carbon fiber (5 μm diameter, 2 mm length) in a ZrB_2-20 vol% SiC matrix increasing the toughness from ~4.3 MPa·m$^{1/2}$ to ~6.6 MPa·m$^{1/2}$ with only ~11% reduction to flexure strength compared to monolithic ZrB_2-20 vol% SiC.[119] Similarly, Yue *et al*. explored the addition of BN

nanotubes and nanoplatelets in ZrB_2-20 vol% SiC to increase toughness, where a slight increase was observed (i.e. 3.7 to 4.6 MPa·m$^{1/2}$) for a 1 wt% addition.[120] Several researchers have performed a number of studies investigating the addition of SiC whiskers (1 µm diameter and 30 µm length) and short chopped (14 µm diameter and 1 mm length) SiC fibers in ZrB_2 and its effect on microstructure, mechanical properties, as well as oxidation behavior.[46,53,121-124] It was shown that either 10 or 20 vol% of either reinforcement increased fracture toughness in ZrB_2. For example, baseline ZrB_2 toughness (3.7 MPa·m$^{1/2}$) was increased to 5.0-5.7 MPa·m$^{1/2}$, while ultimate strengths were reduced by ~30%.[53] Toughening in these materials was attributed to crack branching, bridging, and deflection at reinforcing interfaces due to residual stresses. Additionally, a high degree of interdiffusion was observed between the ZrB_2 matrix and the SiC whiskers or short chopped fibers after hot pressing at 1650°C. However, in all of these studies, failure during flexure testing was still observed to be brittle and/or catastrophic with no significant amount of fiber-matrix debonding.

ZrB$_2$ reinforced with continuous SiC fibers has been studied to a lesser extent. ZrB_2 containing SCS-9a fiber has been investigated.[125-128] Compressive strength and oxidation performance of a ZrB_2-20 vol% SiC containing 35 vol% SCS-9a fibers was investigated by Fernandez and Ramirez-Rico *et al*.[125,126] Room temperature and high temperature (i.e. 1400°C and 1550°C) strengths under atmospheric air were reduced when incorporating SCS-9a fibers. For example, compressive strength was reduced from ~3 GPa to ~330 MPa at room temperature, and ~1 GPa to 100 MPa at 1400°C.   They suggested that the reduced compressive strength was due to significant matrix cracking surrounding SCS-9a fibers. The penny-shaped cracks acted as stress risers during

compressive strength testing, but also served as fast diffusion paths for oxygen ingress during high temperature testing, leading to oxidative damage. Three-point flexure strength of a ZrB_2-20 vol% reaction bonded SiC (RBSiC; reaction of C and Si starting powders during hot pressing to form SiC in-situ) reinforced with 30 vol% SCS-9a fiber was studied by Stuffle *et al*. in the early 90s.[127,128] Specific hot pressing temperatures were not reported beyond "lower", "medium", and "higher". Matrix compositions were observed to be not fully dense under their processing conditions. While room temperature ultimate flexure strength was observed to be greater than 700 MPa, the high temperature strength necessarily suffered (i.e. <200 MPa after exposure to atmospheric air for 1 hour) due to poor oxidation performance caused by an insufficiently dense matrix. These materials demonstrated good composite like graceful failure, where load carrying capability drops step-wise incrementally during failure. Microcracking normal to the SCS-9a fiber was observed due to the mismatch in CTE ($\alpha_{ZrB2-20vol\%RBSiC} = 6.0 \times 10^{-6}$ K^{-1} and $\alpha_{fiber} = 2.6 \times 10^{-6}$ K^{-1}). The microcracking enabled load transfer to the fiber by delocalizing stresses, hence improved noncatastrophic failure. In contrast, future composites may utilize the smaller diameter SiC fibers on the market today as well as interphase coatings to mitigate matrix microcracking. This will allow for not only improved damage tolerance in a ZrB_2 based matrix, but provide graceful failure and maintain better oxidation resistance.

PAPER

I. DENSIFICATION, MICROSTRUCTURE, AND PROPERTIES OF HOT PRESSED ZrB$_2$-ZrSi$_2$ CERAMICS

Benjamin J. Lai, Jeremy L. Watts, Gregory E. Hilmas, William G. Fahrenholtz

Missouri University of Science and Technology

Materials Science and Engineering Dept.

1400 N. Bishop Ave.

Rolla, MO 65409

ABSTRACT

Densification behavior, microstructure, and mechanical properties of ZrB$_2$-ZrSi$_2$ ceramics were studied. ZrB$_2$ ceramics with 5 to 20 vol% additions of ZrSi$_2$ were densified to >95% relative density at temperatures as low as 1400°C by hot pressing. Improved densification behavior of ZrB$_2$ was observed for increasing ZrSi$_2$ addition. The most effective additive amount for densification was 20 vol% ZrSi$_2$ hot pressed at 1400°C (~98% relative density). Microstructural analysis revealed up to 7 vol% of residual ZrO$_2$, ZrSiO$_4$, SiO$_2$, and metallic silicon in the final ceramics. Improved densification behavior was attributed to ductility of the silicide phase, silicon wetting of ZrB$_2$ particles, and reactions of surface oxides. Strength ranged from 390 to 750 MPa and elastic modulus ranged from 440 to 490 GPa. Improved densification combined with decreased strength, modulus, and hardness suggest a trade-off between ZrSi$_2$ content sufficient to achieve adequate densification behavior, but low enough to retain adequate mechanical performance.

Keywords: ZrB$_2$; ZrSi$_2$; Densification; Microstructure; Mechanical properties

1.   INTRODUCTION

Zirconium diboride (ZrB$_2$) is one of several materials known as ultra-high temperature ceramics (UHTCs). These materials have extremely high melting points (>3000°C) and are useful for applications including molten metal crucibles,[1,2] high temperature electrodes,[1,3] cutting tools,[4,5] and hypersonic aerospace vehicles.[6-9] The high degree of metallic bonding character,[10] the relatively high thermal conductivity (60-145 W·(m·K)$^{-1}$)[11] and low electrical resistivity (7.8-22 µΩ·cm)[12] of borides set them apart from other UHTC materials, specifically transition metal carbides and nitrides. Combined with their high thermal conductivity, the extremely high melting temperature (>3000°C) and high strength (>500 MPa) of ZrB$_2$–based ceramics makes them attractive candidates for ultra-high temperature aerospace applications.[11-15]

Future advancements in the mechanical reliability of ZrB$_2$ will require a reinforcing phase to enable graceful failure and improve damage tolerance. Previous studies have shown that addition of SiC whiskers, or short chopped SiC fibers, improve the fracture toughness of ZrB$_2$.[16-19] Toughening is achieved by crack branching, bridging, and deflection at the fiber-matrix interface, where residual stresses are higher due to thermal expansion mismatch.[16] However, in these studies, significant degradation of the SiC whiskers or short fibers has occurred due to the extreme processing conditions.[17] Increased fiber-matrix bonding hinders graceful failing mechanisms (i.e. debond energy, sliding resistance, etc.).[20,21] While these materials have demonstrated an increase in fracture toughness, lower processing temperatures that

still result in nearly fully dense bodies would improve fiber integrity and provide additional increases in toughness and graceful failure.

Densification of ZrB_2-based ceramics typically requires temperatures of 2000°C or higher. Incorporation of combinations of boron carbide (B_4C), carbon (C), and/or silicon carbide (SiC) particles increases the driving force for densification and limits grain growth, which can decrease the peak densification temperatures to below 2000°C.[22-25] Silicon nitride (Si_3N_4) additions to ZrB_2 have been shown to reduce the densification temperature to ~1700°C to achieve near full density by hot pressing.[26-28] Transition metal disilicides, specifically $MoSi_2$ and $ZrSi_2$, improve densification by forming an in-situ liquid phase during processing, allowing for increased densification at significantly reduced temperatures (1400 to 1900°C).[29-33] Additions of 5 to 20 vol% $MoSi_2$ were sufficient to densify ZrB_2 at 1800°C by pressureless sintering.[33] ZrB_2 ceramics containing 30 vol% $ZrSi_2$ were found to achieve full density by pressureless sintering at 1650°C, while additions as low as 20 vol% $ZrSi_2$ were sufficient to achieve full density by hot pressing at 1550°C.[29,30] Research by Guo *et al*. investigated sintering mechanisms and densification behavior of ZrB_2 with $ZrSi_2$ additions ranging from 10 to 40 vol%.[34] These studies focused on: (i) obtaining a sufficiently dense matrix (i.e. containing 5 to 20 vol% $MoSi_2$) for improved oxidation resistance; and (ii) investigating sintering mechanisms (i.e. $ZrSi_2$ content 10 to 40 vol%). However, these studies did not report mechanical properties at low additive concentrations.

In the present study, ZrB_2-based ceramics were fabricated with $ZrSi_2$ as an additive to improve sinterability. Continued advancement in the field of hypersonic aviation will require incorporation of reinforcing fiber phases to improve damage

tolerance; however, current generation commercially available SiC fibers degrade at processing temperatures above 1600°C. Hence, reduced processing temperatures for a ZrB_2-based ceramic will enable future material system compatibility.

2.   EXPERIMENTAL PROCEDURE

2.1   *Specimen Preparation*

Commercially available ceramic powders were used throughout this study. The ZrB_2 powder (Grade B, H.C. Starck, Newton, MA) had a purity of >99% (metals basis) and an average particle size of 2 μm. The $ZrSi_2$ powder (Alfa Aesar, Ward Hill, MA) had a reported purity of >99.5% (metals basis) and a particle size of -325 mesh. Additionally, silicon carbide (UF-25, H.C. Starck, Newton, MA) was used as an additive in one composition to simulate incorporation of SiC media during milling. SiC had a reported purity of >99.9% (metals basis) and an average particle size of 0.45 μm. Following batching, powders were attrition milled (Model 01-HD, Union Process, Akron, OH) for 2 hours in acetone at 600 rpm using a polymer coated container and spindle as well as SiC media. Powder compositions were rotary evaporated (Model R-124, Buchi, Flawil, Germany) at 70°C, 300 mm Hg (40 kPa) vacuum, and 50 rpm rotational speed to remove the solvent and prevent powder segregation during drying. Dried powders were sieved to 60-mesh (<250 μm) prior to hot pressing.

Batched and dried powders were loaded into graphite dies that were lined with graphite foil and coated in boron nitride (BN; Cerac, SP-108, Milwaukee, WI, USA). Billets were initially compacted with a ~6 MPa uniaxial load at room temperature and then hot-pressed (Model HP-20-3060-20, Thermal Technology, Santa Rosa, CA) at temperatures ranging from 1400 to 1600°C. Temperature was monitored by an infrared

pyrometer (Model 0S3708, Omega Engineering, Stamford, CT) above 600°C. After initially evacuating to 140 mtorr (19 Pa) at room temperature, the hot press was backfilled with argon and heating was conducted under flowing argon at nominally ambient pressure. Dies were heated at ~30-40 °C·(min)$^{-1}$ to 1200°C where a 32 MPa uniaxial load was applied. Powder compacts continued to be heated to 1400°C and 1600°C and held for approximately 1 hour at each temperature.

Determination of onset of densification and final stage sintering were inferred from ram travel during hot pressing. Final density values were used to determine sample thicknesses as a function of ram travel during hot pressing. In this way, relative densities of specimens were estimated as a function of hot pressing time and temperature. Peak hot pressing temperatures were held for ~1 hour. Following the high temperature hold, the hot press was cooled at ~20°C·(min)$^{-1}$ to room temperature. Uniaxial load was removed upon cooling to 1200°C. A minimum of two billets were prepared for each powder composition. The sample designations are based on the nominal composition and hot pressing temperature as defined in Table I. As an example, Z10S-1400 is ZrB_2 containing 10 vol% $ZrSi_2$ that was hot pressed at 1400°C.

2.2   Characterization

Following removal from the hot press die, billets were surface ground to a thickness of ~2.5 mm to achieve flat and parallel surfaces as well as removal of any adherent BN. The bulk densities of the billets were measured using Archimedes method with water as the immersion medium. Bulk densities were compared to theoretical values determined by a volumetric rule of mixtures using values of 6.09 g/cm^3 for ZrB_2, 4.88 g/cm^3 for $ZrSi_2$, and 3.21 g/cm^3 for SiC. Microstructural analysis was performed by

scanning electron microscopy (SEM; Model S570, Hitachi, Tokyo, Japan) while

simultaneous elemental composition was evaluated by energy dispersive spectroscopy

(EDS; Model AAT, X-ray Optics, Gainesville, FL). Aerial analyses of microstructures

were performed using ImageJ software (National Institutes of Health, Bethesda, MD).

Specimens were prepared for microscopy by removing a cross-section parallel to hot-

pressing direction and utilizing successively finer diamond abrasive slurries where final

finish was obtained using 0.25 µm diamond paste. Phase analysis was performed by X-

ray diffractometry (XRD; Model X-Pert Pro, PANalytical, Almelo, Netherlands) on

specimens that were ground to -325 mesh (<44 µm) using a high-purity Al_2O_3 mortar and

pestle.

2.3   *Mechanical Property Testing*

Specimens for mechanical property tests were machined from the billets and

ground to final dimensions using 400-grit (37 µm) diamond before final polishing to a

0.25 µm diamond finish. Diamond abrasive wheels were used for all cutting and

grinding surfaces using an automated surface grinder (Model FSG-3A818, Chevalier,

Santa Fe Springs, CA). Flexure strength was measured using a fully-articulated four

point bending fixture consistent with ASTM C1161-using A-type test bars (25 mm x 2

mm x 1.5 mm). A minimum of ten bars were tested for each composition. Hardness was

determined by Vickers indentation (Duramin 5, Struers, Cleveland, OH) consistent with

ASTM C1327-08 using a 0.5 kg (4.9 N) load and a dwell time of 15 seconds. Fracture

toughness was determined by direct crack measurements, described by Anstis *et al*.[35]

Using polished surfaces, Vickers indentations were made (Model V-100-A2, Leco

Corporation, St. Joseph, MI) using a 10 kg load, and indent dimensions and crack lengths

were measured. Toughness was subsequently calculated using Eq. (1); reported toughness values are the average of ten indentations.

$$K_{IC} = \xi \left(\frac{E}{H}\right)^{\frac{1}{2}} \left(\frac{P}{c^{\frac{3}{2}}}\right) \qquad (1)$$

where ξ is a geometric constant (0.016±0.004), E the elastic modulus (GPa), H the Vickers hardness (GPa), P the load (98 N), and c half of the measured radial crack length (m).

3. RESULTS AND DISCUSSION

3.1 *Densification and Microstructure*

Additions of $ZrSi_2$ increased the densification rate and final density of ZrB_2 hot pressed at 1400°C and 1600°C. All compositions achieved greater than 95% relative density, with the exception of Z05S-1400 and Z05S-1600 that achieved only ~76% and ~81% relative densities, respectively. In Fig. 1, typical examples of shrinkage curves during hot pressing are presented. For all compositions utilizing $ZrSi_2$, the higher hot pressing temperature of 1600°C resulted in higher densification rates as well as higher final densities, as compared to compositions hot-pressed to 1400°C. For example, Z10S-1600 reached ~96% relative density after ~30 minutes at peak hot pressing temperature compared to Z10S-1400, which required ~60 minutes to achieve ~95% relative density. An increasing $ZrSi_2$ content also resulted in higher relative densities. For example, Z05S-1400 achieved a relative density of ~77%, compared to a relative density of ~98% for Z20S-1400.

The addition of SiC particles has been shown to increase densification and pin grain growth in ZrB_2 at sintering temperatures greater than 1900°C.[36] Hence, Z10S-

1.5SiC-1400 was investigated to determine if small additions (1.5 vol%) of SiC would affect densification in the ZrB_2-$ZrSi_2$ system at low temperatures (i.e. 1400°C). The addition of 1.5 vol% SiC to Z10S (designated Z10S-1.5SiC-1400) resulted in a minimal increase in relative density compared to Z10S at 1400°C (~95 relative density for Z10S compared to ~96% Z10S-1.5SiC). Further, the addition of SiC in Z10S-1.5SiC-1400 did not increase the densification rate compared to Z10S-1400.

XRD confirmed that ZrB_2 was the dominant phase in all of the densified ceramics (Fig. 2). In contrast, $ZrSi_2$ did not appear in appreciable amounts in any of the XRD patterns. Further, the XRD patterns also revealed the presence of Si, ZrO_2, and $ZrSiO_4$, which could be present as a result of processing conditions that led to the decomposition of $ZrSi_2$ or impurities in the starting powders. Previous studies have shown that reaction holds under mild vacuum (~200 mtorr), at temperatures of 1450°C and 1650°C, reduce the amount of oxide species present on the surfaces of ZrB_2 powder particles and improve densification.[22-24] During these reaction holds, vaporization of B_2O_3 present on the surface of ZrB_2 becomes favorable under mild vacuum, which removes B and O from the system. Typically, ZrB_2 is densified at much higher temperatures (>2000°C) than in the present work, which allows for incorporation of those holds into the processing cycle. However, in the present study, peak densification temperatures are 1400°C or 1600°C, which are lower than one or both of the typical reaction holds. As a result, incorporating vaporization reaction holds into the hot pressing schedule is not feasible. Additionally, silicides may not be stable at elevated temperatures. Due to the proximity of the processing temperature (1400°C) and the melting temperature of the silicide (1620°C), as well as an increased vapor pressure of Si species at these temperatures, using an inert

atmosphere instead of vacuum may reduce loss of the silicide due to volatilization.[37]

Work by Silvestroni and Sciti, in studies of ZrB_2-$MoSi_2$ ceramics, observed weight losses

of up to 2.4% after pressureless sintering at 1850°C.[38] Because of the constraints on

the processing cycle, ZrB_2 remained the dominant phase following hot pressing, but

impurity oxide phases persisted through the processing cycle due to a lack of reaction

holds.

A number of mechanisms could potentially explain the improved densification

observed with $ZrSi_2$ additions. In the 1400°C isothermal section of the B-Si-Zr ternary

phase diagram described by Parthé, an Alkemade triangle connects ZrB_2, $ZrSi_2$, and a Si-

rich liquid phase (Fig. 3).[39] Previous studies have shown that silicide additives

improve densification of borides through one of two mechanisms: (i) the ductility of the

silicide phase provides the capability to effectively fill the void space between the hard

ZrB_2 particles; or (ii) the reaction of surface oxides present on the silicide and diboride

particles, i.e. SiO_2 reacting with B_2O_3 to form a liquid phase well below the hot-pressing

temperature, promotes sintering instead of grain growth.[38,40,41] Whether the liquid is

Si-rich or a borosilicate glass, it could improve densification. In the initial stages of hot-

pressing, a liquid phase could enhance grain rearrangement, which increases the packing

density of hard ZrB_2 particles. The liquid phase could also react with and remove the

oxides species present on the surface of the ZrB_2 particles, specifically ZrO_2 and B_2O_3.

These oxides inhibit densification by enhancing surface diffusion and vapor transport,

which are nondensifying, grain coarsening mechanisms in solid-state sintering.[42]

Removal of oxide species from the surfaces of particles allows for increased grain

boundary diffusion and lattice diffusion from the grain boundary, which enhances

densification relative to grain coarsening. In addition, Si-rich liquids wet ZrB_2 and TiB_2 (contact angle less than 15°).[43] It is conceivable that as the local composition shifts away from the ZrB_2-$ZrSi_2$ Alkemade line, the formation of a small amount of liquid (predominantly Si) facilitates the mechanisms discussed previously. However, after entering the three-phase region, residual Si should form upon cooling. However, crystalline $ZrSi_2$ was not observed in appreciable amounts in the final microstructures. Indeed, analysis using SEM/EDS revealed the presence of a Si containing phase, but no Zr was present in that phase (discussed in more detail below). The observed Si containing phase potentially originates from SiC media during attrition and ball milling, which could alter the activity of Si in the ZrB_2-$ZrSi_2$ system. The $ZrSi_2$ phase was not present in the amounts predicted using the B-Si-Zr phase diagram based on the nominal composition.

More detailed XRD analysis revealed that the compositions produced by hot pressing differed significantly from what should have formed based on the nominal ratio of the starting materials. Supplier information for the $ZrSi_2$ powder reported a purity of >99.5% on a metals basis; however, XRD analysis of the powder revealed a number of phases in addition to $ZrSi_2$. Rietveld refinement of the XRD data was subsequently performed on all of the raw material powders. The results showed that while ZrB_2 powders were phase-pure hexagonal ZrB_2, the $ZrSi_2$ powder consisted of only about 26 vol% $ZrSi_2$ along with ~39 vol% Si, ~27 vol% ZrO_2, and ~8 vol% $ZrSiO_4$ (also included in Fig. 4). The discrepancy in the measured versus reported compositions may not have been detected using the method by which powder purities were assessed. Supplier analysis was performed by inductively coupled plasma mass spectroscopy (ICP-MS)

which characterized the amounts of the metals present; however, this method is only sensitive to the chemistry, not the phases. In contrast, XRD can be used to quantify the distinct crystalline structures that are present, but compositions are inferred from the positions and intensities of the peaks. The discovery of the undesired phases (i.e., ZrO_2, $ZrSiO_4$, etc.) necessitated reevaluation of the densification analysis. In light of the extraneous phases present in the "$ZrSi_2$", the overall composition is shifted further into the ZrB_2-$ZrSi_2$-liquid compatibility region due to the presence of free Si. For the Z10S compositions, as an example, the $ZrSi_2$ content added was significantly less than intended (~2.6 vol%), while Si content was higher (~3.9 vol%). This caused a shift closer to ZrB_2 along the ZrB_2-$ZrSi_2$ Alkemade, but the increased Si content in the overall composition shifted the composition within the Alkemade triangle toward the liquid phase at the Si-rich end of the triangle.

The impurity phases in the $ZrSi_2$ had a significant impact on the phases present in the ZrB_2-$ZrSi_2$ ceramics after hot-pressing. An initial analysis considered a shift in composition away from the ZrB_2-$ZrSi_2$ Alkemade line due to the presence of SiC picked up during attrition milling, which would produce a small amount of liquid by altering the activity of Si in the B-Si-Zr system. A more rigorous analysis based on the measured impurity content of the starting powders suggested a much larger shift away from the nominal ZrB_2-$ZrSi_2$ compositions. Due to limited studies of B-O-Si-Zr phase stability at elevated temperatures, the analysis ignored the oxide phases. The relative amounts of B, Si, and Zr in the non-oxide phases shift the overall composition into the Alkemade triangle containing ZrB_2, $ZrSi_2$, and Si metal at 1400°C. The compositional range estimated from characterization of the precursor powders is shown in Fig. 3. Based on the

measured composition, and ignoring the Zr present in ZrO_2 and $ZrSiO_4$, the compositions shift to the area highlighted in the Zr-B-Si phase diagram. With increasing additive content, an increasing amount of Si-rich liquid phase should form at the processing temperature of 1400°C. Assuming that ZrB_2 remains stoichiometric and phase-pure (i.e. no dissolution of Si or other species), the relative amounts of liquid phase were estimated. The formation of 2.7 vol% liquid was predicted for Z05S, 4.2 vol% for Z7.5S, 5.7 vol% for Z10S, and 12.8 vol% for Z20S. The density of the liquid phase was assumed to be that of pure Si as the composition was mainly Si and elevated temperature liquid density data was not available for B-Si-Zr compositions, but was for liquid Si.[44-46] Based upon these estimates, combined with the densification data, liquid phase contents of more than 4 vol% were required for appreciable densification of ZrB_2 at 1400°C. In addition, increasing the volume fraction of liquid formed at 1400°C beyond 5 vol% only resulted in slight increases in final densities (~97% dense for Z7.5S with 5.7 vol% liquid compared to ~98% for Z20S with 12.8 vol% liquid). For compositions hot-pressed at 1600°C, a significantly greater amount of liquid is expected, which could enable densification with lower additive amounts than required at 1400°C.

The impurities present in the starting powders influenced the final composition and microstructure. All compositions exhibited well-dispersed second phases in the microstructures, examples of which can be seen in Fig. 5. The brighter, light gray phase in the images was identified as ZrB_2, while the darker gray, dispersed intergranular phases are a combination of residual metallic Si, $ZrSi_2$, and an unidentified Si-containing phase. Previous work by Grigoriev *et al.* showed that $ZrSi_2$ additions greater than 10 vol% to ZrB_2-SiC ceramics resulted in the formation of a Zr-Si liquid at the processing

temperature, which formed $ZrSi_2$ along with a residual amorphous phase upon cooling.[32] For silicide additions of less than 10 vol%, the liquid formed at the processing temperature was almost completely converted to a crystalline $Zr(Hf)C(B)$ phase upon cooling. Higher silicide additions, above 10 vol%, led to formation of a Zr-Si-B-(O) liquid at elevated temperatures and a residual amorphous phase upon cooling. A similar phenomenon was expected for the compositions produced in the present study. Indeed for ZrB_2 with 20 vol% $ZrSi_2$ (Z20S), significant amounts of Si and $ZrSi_2$ formed upon cooling from 1400°C. The liquid phase was reactive toward graphite and, as a result, hot pressing Z20S at 1600°C resulted in significant reaction with the graphite dies. After cooling, SEM imaging of Z20S hot pressed at 1400°C revealed the presence of a phase that appeared dark in the microstructures due to its low average atomic mass (designated low Z). The lower Z phase was rich in Si and O. Two possible sources for this phase were the presence of ZrO_2, $ZrSiO_4$, and Si in "$ZrSi_2$" powder and wear of SiC media during attrition and ball milling. Typically, 0.5 vol% to 1.5 vol% SiC was incorporated into batches during milling, estimated from media weight loss measurements. Aerial analysis of microstructures revealed the fraction of low Z phase was ~12.4 vol% for Z7.5S, ~16.4 vol% for Z10S, and ~20.9 vol% for Z20S. The observed low Z phase appeared in greater amounts than predicted from nominal additive content and wear of SiC media. Hence, this phase was likely formed due to the presence of impurity phases in the starting $ZrSi_2$.

The microstructures of Z7.5S, Z10S, and Z20S contained a number of features that can be explained by the actual composition. Relatively large regions of second phases were present in Z10S and Z20S specimens (Fig 5). The diameters of second

phase regions (Fig. 5) were typically less than 20 µm in Z10S but 40 µm or larger in

Z20S. SEM/EDS analysis of Z10S specimens revealed that the second phases included

$ZrSiO_4$ (i.e. ~17 at % Zr, ~18 at %, and ~64 at % O) along with another Si and O-rich

phase that had deformed to fill the void space among ZrB_2 grains (Fig. 6). SEM/EDS

analysis also revealed small amounts (< 0.5 vol%) SiO_2 present in Z7.5S, Z10S, and

Z20S. The SiO_2 could have formed by a reaction between Si metal and the oxide

impurities that were present on the surfaces of the starting powders. The large $ZrSiO_4$

grains were present due to both the small amount present in the starting "$ZrSi_2$" powder,

as well as due to reaction of ZrO_2 and SiO_2 during hot pressing. The change in standard

state Gibbs' free energy of this reaction is estimated to be -6 kJ per mole of $ZrSiO_4$

formed from ZrO_2 and SiO_2 at 1400°C. To confirm the hypothesis that $ZrSiO_4$ formed

during processing, samples of the "$ZrSi_2$" powder that initially consisted of ~48 vol% Si

~17 vol% ZrO_2, ~8 vol% $ZrSiO_4$, and ~27 vol% $ZrSi_2$ were characterized after

pressureless sintering and hot pressing at 1400°C (Table II). Pressureless sintering

resulted in the formation of additional $ZrSi_2$ due to the consumption of Si and ZrO_2.

While the direct reaction of ZrO_2 to form $ZrSi_2$ is not favorable at 1400°C, it is

conceivable that a liquid Zr-Si-O phase present at the processing temperature

recrystallized to form a mixture of $ZrSi_2$, $ZrSiO_4$, and SiO_2. Further, the volume fraction

of $ZrSi_2$ increased (from ~27 to 57 vol%, as shown in Table II) after hot pressing at

1400°C. However, this is presumably due to loss of Si from the system during

processing. During processing at 1400°C, Si deformed and was extruded from the die

where it reacted with the outside of the graphite die (i.e. $Si + C \rightarrow SiC$, $\Delta G_{rxn} = -58$ kJ at

1400°C). In this way, Si was removed from the resulting ceramic. Mass of the billet

before and after hot pressing estimates a mass loss of ~26 wt%, which is in good

agreement to values obtained by Rietveld analysis. SEM analysis of Z7.5S, Z10S, and

Z20S specimens showed concentrations of porosity that were less than predicted from

relative densities calculated from Archimedes measurements. Based on the

microstructural and compositional analyses presented above, the theoretical densities

were recalculated based on the presence of ZrO_2, $ZrSiO_4$, and Si after densification

(Table III). The theoretical densities were calculated based on the phases present after

pressureless sintering of "$ZrSi_2$", which resulted in the loss of some Si. As a result, the

revised relative densities increased with increasing additive content. For example, the

relative densities of Z05S-1400 and Z05S-1600 increased by ~0.6% while Z10S-1400

and Z10S-1600 increased by ~1.5%. This is consistent with the presence of lower

density second phases (i.e. Si, ZrO_2, $ZrSiO_4$, and SiO_2) in the final ceramics. Relative

densities were shifted less than ~1.5% for all compositions with the exception of Z20S-

1400, which increased by ~2.7%. The presence of the oxide phases, as well as elemental

Si, impacted the microstructural development of ZrB_2 ceramics. The concentrations in

the final microstructures ranged from 0.15 vol% SiO_2 in Z05S to 7.1 vol% Si in Z20S

while $ZrSi_2$ remained the dominant second phase.

3.2   Mechanical Properties

The flexural strength, elastic modulus, and Vickers hardness values were

measured for all compositions that reached >97% relative density (Table IV). The

compositions that met this criterion were Z7.5S and Z10S hot pressed at both 1400°C and

1600°C, and Z20S hot pressed at 1400°C. Vickers hardness values for all compositions

were lower than for nominally pure ZrB_2 (~22 GPa)[13] due to the addition of $ZrSi_2$,

which has a reported hardness of 10.5 GPa.[47] The highest observed hardness (~16 GPa) was measured for Z10S hot pressed at either 1400°C or 1600°C. The hardness of Z7.5S was 15.5 GPa after hot pressing at 1400°C and 15.8 GPa after hot pressing at 1600°C. The lowest hardness was 15.0 GPa for Z20S. From the observed hardness, it can be inferred that the higher hot pressing temperature of 1600°C resulted in increased hardness compared to those hot pressed at 1400°C. Further, $ZrSi_2$ additions between 7.5 and 10 vol% resulted in small changes to hardness, but only additions as high as 20 vol% $ZrSi_2$ begin to see markedly reduced hardness due to its higher $ZrSi_2$ content.

The hardness of the ZrB_2-$ZrSi_2$ ceramics was lower than values predicted using a linear volumetric rule of mixtures calculation with published values for the hardness of ZrB_2 (~22 GPa)[13] and $ZrSi_2$ (~10.5 GPa).[47] The most likely explanation for the decreased hardness is the presence of Si and the other oxide impurities from the starting $ZrSi_2$ powders. The reported hardness of Si ranges from 8 to 13 GPa at room temperature, depending on the measurement technique and elastic-plastic transition behavior as a result of loading.[48,49] Based on the prevalence of the low Z phase as well as the presence of Si, it is conceivable that the reductions in hardness from a baseline ZrB_2 material are a result of intergranular Si or a Si-containing amorphous phase. If the presence of Si were the only cause of the reduction in hardness, the volume fractions required to explain the hardness values measured for Z7.5S, Z10S, and Z20S would be 40 to 44 vol%, which is significantly higher than observed in the microstructures. Small amounts of porosity can also reduce hardness as described by Milman *et al.*, in studies of SiC ceramics, which described an exponential decrease in hardness with increasing porosity as defined in Eq. (2):[50]

$$HV = HV_c \exp(-B\theta) \qquad (2)$$

where HV_c is the hardness of a fully dense specimen measured at the same temperature

(GPa), θ is the porosity (vol%), and B is an experimentally determined geometric

parameter as a function of temperature, determined to be 6.3 between 20°C and 200°C

for SiC. Archimedes density measurements predicted less than 0.06 vol % open porosity

for Z7.5S, Z10S, and Z20S, while closed porosity ranged from 1.8 to 3.4 vol%. Using a

similar B parameter for the ZrB_2-$ZrSi_2$ compositions, and the measured hardness and

porosity values, Eq. (2) predicted the hardness of fully dense ZrB_2-$ZrSi_2$ specimens to fall

between 17.2 GPa and 20.0 GPa for Z7.5S, Z10S, and Z20S. Hence, while porosity

reduces hardness, the amount of porosity in these ceramics is not enough to explain the

observed decrease in hardness. Finally, the oxide impurities in the $ZrSi_2$ powder also

have lower hardness values than either ZrB_2 or $ZrSi_2$, but have not been accounted for in

the analysis above. Therefore, it is expected that a combination of impurity phases and

porosity caused the observed reduction in hardness.

The fracture toughness of the ZrB_2-$ZrSi_2$ ceramics did not vary significantly with

$ZrSi_2$ additions between 7.5 vol% and 20 vol%. Fracture toughness remained consistent

at ~4 MPa·m$^{1/2}$ for Z7.5S, Z10S, and Z20S hot pressed at either 1400°C or 1600°C. The

addition of $ZrSi_2$ resulted in a slight increase in fracture toughness compared to phase

pure ZrB_2 hot pressed at 1900°C reported by Chamberlain et al. at 3.5 MPa·m$^{1/2}$.[6]

These results were consistent with reduced elastic modulus and hardness values for ZrB_2

containing $ZrSi_2$, as these properties are used in direct crack fracture toughness

calculations. The presence of lower hardness second phases such as Si increased the

calculated toughness values for compositions containing $ZrSi_2$. Based on Eq. (1), a Si-

containing region of lower hardness would serve to increase mode I critical stress intensity factor (K_{IC}), potentially allowing for local K_I to drop below K_{IC} and requiring more energy for crack propagation. Indentation tests confirmed that radial/median cracks propagated preferentially through softer intergranular phases as shown in Fig. 7, therefore decreasing crack lengths and increasing toughness. The $ZrSi_2$ contents ranging from 7.5 vol% to 20 vol% had no discernible change in fracture toughness behavior or mechanism.

The addition of $ZrSi_2$ decreased the strength of hot-pressed ZrB_2. The strength of Z20S hot-pressed at 1400°C was ~390 MPa, which is ~25 to ~50% lower than strengths of 500 MPa to 700 MPa typically reported for nominally pure ZrB_2.[6,14,23,51] The reduction in strength for Z20S is attributed to the presence of large second phase particles (Fig. 8). Using the measured strength and fracture toughness values, Griffith analysis, defined by Eq. (3), was used to predict the critical flaw size.[52]

$$\sigma_f = \frac{K_{IC}}{Y\sqrt{c}} \tag{3}$$

where σ_f is the failure stress (MPa), K_{IC} is the fracture toughness (MPa·m$^{1/2}$), c is flaw size (m), and Y is a geometric constant based on the failure origin. The Y parameter used for the ZrB_2-$ZrSi_2$ ceramics was determined to be 1.25 based on Eq. (4) developed by Kaur *et al.* for semi-elliptical surface cracks in finite width specimens.[53]

$$Y(C) = 0.2139 + 1.0770 \left(\frac{w}{w+c}\right) \tag{4}$$

where w is the beam thickness (m), and c is the flaw size (m). The predicted critical flaw size for Z20S specimens was in the range of ~50 μm to 90 μm. Image analysis of polished specimens revealed the presence of large second phase agglomerates in Z20S ranging in size from 40 to 65 μm (Fig. 8). Decreased strength in ZrB_2 ceramics with

higher $ZrSi_2$ additions was attributed to increased tendency to form larger second phase regions as the additive amount increased.

The size of the second phase regions observed in SEM images likely underestimates the size of the strength-limiting flaws present in the ceramics. Previous work by Watts *et al*. suggested that failure of ZrB_2 with 30 vol% SiC was dominated by a complex function of local tensile stresses around particles and interparticle spacing, where increasing effective SiC particle size was shown to have a cubic relation to the volume of matrix under stress.[25] Further, they determined that reductions in strength of ZrB_2-SiC composites originated from the local volume of matrix under stress, with stress alleviated by microcracking when the stress exceeded a critical value. Similar behavior is expected for Z20S where the reduced strength is consistent with the size of second phase particles observed by SEM. A reduction in modulus, relative to phase pure ZrB_2 (~530 GPa), was also observed for all compositions incorporating $ZrSi_2$. Z10S compositions had strengths of 543±82 MPa after hot pressing at 1400°C and 475±67 MPa after hot pressing at 1600°C. Z7.5S had strengths of 673±38 MPa and 752±71 MPa after hot-pressing at 1400°C and 1600°C, respectively, with no appreciable reductions in modulus or relative density. The increase in strength of Z7.5S over Z10S compositions is likely due to the lower liquid phase content at elevated temperature during processing where greater liquid phase volume fractions likely resulted in formation of larger second phase particles in Z10S and Z20S.

4. CONCLUSIONS

ZrB_2 containing 5, 7.5, 10, and 20 vol% $ZrSi_2$ was hot-pressed to near theoretical density. Compositions incorporating between 7.5 vol% and 20 vol% $ZrSi_2$ achieved greater than 96% relative density by hot pressing at 1400°C or 1600°C. XRD analysis revealed the presence of oxide impurities (i.e. ZrO_2 and $ZrSi_2O_4$) in the final ceramics. Subsequent analysis revealed the presence of impurities (i.e. Si, ZrO_2, and $ZrSiO_4$) in the starting $ZrSi_2$ powder. Analysis based on the actual composition of the $ZrSi_2$ additive predicted the formation of a Si-rich liquid phase at 1400°C, with the liquid phase content increasing from 4.7 vol% to 12.8 vol% with increasing $ZrSi_2$ additions. Sintering and hot pressing studies with the "$ZrSi_2$" powder showed that additional $ZrSi_2$ formed after processing at 1400°C. The elastic modulus values for the ZrB_2-$ZrSi_2$ ceramics ranged from 440 GPa to 490 GPa. The decreased values compare to phase pure ZrB_2 (~530 GPa) were consistent with incorporating lower modulus phases (i.e. Si, $ZrSi_2$) as well as accounting for porosity. Strengths of ZrB_2 with 7.5 vol% $ZrSi_2$ hot pressed at 1400°C and 1600°C were 673 MPa and 752 MPa, respectively, the highest of the compositions studied. Increasing the $ZrSi_2$ addition above 7.5 vol% reduced strength. Strength was 543 MPa for 10 vol% $ZrSi_2$ and 388 MPa for 20 vol% $ZrSi_2$. Reductions in strengths were attributed to the presence of impurity/oxide phase particles with sizes in the range of 50 μm to 90 μm. Hardness values ranging from 15 GPa to 16 GPa for all Z7.5S, Z10S, and Z20S materials, where slight differences likely resulted from small changes in relative density and the amount of the impurity phases. Toughness showed no significant increase for increasing $ZrSi_2$ addition, with values ranging 4.0 MPa·m$^{1/2}$ to 4.3 MPa·m$^{1/2}$ for all processing conditions. Reductions to strength, elastic modulus, and hardness of

ZrB$_2$ lend to a trade-off between minimization of ZrSi$_2$ content to retain strength, modulus and hardness while increasing content to promote densification. ZrB$_2$ with 7.5 vol% ZrSi$_2$ hot pressed at 1600°C yielded an optimum combination of high strength, modulus, hardness, and toughness while maintaining sufficient densification.

REFERENCES

[1] B. Stucker, W. Bradley, P. T. Eubank, S. Norasetthekul, and B. Bozkurt, "Zirconium Diboride/Copper Edm Electrodes from Selective Laser Sintering," pp. 257-65 in *Solid Freeform Fabr. Symp. Proc.*, 1997.

[2] J. Sung, D. M. Goedde, G. S. Girolami, and J. R. Abelson, "Remote-Plasma Chemical Vapor Deposition of Conformal ZrB_2 Films at Low Temperature: A Promising Diffusion Barrier for Ultralarge Scale Integrated Electronics," *J. Appl. Phys.,* **91**[6] 3904-11 (2002).

[3] S. Norasetthekul, P. T. Eubank, W. L. Bradley, B. Bozkurt, and B. Stucker, "Use of Zirconium Diboride-Copper as an Electrode in Plasma Applications," *J. of Mater. Sci.,* **34**[6] 1261-70 (1999).

[4] S. K. Mishra, S. Das, S. K. Das, and P. Ramachandrarao, "Sintering Studies on Ultrafine ZrB_2 Powder Produced by a Self-Propagating High-Temperature Synthesis Process," *J. Mater. Res.,* **15** 2499-504 (2000).

[5] Y. Murata, "Cutting Tool Tips and Ceramics Containing Hafnium Nitride and Zirconium Diboride," U. S. Patent, 3487594, 1970.

[6] A. L. Chamberlain, W. G. Fahrenholtz, G. E. Hilmas, and D. T. Ellerby, "High-Strength Zirconium Diboride-Based Ceramics," *J. Am. Ceram. Soc.,* **87**[6] 1170-2 (2004).

[7] A. L. Chamberlain, W. G. Fahrenholtz, G. Hilmas, and D. T. Ellerby, "Oxidation of ZrB_2-SiC Ceramics under Atmospheric and Reentry Conditions," *Refractories App. Trans.,* **1**[2] 2-8 (2004).

[8] W. G. Fahrenholtz, G. E. Hilmas, I. G. Talmy, and J. A. Zaykoski, "Refractory Diborides of Zirconium and Hafnium," *J. Am. Ceram. Soc.,* **90**[5] 1347-64 (2007).

[9] X. Zhang, P. Hu, J. Han, and S. Meng, "Ablation Behavior of ZrB_2–SiC Ultra High Temperature Ceramics under Simulated Atmospheric Re-Entry Conditions," *Compos. Sci. Technol.,* **68**[7–8] 1718-26 (2008).

[10] P. Vajeeston, P. Ravindran, C. Ravi, and R. Asokamani, "Electronic Structure, Bonding, and Ground-State Properties of AlB_2-Type Transition-Metal Diborides," *Phys. Rev. B.,* **63**[4] 045115 (2001).

[11] J. W. Zimmermann, G. E. Hilmas, W. G. Fahrenholtz, R. B. Dinwiddie, W. D. Porter, and H. Wang, "Thermophysical Properties of ZrB_2 and ZrB_2–SiC Ceramics," *J. Am. Ceram. Soc.,* **91**[5] 1405-11 (2008).

[12] M. Rahman, C. C. Wang, W. Chen, S. A. Akbar, and C. Mroz, "Electrical Resistivity of Titanium Diboride and Zirconium Diboride," *J. Am. Ceram. Soc.,* **78**[5] 1380-2 (1995).

[13] R. A. Cutler, "Engineering Properties of Borides," pp. 787-803 In *Ceramics and Glasses, Engineered Materials Handbook,* **Vol. 4**, Edited by S. J. Schneider. ASM International, Materials Park, OH, 1992.

[14] A. L. Chamberlain, W. G. Fahrenholtz, and G. E. Hilmas, "Low-Temperature Densification of Zirconium Diboride Ceramics by Reactive Hot Pressing," *J. Am. Ceram. Soc.,* **89**[12] 3638-45 (2006).

[15] H. Kinoshita, S. Otani, S. Kamiyama, H. Amano, I. Akasaki, J. Suda, and H. Matsunami, "Zirconium Diboride (0001) as an Electrically Conductive Lattice-Matched Substrate for Gallium Nitride," *Jpn. J. Appl. Phys.,* **40** L1280-L2 (2001).

[16] S. Guicciardi, L. Silvestroni, M. Nygren, and D. Sciti, "Microstructure and Toughening Mechanisms in Spark Plasma-Sintered ZrB_2 Ceramics Reinforced by SiC Whiskers or SiC-Chopped Fibers," *J. Am. Ceram. Soc.,* **93**[8] 2384-91 (2010).

[17] D. Sciti, S. Guicciardi, and L. Silvestroni, "SiC Chopped Fibers Reinforced ZrB_2: Effect of the Sintering Aid," *Scripta Mater.,* **64**[8] 769-72 (2011).

[18] D. Sciti, L. Silvestroni, G. Saccone, and D. Alfano, "Effect of Different Sintering Aids on Thermo–Mechanical Properties and Oxidation of SiC Fibers − Reinforced ZrB_2 Composites," *Mater. Chem. Phys.,* **137**[3] 834-42 (2013).

[19] X. Zhang, L. Xu, S. Du, J. Han, P. Hu, and W. Han, "Fabrication and Mechanical Properties of ZrB_2–SiC_w Ceramic Matrix Composite," *Mater. Lett.,* **62**[6–7] 1058-60 (2008).

[20] A. G. Evans, F. W. Zok, and J. Davis, "The Role of Interfaces in Fiber-Reinforced Brittle Matrix Composites," *Compos. Sci. Technol.,* **42**[1–3] 3-24 (1991).

[21] F. Rebillat, J. Lamon, R. Naslain, E. Lara-Curzio, M. K. Ferber, and T. M. Besmann, "Properties of Multilayered Interphases in SiC/SiC Chemical-Vapor-Infiltrated Composites with "Weak" and "Strong" Interfaces," *J. Am. Ceram. Soc.,* **81**[9] 2315-26 (1998).

[22] S. C. Zhang, G. E. Hilmas, and W. G. Fahrenholtz, "Pressureless Densification of Zirconium Diboride with Boron Carbide Additions," *J. Am. Ceram. Soc.,* **89**[5] 1544-50 (2006).

[23] W. G. Fahrenholtz, G. E. Hilmas, S. C. Zhang, and S. Zhu, "Pressureless Sintering of Zirconium Diboride: Particle Size and Additive Effects," *J. Am. Ceram. Soc.,* **91**[5] 1398-404 (2008).

[24] M. J. Thompson, W. G. Fahrenholtz, and G. E. Hilmas, "Elevated Temperature Thermal Properties of ZrB_2 with Carbon Additions," *J. Am. Ceram. Soc.,* **95**[3] 1077-85 (2012).

[25] J. Watts, G. Hilmas, and W. G. Fahrenholtz, "Mechanical Characterization of ZrB_2–SiC Composites with Varying SiC Particle Sizes," *J. Am. Ceram. Soc.,* **94**[12] 4410-8 (2011).

[26] L. Silvestroni and D. Sciti, "Oxidation of ZrB_2 Ceramics Containing SiC as Particles, Whiskers, or Short Fibers," *J. Am. Ceram. Soc.,* **94**[9] 2796-9 (2011).

[27] F. Monteverde and A. Bellosi, "Effect of the Addition of Silicon Nitride on Sintering Behaviour and Microstructure of Zirconium Diboride," *Scripta Mater.,* **46**[3] 223-8 (2002).

[28] F. Monteverde, S. Guicciardi, and A. Bellosi, "Advances in Microstructure and Mechanical Properties of Zirconium Diboride Based Ceramics," *Mater. Sci. Eng., A,* **346**[1–2] 310-9 (2003).

[29] S.-Q. Guo, Y. Kagawa, T. Nishimura, and H. Tanaka, "Pressureless Sintering and Physical Properties of ZrB_2-Based Composites with $ZrSi_2$ Additive," *Scripta Mater.,* **58**[7] 579-82 (2008).

[30] S.-Q. Guo, Y. Kagawa, and T. Nishimura, "Mechanical Behavior of Two-Step Hot-Pressed ZrB_2-Based Composites with $ZrSi_2$," *J. Eur. Ceram. Soc.,* **29**[4] 787-94 (2009).

[31] O. N. Grigoriev, B. A. Galanov, V. A. Kotenko, S. M. Ivanov, A. V. Koroteev, and N. P. Brodnikovsky, "Mechanical Properties of ZrB_2-SiC($ZrSi_2$) Ceramics," *J. Eur. Ceram. Soc.,* **30**[11] 2173-81 (2010).

[32] O. N. Grigoriev, B. A. Galanov, V. A. Lavrenko, A. D. Panasyuk, S. M. Ivanov, A. V. Koroteev, and K. G. Nickel, "Oxidation of ZrB_2–SiC–$ZrSi_2$ Ceramics in Oxygen," *J. Eur. Ceram. Soc.,* **30**[11] 2397-405 (2010).

[33] D. Sciti, M. Brach, and A. Bellosi, "Oxidation Behavior of a Pressureless Sintered ZrB_2–$MoSi_2$ Ceramic Composite," *J. Mater. Res.,* **20**[4] 922-30 (2005).

[34] S. Guo, T. Nishimura, and Y. Kagawa, "Low-Temperature Hot Pressing of ZrB_2-Based Ceramics with $ZrSi_2$ Additives," *Int. J. Appl. Ceram. Tec.,* **8**[6] 1425-35 (2011).

[35] G. R. Anstis, P. Chantikul, B. R. Lawn, and D. B. Marshall, "A Critical Evaluation of Indentation Techniques for Measuring Fracture Toughness: I, Direct Crack Measurements," *J. Am. Ceram. Soc.,* **64**[9] 533-8 (1981).

[36] S. C. Zhang, G. E. Hilmas, and W. G. Fahrenholtz, "Pressureless Sintering of ZrB_2–SiC Ceramics," *J. Am. Ceram. Soc.,* **91**[1] 26-32 (2008).

[37] V. G. Sevast'yanov, P. Y. Nosatenko, V. V. Gorskii, Y. S. Ezhov, D. V. Sevast'yanov, E. P. Simonenko, and N. T. Kuznetsov, "Experimental and Theoretical Determination of the Saturation Vapor Pressure of Silicon in a Wide Range of Temperatures," *Russian Journal of Inorganic Chemistry,* **55**[13] 2073-88 (2010).

[38] L. Silvestroni and D. Sciti, "Effects of $MoSi_2$ Additions on the Properties of Hf– and Zr–B_2 Composites Produced by Pressureless Sintering," *Scripta Mater.,* **57**[2] 165-8 (2007).

[39] E. Parthé and J. T. Norton, "B-Si-Zr Isothermal Section at 1400°C." In *ASM Alloy Phase Diagrams Center***. ASM International, Materials Park, OH, USA, 2007.

[40] D. Sciti, L. Silvestroni, and A. Bellosi, "Fabrication and Properties of HfB_2–$MoSi_2$ Composites Produced by Hot Pressing and Spark Plasma Sintering," *J. Mater. Res.,* **21** 1460-6 (2006).

[41] G. Baret, R. Madar, and C. Bernard, "Silica-Based Oxide Systems," *J. Electrochem. Soc.,* **138**[9] 2830-5 (1991).

[42] M. N. Rahaman, "Ceramic Processing," Taylor & Francis Group, LLC, Boca Raton, FL, 2007.

[43] A. Passerone, M. Muolo, and D. Passerone, "Wetting of Group IV Diborides by Liquid Metals," *J. of Mater. Sci.,* **41**[16] 5088-98 (2006).

[44] Y. Waseda, "The Structure of Non-Crystalline Materials: Liquids and Amorphous Solids," McGraw-Hill, New York, NY, 1980.

[45] J. R. Chelikowsky, N. Troullier, and N. Binggeli, "First-Principles Simulation of Liquid Silicon Using Langevin Dynamics with Quantum Interatomic Forces," *Phys. Rev. B.,* **49**[1] 114-9 (1994).

[46] I. Štich, R. Car, and M. Parrinello, "Bonding and Disorder in Liquid Silicon," *Phys. Rev. Lett.,* **63**[20] 2240-3 (1989).

[47] W. Martienssen and H. Warlimont, "Springer Handbook of Condensed Matter and Materials Data," pp. 474-5 **Vol. 1**, Springer, Heidelberg, Germany, 2005.

[48] D. L. Callahan and J. C. Morris, "Extent of Phase Transformation in Silicon Hardness Indentations," *J. Mater. Res.,* **7**[7] 1614-7 (1992).

[49] V. Domnich, Y. Aratyn, and W. M. K. andYury Gogotsi, "Temperature Dependence of Silicon Hardness: Experimental Evidence of Phase Transformations," *Rev. Adv. Mater. Sci,* **17** 33-41 (2008).

[50] Y. V. Milman, S. I. Chugunova, I. V. Goncharova, T. Chudoba, W. Lojkowski, and W. Gooch, "Temperature Dependence of Hardness in Silicon–Carbide Ceramics with Different Porosity," *Int. J. Refract. Met. Hard Mater.,* **17**[5] 361-8 (1999).

[51] E. W. Neuman, G. E. Hilmas, and W. G. Fahrenholtz, "Strength of Zirconium Diboride to 2300°C," *J. Am. Ceram. Soc.,* **96**[1] 47-50 (2013).

[52] J. Wachtman, "Mechanical Properties of Ceramics," John Wiley & Sons, Inc., New York, 1996.

[53] S. Kaur, D. K. Shetty, and R. A. Cutler, "R Curves and Crack-Stability Map: Application to Ce-TZP/Al_2O_3," *J. Am. Ceram. Soc.,* **90**[11] 3554-8 (2007).

Table I. Sample Designations, Nominal Compositions, and Densities.

Sample Designation	Composition			Hot Pressing Temperature	Theoretical Density	Bulk Density	Relative Density
	(vol%)			(°C)	(g/cm^3)	(g/cm^3)	(%)
	ZrB$_2$	ZrSi$_2$	SiC				
Z05S-1400	95	5	0	1400	6.03	4.59	76.13
Z05S-1600	95	5	0	1600	6.03	4.87	80.77
Z7.5S-1400	92.5	7.5	0	1400	6.00	5.74	95.68
Z7.5S-1600	92.5	7.5	0	1600	6.00	5.81	96.85
Z10S-1400	90	10	0	1400	5.97	5.68	95.16
Z10S-1.5SiC-1400	88.67	9.85	1.5	1400	5.93	5.70	96.14
Z10S-1600	90	10	0	1600	5.97	5.74	96.16
Z20S-1400	80	20	0	1400	5.85	5.56	95.13

Table II. Composition of Component Powders Determined from Rietveld Refinement of XRD Patterns.

Component	Raw ZrB_2 (vol%)	Raw "$ZrSi_2$" (vol%)	Hot Pressed "$ZrSi_2$" (vol%)	Pressureless Sintered "$ZrSi_2$" (vol%)
ZrB_2	100	-	-	-
$ZrSi_2$	-	27.3	57.0	41.1
Si	-	47.5	8.1	35.6
ZrO_2 (monoclinic)	-	17.4	14.5	11.4
$ZrSiO_4$	-	7.8	14.1	8.7
SiO_2 (β-Cristobalite)	-	-	6.3	3.1

Table III. Revised Theoretical and Relative Densities

Sample Designation	Theoretical Density	Bulk Density	Relative Density
	(g/cm^3)	(g/cm^3)	(%)
Z05S-1400	5.98	4.59	76.70
Z05S-1600	5.98	4.87	81.37
Z7.5S-1400	5.93	5.74	96.76
Z7.5S-1600	5.93	5.81	97.94
Z10S-1400	5.88	5.68	96.61
Z10S-1.5SiC-1400	5.84	5.70	97.59
Z10S-1600	5.88	5.74	97.63
Z20S-1400	5.69	5.56	97.82

Table IV. Mechanical Properties of ZrB_2-$ZrSi_2$ Hot-Pressed Materials

Material	Composition (vol%)		Hardness (GPa)			Toughness ($MPa \cdot m^{1/2}$)			Elastic Modulus (GPa)			Flexure Strength (MPa)		
	ZrB_2	$ZrSi_2$												
Z05S-1400	95	5	-			-			-			-		
Z05S-1600	95	5	-			-			-			-		
Z7.5S-1400	92.5	7.5	15.5	±	0.5	4.0	±	0.2	462	±	23	673	±	38
Z7.5S-1600	92.5	7.5	15.8	±	0.3	4.2	±	0.1	471	±	19	752	±	71
Z10S-1400	90	10	16.1	±	0.3	4.2	±	0.1	486	±	13	543	±	82
Z10S-1600	90	10	16.2	±	0.5	4.3	±	0.2	493	±	11	475	±	67
Z20S-1400	80	20	15.0	±	0.2	4.3	±	0.2	439	±	9	388	±	47
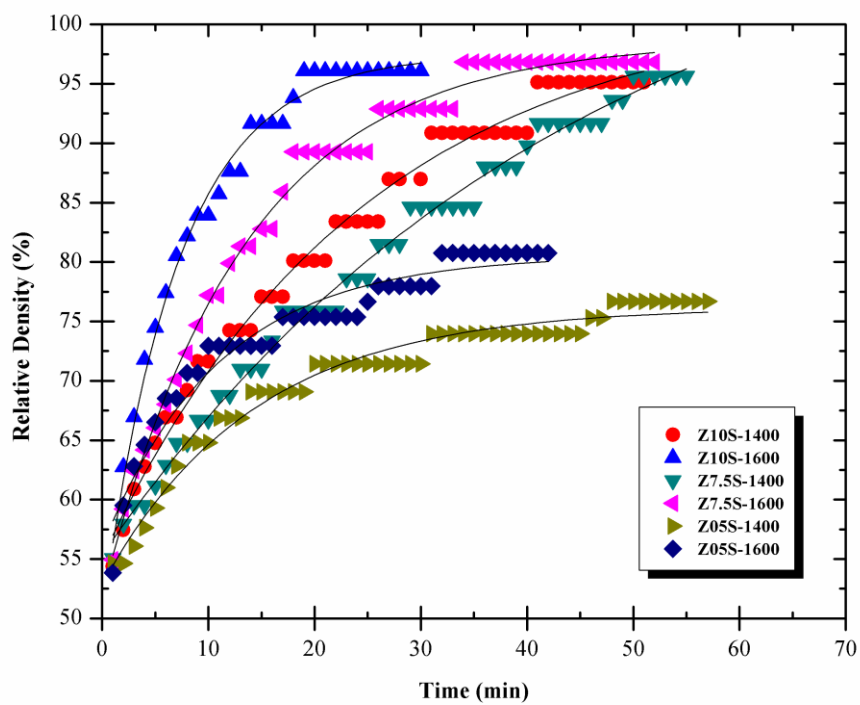
Fig. 1. Typical examples of shrinkage curves obtained during hot-pressing cycle for selected compositions.
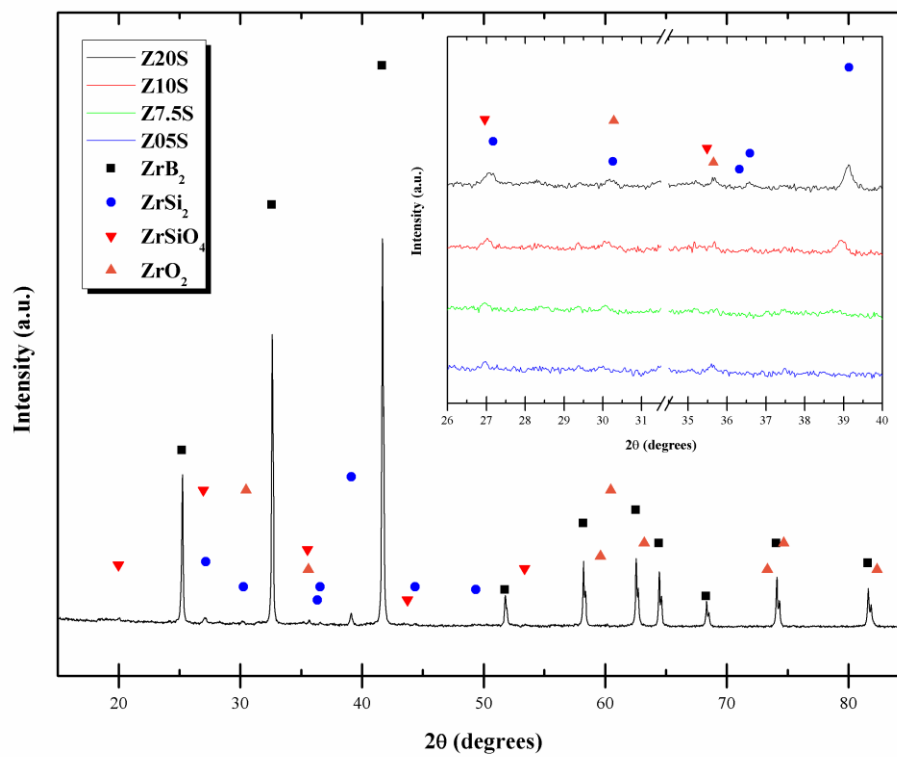
Fig. 2. XRD patterns for selected compositions showing presence of dominant ZrB_2 phase and trace amounts of oxide phases (ZrO_2 and $ZrSiO_4$).
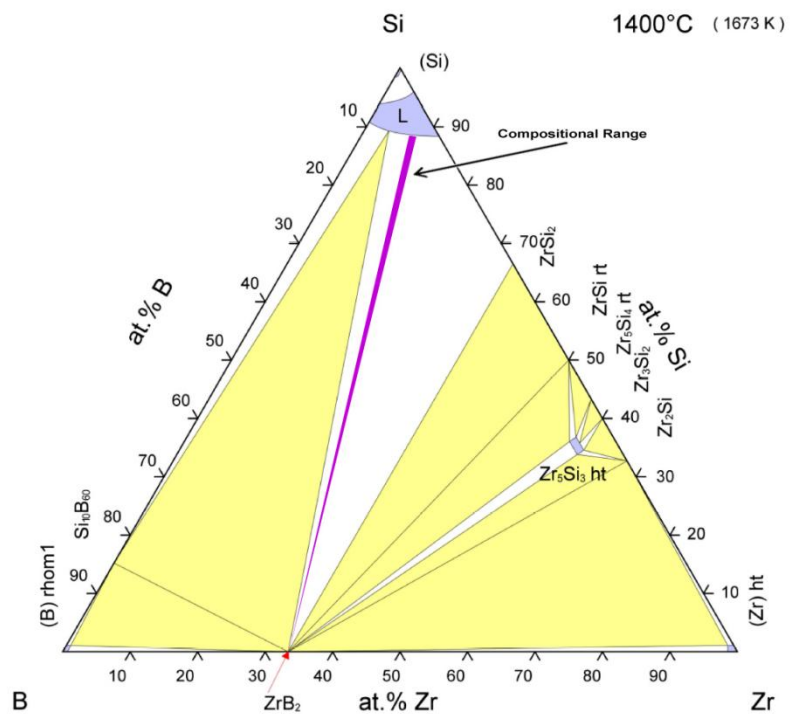
Fig. 3. Isothermal section of B-Si-Zr ternary phase diagram, taken from Parthé *et al.*, showing Si liquid in equilibrium with ZrB_2 and $ZrSi_2$.[39] The compositional range predicted from the measured composition of the "$ZrSi_2$" powder is shown.
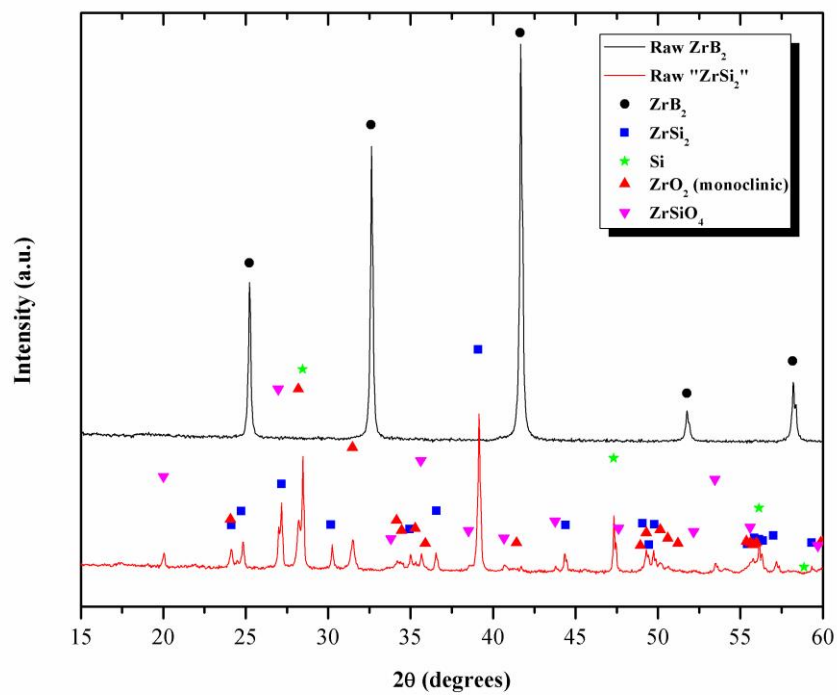
Fig. 4. XRD patterns for starting ZrB_2 and "$ZrSi_2$" powders.
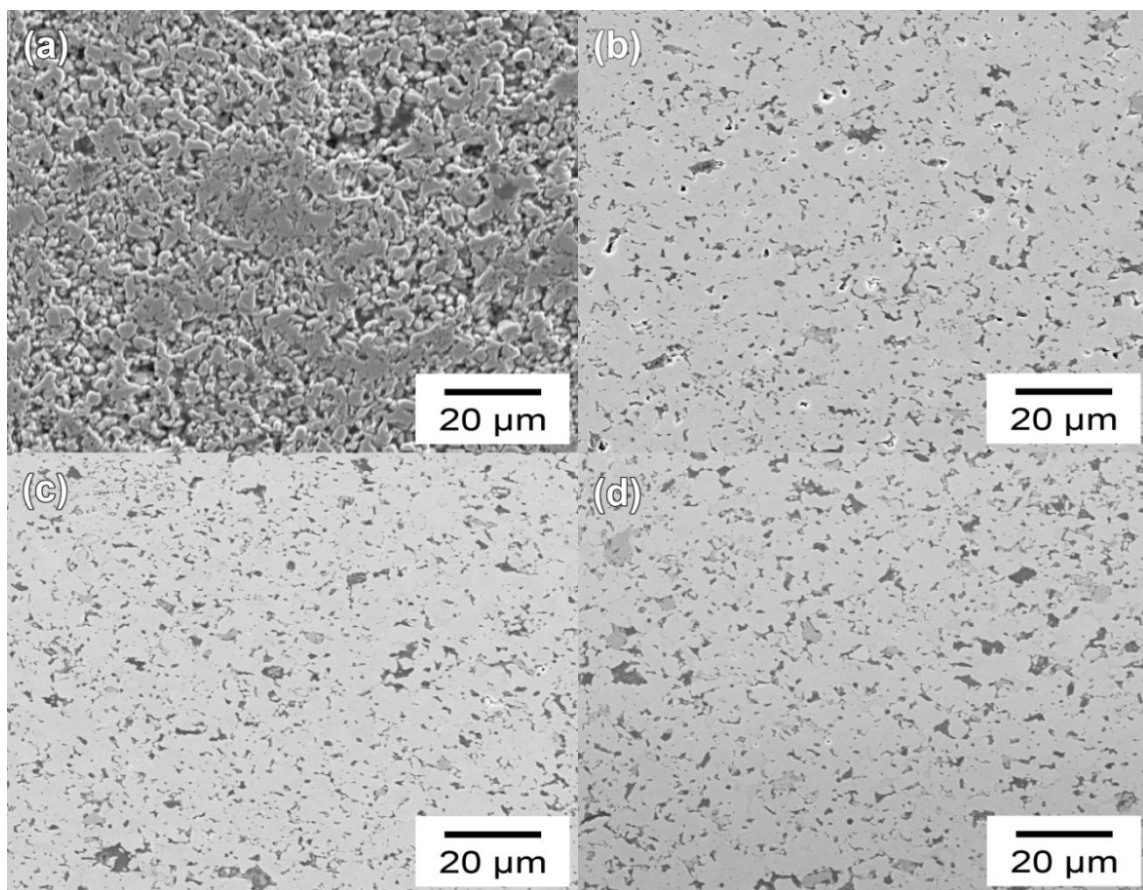
Fig. 5. Polished cross sections of (a) Z05S, (b) Z7.5S, (c) Z10S, and (d) Z20S after hot pressing at 1400°C.
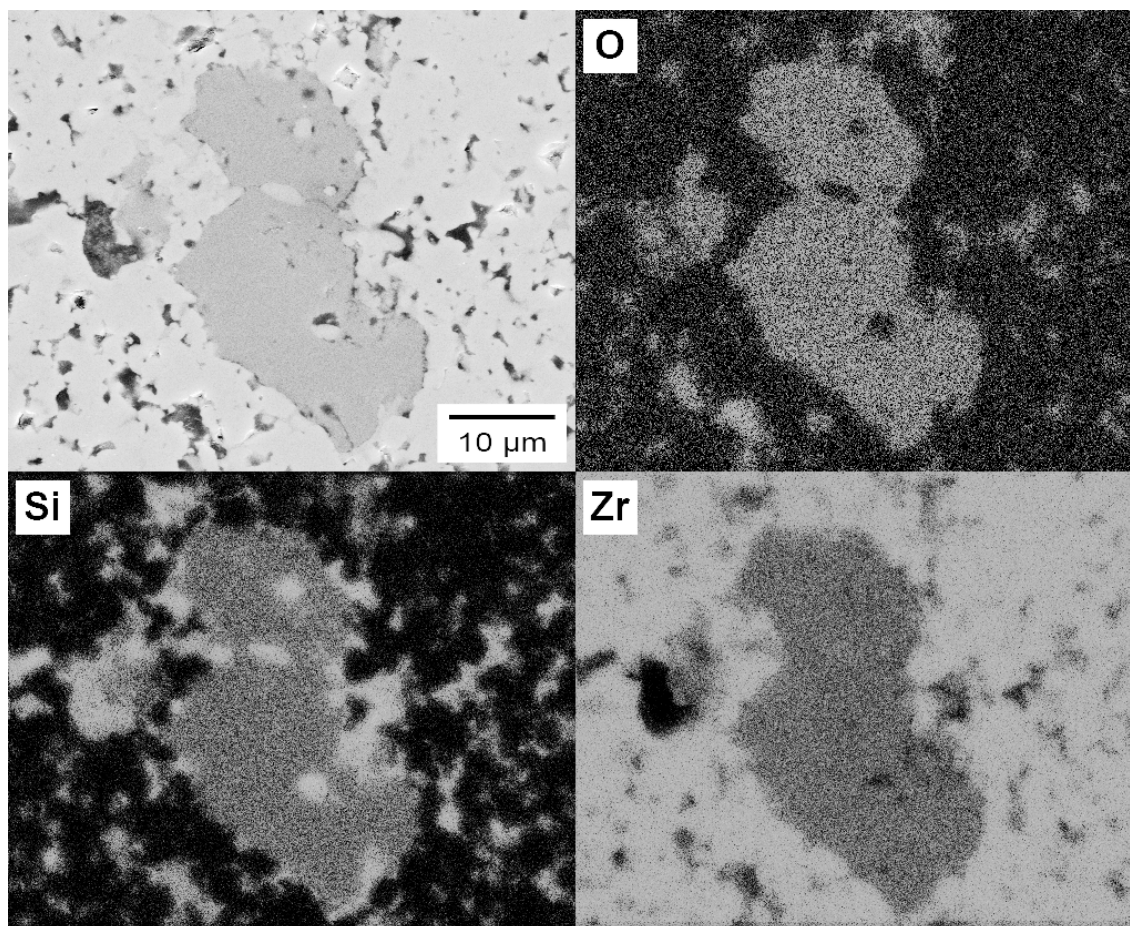
Fig. 6. Representative SEM image of Z10S second phase agglomerate with accompanying EDS phase mapping showing O, Si, and Zr distribution.
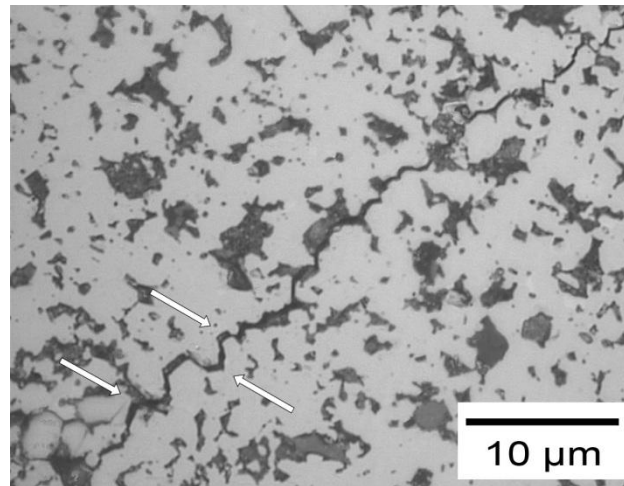
Fig. 7. Radial median crack extending from indent tip in Z20S showing deflection along
ZrB$_2$ particle edge through softer intergranular phase.
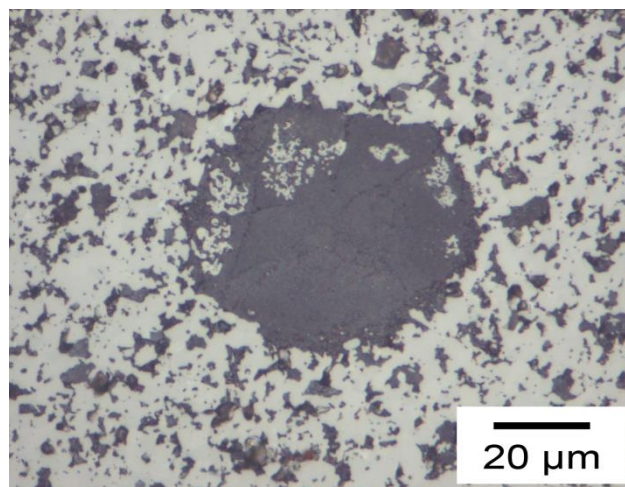
Fig. 8. Optical micrograph of Z20S material showing agglomeration of the Si-rich low Z phase.

II. ZrB$_2$-ZrSi$_2$ MATRIX COMPOSITES REINFORCED WITH CONTINUOUS SiC FIBER

Benjamin J. Lai, Jeremy L. Watts, Gregory E. Hilmas, William G. Fahrenholtz

Missouri University of Science and Technology

Materials Science and Engineering Dept.

1400 N. Bishop Ave.

Rolla, MO 65409

ABSTRACT

Flexural strength and elastic modulus were used to characterize the mechanical properties and performance of ZrB$_2$-ZrSi$_2$ matrix composites containing continuous SiC fiber. Dense ZrB$_2$-ZrSi$_2$ matrices consisting of 90 vol% ZrB$_2$ and 10 vol% ZrSi$_2$ reinforced with commercially available continuous SiC fiber (i.e. CG-Nicalon, Hi-Nicalon, or Sylramic iBN) were produced via slurry coating/impregnation, followed by hot pressing at 1400°C. Composite specimens display a high degree of slurry penetration into fiber tows and improved retention of fiber integrity after hot pressing. Flexural strengths decreased for all composite specimens incorporating SiC fiber (50-86%) as compared to a baseline ZrB$_2$-ZrSi$_2$ matrix composition, but strain to failure was increased (0.2 to 3.0%) as well as inelastic work of fracture (1.2 to 3.5 kJ·m^{-2}).

Keywords: ZrB$_2$; Ceramic matrix composite; Continuous SiC fiber; Mechanical properties

1. INTRODUCTION

The ultra-high temperature ceramics (UHTCs), with extremely high melting temperatures (>3000°C), are ideal candidates for thermal protections systems (TPS),

propulsion systems, and hypersonic aerospace vehicles.[1-4] Zirconium diboride (ZrB_2) is set apart from other UHTC materials due to its high thermal conductivity (60-145 $W \cdot (m \cdot K)^{-1}$)[5,6] and low electrical resistivity (7.8-22 $\mu\Omega \cdot cm$),[7] as well as its high strength (>500 MPa),[2] and resistance to chemical attack.[8] The combination of high thermal conductivity and ultra-high temperature stability make ZrB_2 a desirable material for sharp leading edge components (i.e. those employed on hypersonic capable vehicles).

However, in such applications a material is not only subjected to extreme temperatures due to aerothermal heating, but also is subject to high-stress due to nonuniform loading as well as thermal shock conditions caused by near instantaneous heating. Due to its inherently brittle nature, ZrB_2-based monolithic ceramics fall short of desirable behavior, where catastrophic failure is common with relatively low, instantaneous temperature changes (~400°C).[9] To potentially overcome these limitations, continuous fiber reinforcement has been proposed for several systems, such as SiC/SiC, C/SiC, SiC/Si_3N_4, but is limited with regard to ZrB_2-based systems.[10-14]

The technical literature regarding current state-of-the-art SiC/SiC and C/SiC composites is extensive, especially regarding mechanical testing at room temperature and elevated temperature. C/SiC and SiC/SiC composites have been of interest recently for their higher temperature capabilities (i.e. ~1600°C) and highly damage tolerant mechanical performance.[15-21] However, application of C/SiC and SiC/SiC composite systems to ultra-high temperature regimes (i.e. >2000°C typically seen in hypersonic flight conditions) is limited due to significant ablation,[22-24] embrittlement,[25-27] and oxygen ingress (i.e. active oxidation dominates above a critical temperature, where previously passive oxidation aids in protection at lower temperatures due to formation of

viscous silica).[28-32] Use of continuous fiber-reinforced ceramic matrix composites (CFCCs) under these severe conditions necessitates a compatible ultra-high temperature matrix to resist ablation arising from thermomechanical, thermochemical, and thermophysical influences. In recent years, ZrB_2-based systems have seen significant improvements to oxidation resistance.[33] Additionally, significant advancements have been made regarding characterization of oxidation behavior (i.e. mechanisms operating in defined temperature regimes) in ZrB_2-based systems.[34-36] CFCCs utilizing an ultra-high temperature matrix and high-strength continuous fibers offer a beneficial combination of a higher use temperature while maintaining an oxidation/ablation resistant matrix along with a reinforcing phase that imparts graceful failure and damage tolerance.

Densification of ZrB_2-based ceramics typically requires very high temperatures (>2000°C), which is a regime unsuitable for processes incorporating silicon carbide (SiC) fiber reinforcements. Commercially available SiC fibers have reported maximum use temperatures in the range of 1000°C to 1600°C, depending on the manufacturer and grade, where decreasing relative oxygen content results in a higher grade fiber.[37-41] Due to this discrepancy, the high temperatures utilized in densifying pure ZrB_2 materials limit the applicability of SiC fiber reinforcement in these materials. Utilizing additives and second phases, the processing temperatures required to achieve full density in a ZrB_2-based system can be effectively reduced, increasing the viability of utilizing a continuous SiC fiber reinforcement. Traditionally ZrB_2 materials incorporate combinations of boron carbide (B_4C), carbon (C), as well as fine SiC particulate to effectively reduce processing temperatures, often bringing peak densification temperatures below 2000°C.[42-45] In light of maximum use temperatures of commercially available SiC fibers and their

limited ultra-high temperature capabilities, further reductions in processing temperature are required in the ZrB_2-based systems. Silicon nitride (Si_3N_4) additions to ZrB_2 have been shown to reduce the densification temperature to ~1700°C to achieve near full density by hot pressing.[46-48] Transition metal disilicides, specifically $MoSi_2$ and $ZrSi_2$, have been used to form an in-situ liquid phase during processing, allowing for increased densification at significantly reduced processing temperatures (1400 to 1900°C).[42,56-59] Additions of 5 to 20 vol% $MoSi_2$ were sufficient to densify ZrB_2 at 1800°C by pressureless sintering.[35] ZrB_2 ceramics containing 30 vol% $ZrSi_2$ were found to achieve full density by pressureless sintering at 1650°C,[49] while additions as low as 20 vol% $ZrSi_2$ were sufficient to achieve full density by hot pressing at 1550°C.[50] This increased sinterability allows for ZrB_2-based materials to form a compatible matrix material to various grades of commercially available SiC fibers.

In the present study, ZrB_2-based composite materials were fabricated employing $ZrSi_2$ as an additive for the purpose of incorporating various grades of commercially available SiC fibers. Future advancement in areas such as hypersonic aviation will require high temperature, damage tolerant materials. Incorporation of continuous SiC fibers in a ZrB_2 matrix offers a desirable combination of ultra-high temperature capability and graceful failing/damage-tolerant structure.

2. EXPERIMENTAL PROCEDURE

2.1 *Slurry and Specimen Preparation*

Commercially available ceramic powders were used throughout the study. The ZrB_2 powder (Grade B, H.C. Starck, Newton, MA) used had a purity of >99% (metals

basis) and an average particle size of 2 μm. The $ZrSi_2$ powder (Alfa Aesar, Ward Hill, MA) had a reported purity of >99.5% (metals basis) and a particle size of -325 mesh. Following batching, powders were attrition milled (Model 01-HD, Union Process, Akron, OH) for 2 hours in acetone at 600 rpm using a polymer coated container and spindle as well as SiC media. Powder compositions were then rotary evaporated (Model R-124, Buchi, Flawil, Germany) at 70°C, 300 mm Hg (40 kPa) vacuum, and a 50 rpm rotational speed to prevent sedimentation during drying. Dried powders were then sieved to 60-mesh (<250 μm) before any further processing. A number of commercial SiC fibers were utilized, specifically: plain weave Ceramic Grade (CG) Nicalon, Hi-Nicalon, as well as an in-situ BN coated Sylramic SiC fiber (Syralmic iBN; COI Ceramics, Magna, UT). Additionally, it became advantageous to incorporate a specialized chemical vapor deposition (CVD) coating procedure for continuous fiber tow (yarn). Due to supplier specifications and material limitations, a CVD coating was only applied to the Hi-Nicalon continuous fiber tow. Si-doped BN coatings about 0.2 μm thick were deposited by Hyper-Therm High-Temperature Composites, Inc. (Huntington Beach, CA).

Two methods to incorporate a ZrB_2-$ZrSi_2$ matrix into a SiC fiber reinforced composite were utilized. The first employed an acetone-based suspension of ZrB_2-$ZrSi_2$ (Z20S-A). The second utilized a modified polyvinyl butyral (PVB; B-79, Maroon Inc., Avon, OH) based tape-casting slurry composition. Necessarily, an analysis of surface area as well as gravitational sedimentation was conducted on milled powders to determine dispersant concentrations. It was determined that a concentration of 0.1 mg·m^{-2} DISPERBYK-110 (BYK, Wesel, Germany) dispersant was optimal for both ZrB_2 and $ZrSi_2$ powders in an azeotropic mixture of methyl ethyl ketone (MEK) and ethanol

(EtOH) (MEK to EtOH: 60:40 by weight). Slurry compositions were prepared by ball

milling ceramic powders in MEK:EtOH solvent in 24 hour stages per each organic

additive using SiC media (Table I). Ceramic powders were initially ball milled with

BYK-110 dispersant for 24 hours to achieve good mixing. Immediately following

mixing the solid PVB was added and milled for an additional 24 hours. Two organic

plasticizers were utilized to achieve flexibility and ease handling during processing.

Specifically, polyethylene glycol (PEG 400; Fisher Scientific, Fair Lawn, NJ) and benzyl

butyl phthalate (Santicizer 160; Ferro, Walton Hills, OH), were added to slurry

compositions following the PVB binder. After mixing, the slurries were evacuated by

vacuum desiccator to remove small air bubbles and/or entrained air and filtered by

peristaltic pump through a 25 μm screen to remove any undissolved binder or large

agglomerates. Slurries were then slow-rolled at a rotational speed of 20 rpm to further

facilitate the removal of entrained air.

     Ceramic slurries were then utilized in a number of fabrication methods to prepare

composite materials. Slurries were employed in batch production of ceramic green tapes

using a bench top tape caster (Lab Scale Tape Caster, Gardner Laboratory, Silver Spring,

MD); where following filling of a reservoir, tapes were formed via doctor blade set to 15

mil (380 μm) thickness and 40 cm·min^{-1} casting speed on silicone coated Mylar.

Modified slurry compositions were utilized to infiltrate and coat Hi-Nicalon and Sylramic

iBN continuous fiber tow (i.e. a reduced solids loading of ~17 vol%), where a schematic

representation can be seen in Fig. 1. Coated and infiltrated continuous tow was then

allowed to dry and cut to length for the desired architectural layup. Both unidirectional

[0°] and bidirectional [0°/90°] architectural layups were constructed employing ZrB_2-

based green tapes in formation of composite specimens. Initial layups incorporated green tapes as interlayers (Fig. 1), but later processing resulted in removal of interlayer green tapes to increase overall fiber loading in composite specimens. Layups were loaded into graphite dies that were lined with graphite foil and coated in boron nitride (BN; Cerac, SP-108, Milwaukee, WI, USA) and laminated with a ~6 MPa uniaxial load at 90°C for 30 minutes. Specimens then underwent binder burnout overnight (~18 hours) followed by hot pressing (Model HP-20-3060-20, Thermal Technology, Santa Rosa, CA) at temperatures ranging from 1400 to 1600°C. Temperature during hot pressing was monitored by an infrared pyrometer (Model 0S3708, Omega Engineering, Stamford, CT) above 600°C. Following overnight burnout under vacuum of 140 mtorr (19 Pa) to 700°C over 18 hours, the hot press was backfilled with argon and heating was conducted under flowing inert atmospheric pressure argon. Dies were heated at ~30-40 °C·(min)$^{-1}$ up to 1200°C where 32 MPa uniaxial load was applied. Specimens continued to be heated to 1400°C and 1600°C and held for approximately 1 hour at temperature and pressure. Following the high temperature hold the hot press was cooled at ~20°C·(min)$^{-1}$ to room temperature. Uniaxial load was removed upon cooling to 1200°C.

2.2 *Characterization*

Following removal from the hot press die, the billets were surface ground to a thickness of ~1.5 to 2 mm to achieve flat and parallel surfaces as well as removal of any adherent BN. Microstructure was evaluated by scanning electron microscopy (SEM; Model S570, Hitachi, Tokyo, Japan) while simultaneous elemental composition was evaluated by energy dispersive spectroscopy (EDS; Model AAT, X-ray Optics,

Gainesville, FL). Specimens were prepared for microscopy by removing a cross-section parallel to the hot-pressing direction and utilizing successively finer diamond abrasive slurries where final finish was obtained using 0.25 μm diamond.

2.3   *Mechanical Property Testing*

Specimens for mechanical property tests were machined from the billets and ground to final dimensions using 400-grit (37 μm) before final polishing to 0.25 μm diamond finish. Diamond abrasive wheels were used for all cutting and grinding using an automated surface grinder (Chevalier, FSG-3A818, Santa Fe Springs, CA). Flexure strength was measured using a fully-articulated four point bending fixture consistent with ASTM Standard C1161-02c using modified B-type bars (25 mm x 4 mm x 2-3 mm). A minimum of six test bars were tested for each composite.

3.   RESULTS AND DISCUSSION

3.1   *Densification and Microstructure*

Incorporation of $ZrSi_2$ improved the density of the ZrB_2 matrix for all fiber-reinforced composites. Previous work has shown that ZrB_2 incorporating nominal $ZrSi_2$ additions effectively reduces sintering temperatures without significant reductions in strength or modulus.[51,52] Further, additions as low as 7.5 vol% yielded a fully dense (>97% relative) ZrB_2 matrix at 1400°C that had a strength of 673 MPa.[53] The "$ZrSi_2$" consisted of ~39 vol% Si, ~27 vol% ZrO_2, ~8 vol% $ZrSiO_4$, and only ~26 vol% $ZrSi_2$. Additions of less than 10 vol% of this powder were not sufficient to densify ZrB_2 in the presence of continuous SiC fibers. However, initial trials with an addition of 20 vol% $ZrSi_2$ hot pressed at 1600°C showed significant degradation of CG-Nicalon fibers (Fig.

2a). Hence, fibers with improved stability at elevated temperatures were essential to preserve fiber integrity and ultimately improve mechanical performance. Composite specimens incorporating Sylramic iBN fiber hot pressed under the same conditions and the same matrix composition show improved fiber integrity, Fig. 2b. For brittle matrix composites, the fiber-matrix interface influences the performance of the resulting composite. The debond energy and sliding resistance along the debond length or region are critical parameters.[54-59] Specimens exhibiting a high degree of interdiffusion between the fiber and matrix have strong bonding at the fiber-matrix interface, which typically results in brittle fracture due to the inability of the interface to arrest or deflect cracks. The Z20S-A specimens containing CG-Nicalon fiber hot-pressed at 1600°C had a significant amount of degradation presumably due to the relatively high oxygen content (~12 wt%) and significant amount Si-C-O amorphous phase in the CG-Nicalon fiber. It is also conceivable that an increased volume fraction of liquid phase was formed at temperature. Previous work by Lai *et al*. showed that with the present matrix composition ~13 vol% liquid (predominantly Si) is expected at 1400°C, so a significantly greater amount is expected at higher temperatures.[53] Therefore, additive content must be minimized while permitting sufficient densification of the matrix phase to allow for adequate mechanical performance. In the present study, $ZrSi_2$ additive utilized during hot-pressing was optimized at 10 vol% for fiber reinforced ZrB_2-$ZrSi_2$ matrix composites.

A hot-pressing temperature of 1400°C was sufficient to densify composites containing 10 vol% $ZrSi_2$ in the ZrB_2 matrix (i.e., >95% relative density). Hot pressing at 1400°C was chosen to minimize possible thermal degradation of fibers as well as reduce fiber-matrix interdiffusion. From Fig. 3, spontaneous microcracking was observed in

Z10S composites produced using Sylramic fiber in [0°/90°] architectures (Z10S-Syl$_{0°/90°}$). Microcracking likely resulted from the thermal expansion mismatch between the matrix and fibers, which will be discussed in detail later. It was determined that a thin (<50 nm) in-situ BN coating originating from boron addition in the Sylramic iBN fibers was insufficient to serve as a diffusion barrier between the ZrB_2-$ZrSi_2$ matrix and the fibers. Subsequently, Hi-Nicalon fibers with a 0.2 μm thick coating consisting of Si doped BN were employed to produce composites Z10S-Hi(BN)$_{0°}$ and Z10S-Hi(BN)$_{0°/90°}$ (Fig. 4). In addition to improved resistance to attack during densification, BN coated Hi-Nicalon composites showed improved slurry penetration into the tow as well as good retention of BN coating after hot pressing, both of which are essential features to obtain composite behavior.

3.2   Mechanical Properties

The mechanical properties of ZrB_2 matrix composites produced in the study are summarized in Table II. By inspection of microstructures, composite materials utilizing CG-Nicalon fibers and a Z20S matrix phase were not suitable for mechanical testing due to significant damage to the SiC fibers during hot-pressing. For comparison, the strength and elastic modulus of ZrB_2 containing 10 vol% $ZrSi_2$ (i.e., no fibers) is offered. Flexure strength decreased significantly for all composites incorporating continuous SiC fiber. Without fibers, Z10S had strengths of ~540 MPa compared to strengths ranging from ~80 MPa for Z10S-Syl$_{0°/90°}$ to nearly 500 MPa for Z10S-Syl$_{0°}$. The maximum flexural strength reductions were less for compositions utilizing unidirectional ([0°]) fiber architectures and untreated fibers, where reductions on the order of ~8 and ~26% were observed for Sylramic iBN (Z10S-Syl$_{0°}$) and Hi-Nicalon (Z10S-Hi$_{0°}$) fiber reinforced

specimens relative to the Z10S matrix. Specimens incorporating BN coated Hi-Nicalon in unidirectional (Z10S-Hi(BN)$_{0°}$) and bidirectional (Z10S-Hi(BN)$_{0°/90°}$) layups resulted in significant reductions in apparent peak flexural strength, with a reduction in strength of over 50% (i.e. ~260 MPa) compared to the nominally pure, dense matrix. Undoubtedly the most significant decrease in strength was observed for specimens utilizing bidirectional Sylramic iBN fiber (Z10S-Syl$_{0°/90°}$), which exhibited up to an 86% strength reduction (~80 MPa). However, continuous fibers were not added to improve strength, but to enhance fracture toughness and promote graceful failure. Hence, the stress-strain behavior during testing was examined as well.

The fiber architecture, condition/presence of fiber-matrix interfacial coating, and type of fiber had significant impacts on the composite failure behavior. Fig. 5 depicts the typical stress-strain response for composites tested in four point flexure. Composites containing Hi-Nicalon with a unidirectional architecture showed purely brittle failure at peak stresses of ~500 MPa. The brittle response was presumably due to the lack of interfacial BN coating resulting in strong bonding at the fiber-matrix interface. Similarly, a high degree of brittle failure was observed for unidirectional Sylramic iBN fiber composites. Typical behavior in these composites consists of (i) the initial elastic loading of the composite, (ii) initiation of a crack perpendicular to the specimen length, (iii) crack propagation through the brittle matrix that arrests at a region of higher fiber loading (i.e. a tow bundle), (iv) resumption of loading until the stress overcomes the crack initiation stress, and (v) ultimate failure. Comparatively, unidirectional specimens lacking a fiber interface coating exhibited higher characteristic strengths (>500 MPa) but were unable to tolerate higher strains. This behavior can be explained by several factors. Due to the

high strength of the matrix phase, it is conceivable that just prior to crack initiation a significant amount of strain energy has accumulated at the tensile surface, and before sufficient strain energy can be released via crack initiation and propagation, the crack has already propagated through a significant amount of material. As a crack propagates nearer the neutral axis during testing, the tensile loading experienced falls off, so the observed behavior where cracks arrest and the composite continues loading is consistent with expectation. It should be noted that the beam equation used to calculate all stresses assumed a constant cross-sectional area measured prior to testing. Following first crack initiation and propagation, the cross-sectional area is reduced so the true maximum load was higher than reported. Strength values have been reported using constant cross-sectional area, for the sake of simplicity and consistency as well as the differing failure behaviors present for separate composites.

The behavior of Z10S-Syl$_{0°/90°}$ compositions differed significantly from all of the other compositions. The average strength was 78 MPa, which was significantly less than other compositions, but the strain to failure was greater than 3%. It should be noted that specimens tested for Z10S-Syl$_{0°/90°}$ compositions exhibited a significant amount of spontaneous microcracking prior to testing. As a result, a number of compliance changes occurred during loading, presumably originating from growth and/or linking of microcracks in the matrix under the highest shear (i.e. the region between the upper and outer loading pins). Microcracking occurred during cooldown from the densification temperature due to a difference in thermal expansion coefficient between the ZrB_2 matrix and SiC fibers (5.26×10^{-6} K^{-1}, and 3.76×10^{-6} K^{-1} respectively, at room temperature).[60] The addition of second phase Si, $ZrSi_2$, as well as ZrO_2 and $ZrSiO_4$

influences the CTE of the matrix, where a linear expansivity of 5.35×10^{-6} K^{-1} is

expected for Z10S matrix based on impurity content in raw powders and a linear rule of

mixtures.[61-64] The difference in expansivities puts the β-SiC fibers in compression

and the predominantly ZrB$_2$ matrix in tension, consistent with previous work by Watts *et

al*. that defined the tensile stress concentrations in ZrB$_2$ originating from SiC

particulate.[45,65,66] Matrix cracking was observed in Z10S-Syl$_{0°}$ composites as well,

however, to a reduced degree. Therefore it is likely that spontaneous matrix cracking in

Z10S-Syl$_{0°/90°}$ results from a combination of CTE mismatch between the matrix and the

fiber as well as complication of thermal residual stresses arising from transverse plies.

This was consistent with behavior predicted by Beyerle *et al*. that showed evidence of

tunneling cracks in 90° layers arising from machining damage and thermal residual

stresses in [0°/90°] composites.[67] In other compositions, microcracking was mitigated

by employing an inert interfacial BN coating on the SiC fiber surfaces.

The effect of the interfacial coating on mechanical behavior and performance was

observed in the specimens tested in this study. The interfacial coating on Sylramic iBN

fiber degraded during processing, resulting in strong bonding at the fiber-matrix

interface. The strong bonding inhibited load transfer to the fibers and enhanced the effect

of thermal residual stresses. The in-situ BN coating of Sylramic iBN fibers was <50 nm.

Subsequently, composites were prepared with Hi-Nicalon fibers with a 0.2 µm thick Si

doped BN coating. Coating composition and thickness were chosen to maximize

mechanical debond characteristics and high temperature environmental stability while

maintaining flexibility.[68] As shown in Fig. 5, Z10S-Hi(BN)$_{0°}$ and Z10S-Hi(BN)$_{0°/90°}$

had similar strengths at ~260 MPa. The bidirectional Z10S-Hi(BN)$_{0°/90°}$ composites

exhibited a smaller standard deviation in strength ($\pm$19 vs. $\pm$69 MPa), presumably due to the presence of the transverse 90° fiber tows acting as a consistent critical flaw.[69] As the Z10S-Hi(BN)$_{0°}$ material loads, individual fibers and bundles begin to see increased tensile stress and fail independently without allowing the crack to propagate unimpeded through the specimen. This behavior is consistent with expectation while employing a sufficiently thick interfacial coating, where load transfer to the fiber is desired.[26] Following initial matrix cracking, the Z10S-Hi(BN)$_{0°}$ composites showed graceful failure with significant load retention after the onset of matrix cracking and strains at failure of more than 1%.

The inelastic work of fracture for Z10S matrix composites was highly dependent on fiber architecture and type. Inelastic work of fracture was calculated from the cross-sectional area of the bar and summation of the area under the load-deflection curves (i.e. load and displacement were recorded in 10 millisecond intervals). Both Z10S-Syl$_{0°/90°}$ and Z10S-Hi(BN)$_{0°/90°}$ exhibited the lowest work of fracture of the composites studied at 0.7 and 0.6 kJ$\cdot$m^{-2} respectively. Despite the bidirectional composite specimens high strain at failure, the peak load was significantly reduced resulting in reduced work of fracture. Alternatively, unidirectional composites retained higher strength and displayed increased work of fracture. In light of Z10S-Hi$_{0°}$ composite specimens' tendency to fail catastrophically, the work of fracture from the linear-elastic regions are simply offered for comparison. Z10S-Syl$_{0°}$ specimens displayed an increase in average work of fracture at 2.1 kJ$\cdot$m^{-2} after large initial failures at ~500 MPa and reloading. The presence of the interfacial BN coating on Z10S-Hi(BN)$_{0°}$ composite specimens assisted in load transfer from the matrix to the fiber, improved matrix crack deflection, and dissipated energy

during failure, effectively increasing inelastic work of fracture. Z10S-Hi(BN)$_{0°}$ specimens had an average work of fracture of 3.5 kJ·m^{-2}. This is a significant improvement (~3X increase) compared to Z10S-Hi$_{0°}$ composites lacking interfacial coating.

4. CONCLUSIONS

ZrB_2-$ZrSi_2$ matrix composites reinforced with various grades of continuous SiC fiber were fabricated and tested. A nominal matrix composition consisting of 90 vol% ZrB_2 and 10 vol% $ZrSi_2$ was determined to maximize matrix densification and minimize fiber-matrix interaction. While a 20 vol % $ZrSi_2$ addition to ZrB_2 yielded sufficiently dense matrix phases (>96% relative density), significant fiber degradation was observed using CG-Nicalon and Hi-Nicalon fibers. $ZrSi_2$ concentrations of 10 vol% in ZrB_2 showed greater than 95% matrix density while incorporating a continuous SiC fiber reinforcement. SiC fiber reinforcement decreased the ultimate flexural strength for all composites examined but increased strain to failure and increased work of fracture. Minimization of fiber-matrix interaction was accomplished by utilizing an inert 0.2 μm BN(Si) coating applied by CVD. Alternatively, an in-situ BN coating provided by nitrogen atmosphere heat treatment of boron-doped SiC fiber (i.e. Sylramic iBN fiber) proved insufficient to prevent appreciable fiber-matrix interdiffusion at the processing temperature of 1400°C. Z10S-Hi$_{0°}$ composites reinforced with uncoated Hi-Nicalon fiber displayed brittle fracture at peak stresses. Z10S-Syl$_{0°}$ composites utilizing Sylramic iBN fiber and a thin (i.e. <50 nm) BN interfacial coating had the highest strength at ~500 MPa but the lowest strain to failure at ~0.2%. Z10S-Syl$_{0°/90°}$ showed the most significant reduction in strength at 78 MPa, attributed to strong bonding at the fiber-matrix interface

and subsequent spontaneous matrix cracking. Z10S-Hi(BN)$_{0°/90°}$ and Z10S-Hi(BN)$_{0°}$ composites had ~260 MPa max flexural strength. A 0.2 μm thick BN interphase coating provided significant protection to Hi-Nicalon fibers in composites hot pressed at 1400°C, allowing for increased global load sharing behavior between the fibers and the matrix. Z10S-Hi(BN)$_{0°/90°}$ showed some evidence of non-catastrophic failure, but the presence of a weak interphase in 90° plies limited non-brittle failure mechanisms. Z10S-Hi(BN)$_{0°}$ displayed the most compelling combination of ultimate flexure strength at ~260 MPa, high strain to failure (>1%), and increased work of fracture at 3.5 kJ·m^{-2}.

ACKNOWLEDGEMENTS

REFERENCES

[1] A. L. Chamberlain, W. G. Fahrenholtz, G. Hilmas, and D. T. Ellerby, "Oxidation of ZrB$_2$-SiC Ceramics under Atmospheric and Reentry Conditions," *Refractories App. Trans.,* **1**[2] 2-8 (2004).

[2] A. L. Chamberlain, W. G. Fahrenholtz, G. E. Hilmas, and D. T. Ellerby, "High-Strength Zirconium Diboride-Based Ceramics," *J. Am. Ceram. Soc.,* **87**[6] 1170-2 (2004).

[3] W. G. Fahrenholtz, G. E. Hilmas, I. G. Talmy, and J. A. Zaykoski, "Refractory Diborides of Zirconium and Hafnium," *J. Am. Ceram. Soc.,* **90**[5] 1347-64 (2007).

[4] X. Zhang, P. Hu, J. Han, and S. Meng, "Ablation Behavior of ZrB$_2$–SiC Ultra High Temperature Ceramics under Simulated Atmospheric Re-Entry Conditions," *Compos. Sci. Technol.,* **68**[7–8] 1718-26 (2008).

[5] J. W. Zimmermann, G. E. Hilmas, W. G. Fahrenholtz, R. B. Dinwiddie, W. D. Porter, and H. Wang, "Thermophysical Properties of ZrB$_2$ and ZrB$_2$–SiC Ceramics," *J. Am. Ceram. Soc.,* **91**[5] 1405-11 (2008).

[6] H. Kinoshita, S. Otani, S. Kamiyama, H. Amano, I. Akasaki, J. Suda, and H. Matsunami, "Zirconium Diboride (0001) as an Electrically Conductive Lattice-Matched Substrate for Gallium Nitride," *Jpn. J. Appl. Phys.,* **40** L1280-L2 (2001).

[7] M. Rahman, C. C. Wang, W. Chen, S. A. Akbar, and C. Mroz, "Electrical Resistivity of Titanium Diboride and Zirconium Diboride," *J. Am. Ceram. Soc.,* **78**[5] 1380-2 (1995).

[8] S. K. Mishra, S. Das, S. K. Das, and P. Ramachandrarao, "Sintering Studies on Ultrafine ZrB$_2$ Powder Produced by a Self-Propagating High-Temperature Synthesis Process," *J. Mater. Res.,* **15** 2499-504 (2000).

[9] J. W. Zimmermann, G. E. Hilmas, and W. G. Fahrenholtz, "Thermal Shock Resistance of ZrB$_2$ and ZrB$_2$–30% SiC," *Mater. Chem. Phys.,* **112**[1] 140-5 (2008).

[10] F. Lamouroux, S. Bertrand, R. Pailler, R. Naslain, and M. Cataldi, "Oxidation-Resistant Carbon-Fiber-Reinforced Ceramic-Matrix Composites," *Compos. Sci. Technol.,* **59**[7] 1073-85 (1999).

[11] K. Nakano, A. Kamiya, Y. Nishino, T. Imura, and T.-W. Chou, "Fabrication and Characterization of Three-Dimensional Carbon Fiber Reinforced Silicon Carbide and Silicon Nitride Composites," *J. Am. Ceram. Soc.,* **78**[10] 2811-4 (1995).

[12] Y. Zhu, Z. Huang, S. Dong, M. Yuan, and D. Jiang, "Manufacturing 2D Carbon-Fiber-Reinforced SiC Matrix Composites by Slurry Infiltration and PIP Process," *Ceram. Int.,* **34**[5] 1201-5 (2008).

[13] S. Zhu, M. Mizuno, Y. Nagano, J. Cao, Y. Kagawa, and H. Kaya, "Creep and Fatigue Behavior in an Enhanced SiC/SiC Composite at High Temperature," *J. Am. Ceram. Soc.,* **81**[9] 2269-77 (1998).

[14] G. Morscher, P. Pirouz, and A. H. Heuer, "Temperature Dependence of Interfacial Shear Strength in SiC-Fiber-Reinforced Reaction-Bonded Silicon Nitride," *J. Am. Ceram. Soc.,* **73**[3] 713-20 (1990).

[15] W.-Z. Zhang, Y. Zeng, L. Gbologah, X. Xiong, and B.-Y. Huang, "Preparation and Oxidation Property of ZrB_2-$MoSi_2$/SiC Coating on Carbon/Carbon Composites," *T. Nonferr. Metal Soc.,* **21**[7] 1538-44 (2011).

[16] S. Guo and Y. Kagawa, "Tensile Fracture Behavior of Continuous SiC Fiber-Reinforced SiC Matrix Composites at Elevated Temperatures and Correlation to in Situ Constituent Properties," *J. Eur. Ceram. Soc.,* **22**[13] 2349-56 (2002).

[17] D. Singh, J. P. Singh, and M. J. Wheeler, "Mechanical Behavior of SiC(F)/SiC Composites and Correlation to in Situ Fiber Strength at Room and Elevated Temperatures," *J. Am. Ceram. Soc.,* **79**[3] 591-6 (1996).

[18] J. J. Brennan, "Interfacial Characterization of a Slurry-Cast Melt-Infiltrated SiC/SiC Ceramic-Matrix Composite," *Acta Mater.,* **48**[18–19] 4619-28 (2000).

[19] J. A. DiCarlo, H. M. Yun, and J. B. Hurst, "Fracture Mechanisms for SiC Fibers and SiC/SiC Composites under Stress-Rupture Conditions at High Temperatures," *Applied Mathematics and Computation,* **152**[2] 473-81 (2004).

[20] T. Mah, M. G. Mendiratta, A. P. Katz, R. Ruh, and K. S. Mazdiyasni, "Room-Temperature Mechanical Behavior of Fiber-Reinforced Ceramic-Matrix Composites," *J. Am. Ceram. Soc.,* **68**[1] C-27-C-30 (1985).

[21] F. E. Heredia, S. M. Spearing, A. G. Evans, P. Mosher, and W. A. Curtin, "Mechanical Properties of Continuous-Fiber-Reinforced Carbon Matrix Composites and Relationships to Constituent Properties," *J. Am. Ceram. Soc.,* **75**[11] 3017-25 (1992).

[22] S. Tang, J. Deng, W. Liu, and K. Yang, "Mechanical and Ablation Properties of 2D-Carbon/Carbon Composites Pre-Infiltrated with a SiC Filler," *Carbon,* **44**[14] 2877-82 (2006).

[23] D. Cho and B. Il Yoon, "Microstructural Interpretation of the Effect of Various Matrices on the Ablation Properties of Carbon-Fiber-Reinforced Composites," *Compos. Sci. Technol.,* **61**[2] 271-80 (2001).

[24] J. Yin, X. Xiong, H. Zhang, and B. Huang, "Microstructure and Ablation Performances of Dual-Matrix Carbon/Carbon Composites," *Carbon,* **44**[9] 1690-4 (2006).

[25] F. E. Heredia, J. C. McNulty, F. W. Zok, and A. G. Evans, "Oxidation Embrittlement Probe for Ceramic-Matrix Composites," *J. Am. Ceram. Soc.,* **78**[8] 2097-100 (1995).

[26] R. E. Tressler, "Recent Developments in Fibers and Interphases for High Temperature Ceramic Matrix Composites," *Composites Part A: Applied Science and Manufacturing,* **30**[4] 429-37 (1999).

[27] R. R. Naslain, "SiC-Matrix Composites: Nonbrittle Ceramics for Thermo-Structural Application," *Int. J. Appl. Ceram. Tec.,* **2**[2] 75-84 (2005).

[28] Q.-G. Fu, H.-J. Li, X.-H. Shi, K.-Z. Li, and G.-D. Sun, "Silicon Carbide Coating to Protect Carbon/Carbon Composites against Oxidation," *Scripta Mater.,* **52**[9] 923-7 (2005).

[29] B. Schneider, A. Guette, R. Naslain, M. Cataldi, and A. Costecalde, "A Theoretical and Experimental Approach to the Active-to-Passive Transition in the Oxidation of Silicon Carbide: Experiments at High Temperatures and Low Total Pressures," *J. of Mater. Sci.,* **33**[2] 535-47 (1998).

[30] H. Hatta, T. Aoki, Y. Kogo, and T. Yarii, "High-Temperature Oxidation Behavior of SiC-Coated Carbon Fiber-Reinforced Carbon Matrix Composites," *Composites Part A: Applied Science and Manufacturing,* **30**[4] 515-20 (1999).

[31] W. L. Vaughn and H. G. Maahs, "Active-to-Passive Transition in the Oxidation of Silicon Carbide and Silicon Nitride in Air," *J. Am. Ceram. Soc.,* **73**[6] 1540-3 (1990).

[32] M. J. H. Balat, "Determination of the Active-to-Passive Transition in the Oxidation of Silicon Carbide in Standard and Microwave-Excited Air," *J. Eur. Ceram. Soc.,* **16**[1] 55-62 (1996).

[33] M. M. Opeka, I. G. Talmy, and J. A. Zaykoski, "Oxidation-Based Materials Selection for 2000°C + Hypersonic Aerosurfaces: Theoretical Considerations and Historical Experience," *J. of Mater. Sci.,* **39**[19] 5887-904 (2004).

[34] F. Monteverde and L. Scatteia, "Resistance to Thermal Shock and to Oxidation of Metal Diborides–SiC Ceramics for Aerospace Application," *J. Am. Ceram. Soc.,* **90**[4] 1130-8 (2007).

[35] D. Sciti, M. Brach, and A. Bellosi, "Oxidation Behavior of a Pressureless Sintered ZrB_2–$MoSi_2$ Ceramic Composite," *J. Mater. Res.,* **20**[4] 922-30 (2005).

[36] D. Sciti, M. Brach, and A. Bellosi, "Long-Term Oxidation Behavior and Mechanical Strength Degradation of a Pressurelessly Sintered ZrB_2–$MoSi_2$ Ceramic," *Scripta Mater.,* **53**[11] 1297-302 (2005).

[37] K. L. Luthra, "Thermochemical Analysis of the Stability of Continuous "SiC" Fibers," *J. Am. Ceram. Soc.,* **69**[10] C-231-C-3 (1986).

[38] T. Mah, N. L. Hecht, D. E. McCullum, J. R. Hoenigman, H. M. Kim, A. P. Katz, and H. A. Lipsitt, "Thermal Stability of SiC Fibres (Nicalon)," *J. of Mater. Sci.,* **19**[4] 1191-201 (1984).

[39] S. M. Johnson, R. D. Brittain, R. H. Lamoreaux, and D. J. Rowcliffe, "Degradation Mechanisms of Silicon Carbide Fibers," *J. Am. Ceram. Soc.,* **71**[3] C-132-C-5 (1988).

[40] T. J. Clark, R. M. Arons, J. B. Stamatoff, and J. Rabe, "Thermal Degradation of Nicalon SiC Fibers," *Proceedings of the 9th Annual Conference on Composites and Advanced Ceramic Materials: Ceramic Engineering and Science Proceedings,* **6**[7-8] 576-88 (1985).

[41] D. J. Pysher, K. C. Goretta, R. S. Hodder, and R. E. Tressler, "Strengths of Ceramic Fibers at Elevated Temperatures," *J. Am. Ceram. Soc.,* **72**[2] 284-8 (1989).

[42] S. C. Zhang, G. E. Hilmas, and W. G. Fahrenholtz, "Pressureless Densification of Zirconium Diboride with Boron Carbide Additions," *J. Am. Ceram. Soc.,* **89**[5] 1544-50 (2006).

[43] W. G. Fahrenholtz, G. E. Hilmas, S. C. Zhang, and S. Zhu, "Pressureless Sintering of Zirconium Diboride: Particle Size and Additive Effects," *J. Am. Ceram. Soc.,* **91**[5] 1398-404 (2008).

[44] M. J. Thompson, W. G. Fahrenholtz, and G. E. Hilmas, "Elevated Temperature Thermal Properties of ZrB_2 with Carbon Additions," *J. Am. Ceram. Soc.,* **95**[3] 1077-85 (2012).

[45] J. Watts, G. Hilmas, and W. G. Fahrenholtz, "Mechanical Characterization of ZrB_2–SiC Composites with Varying SiC Particle Sizes," *J. Am. Ceram. Soc.,* **94**[12] 4410-8 (2011).

[46] L. Silvestroni and D. Sciti, "Oxidation of ZrB_2 Ceramics Containing SiC as Particles, Whiskers, or Short Fibers," *J. Am. Ceram. Soc.,* **94**[9] 2796-9 (2011).

[47] F. Monteverde and A. Bellosi, "Effect of the Addition of Silicon Nitride on Sintering Behaviour and Microstructure of Zirconium Diboride," *Scripta Mater.,* **46**[3] 223-8 (2002).

[48] F. Monteverde, S. Guicciardi, and A. Bellosi, "Advances in Microstructure and Mechanical Properties of Zirconium Diboride Based Ceramics," *Mater. Sci. Eng., A,* **346**[1–2] 310-9 (2003).

[49] S.-Q. Guo, Y. Kagawa, T. Nishimura, and H. Tanaka, "Pressureless Sintering and Physical Properties of ZrB_2-Based Composites with $ZrSi_2$ Additive," *Scripta Mater.,* **58**[7] 579-82 (2008).

[50] S.-Q. Guo, Y. Kagawa, and T. Nishimura, "Mechanical Behavior of Two-Step Hot-Pressed ZrB_2-Based Composites with $ZrSi_2$," *J. Eur. Ceram. Soc.,* **29**[4] 787-94 (2009).

[51] O. N. Grigoriev, B. A. Galanov, V. A. Kotenko, S. M. Ivanov, A. V. Koroteev, and N. P. Brodnikovsky, "Mechanical Properties of ZrB_2-SiC($ZrSi_2$) Ceramics," *J. Eur. Ceram. Soc.,* **30**[11] 2173-81 (2010).

[52] O. N. Grigoriev, B. A. Galanov, V. A. Lavrenko, A. D. Panasyuk, S. M. Ivanov, A. V. Koroteev, and K. G. Nickel, "Oxidation of ZrB_2–SiC–$ZrSi_2$ Ceramics in Oxygen," *J. Eur. Ceram. Soc.,* **30**[11] 2397-405 (2010).

[53] B. Lai, J. Watts, G. Hilmas, and W. G. Fahrenholtz, "Placeholder Reference for Future Publication (ZrB_2 Hot Pressed with $ZrSi_2$ Additions)," *J. Eur. Ceram. Soc.* (2013).

[54] A. G. Evans, F. W. Zok, and J. Davis, "The Role of Interfaces in Fiber-Reinforced Brittle Matrix Composites," *Compos. Sci. Technol.,* **42**[1–3] 3-24 (1991).

[55] L. S. Sigl and A. G. Evans, "Effects of Residual Stress and Frictional Sliding on Cracking and Pull-out in Brittle Matrix Composites," *Mech. Mater.,* **8**[1] 1-12 (1989).

[56] D. B. Marshall, "Analysis of Fiber Debonding and Sliding Experiments in Brittle Matrix Composites," *Acta Metallurgica et Materialia,* **40**[3] 427-41 (1992).

[57] T. A. Parthasarathy, D. B. Marshall, and R. J. Kerans, "Analysis of the Effect of Interfacial Roughness on Fiber Debonding and Sliding in Brittle Matrix Composites," *Acta Metallurgica et Materialia,* **42**[11] 3773-84 (1994).

[58] D. B. Marshall and A. G. Evans, "Failure Mechanisms in Ceramic-Fiber/Ceramic-Matrix Composites," *J. Am. Ceram. Soc.,* **68**[5] 225-31 (1985).

[59] M. D. Thouless, "Frictional Sliding and Pull-out of a Fibre," *Scripta Metallurgica et Materialia,* **27**[9] 1211-4 (1992).

[60] Y. Touloukian, C. Ho, and D. Dewitt, "Thermal Expansion: Nonmetallic Solids," **Vol. 13**, IFI/Plenum, New York, 1970.

[61] Y. Okada and Y. Tokumaru, "Precise Determination of Lattice Parameter and Thermal Expansion Coefficient of Silicon between 300 and 1500 K " *J. Appl. Phys.,* **56**[2] 314-20 (1984).

[62] I. Engstrom and B. Lonnberg, "Thermal Expansion Studies of the Group IV-VII Transition Metal Disilicides," *J. Appl. Phys.,* **63**[9] 4476-84 (1988).

[63] R. N. Patil, "Axial Thermal Expansion of ZrO_2 and HfO_2 in the Range Room Temperature to 1400°C," *J. Appl. Crystallogr.,* **2** 281-8 (1969).

[64] E. C. Subbarao, D. K. Agrawal, H. A. McKinstry, C. W. Sallese, and R. Roy, "Thermal Expansion of Compounds of Zircon Structure," *J. Am. Ceram. Soc.,* **73**[5] 1246-52 (1990).

[65] J. Watts, G. Hilmas, W. G. Fahrenholtz, D. Brown, and B. Clausen, "Stress Measurements in ZrB_2–SiC Composites Using Raman Spectroscopy and Neutron Diffraction," *J. Eur. Ceram. Soc.,* **30**[11] 2165-71 (2010).

[66] J. Watts, G. Hilmas, W. G. Fahrenholtz, D. Brown, and B. Clausen, "Measurement of Thermal Residual Stresses in ZrB_2–SiC Composites," *J. Eur. Ceram. Soc.,* **31**[9] 1811-20 (2011).

[67] D. S. Beyerle, S. M. Spearing, and A. G. Evans, "Damage Mechanisms and the Mechanical Properties of a Laminated 0/90 Ceramic/Matrix Composite," *J. Am. Ceram. Soc.,* **75**[12] 3321-30 (1992).

[68] G. S. Corman and K. L. Luthra, "Silicon-Doped Boron Nitride Coated Fibers in Silicon Melt Infiltrated Composites," U. S. Patent, 5952100, 1999.

[69] J. Wachtman, "Mechanical Properties of Ceramics," John Wiley & Sons, Inc., New York, 1996.

Table I. Representative Composition of Organic Solvent Tape Casting Slurries

Role	Compound	Vol%
Powder	ZrB_2-10vol% $ZrSi_2$	19.85
Solvent	60:40 mixture of MEK:EtOH	63.88
Dispersant	BYK-110	0.09
Binder	Polyvinyl butyral (B-79)	8.36
Plasticizer 1	Benzyl butyl phthalate (Santicizer, S160)	4.98
Plasticizer 2	Polyethylene glycol (PEG 400)	2.84

Table II. Mechanical Properties of Selected ZrB_2 Matrix Composites Hot Pressed at 1400°C.

Composite	Fiber	Architecture	Elastic Modulus (GPa)	Max Flexure Stress (MPa)	Work of Fracture $(kJ \cdot m^{-2})$
Z10S	-	-	486 ± 13	543 ± 82	-
Z20S-CG$_{PW}$	CG-Nicalon	Plain Weave	-	-	-
Z10S-Hi$_{0°}$	Hi-Nicalon	Unidirectional	415 ± 29	414 ± 49	1.2 ± 0.3
Z10S-Syl$_{0°}$	Sylramic iBN	Unidirectional	378 ± 22	498 ± 79	2.1 ± 1.0
Z10S-Syl$_{0°/90°}$	Sylramic iBN	[0°/90°]	-	78 ± 15	0.7 ± 0.1
Z10S-Hi(BN)$_{0°}$	BN(Si) Coated Hi-Nicalon	Unidirectional	365 ± 36	264 ± 69	3.5 ± 0.8
Z10S-Hi(BN)$_{0°/90°}$	BN(Si) Coated Hi-Nicalon	[0°/90°]	411 ± 11	259 ± 19	0.6 ± 0.1

Schematic unidirectional layup

ZrB$_2$-ZrSi$_2$ slurry
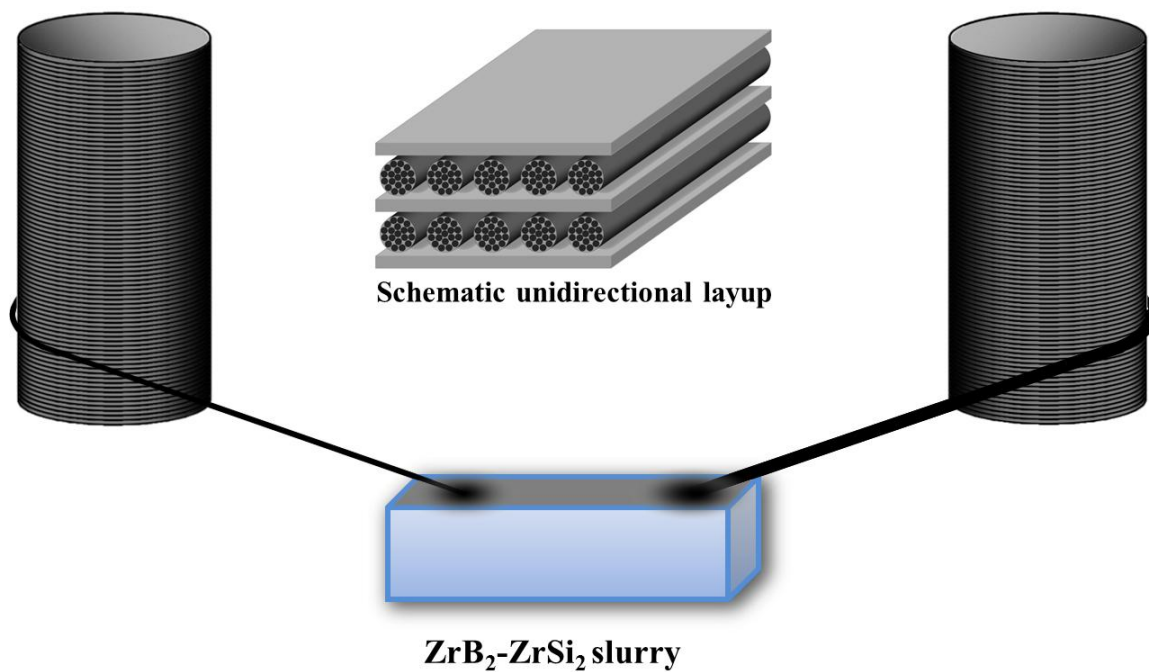
Fig. 1. Schematic representation of continuous fiber tow coating/infiltration with ceramic slurry. Representative unidirectional architecture with interpenetrating tape layers is also presented.
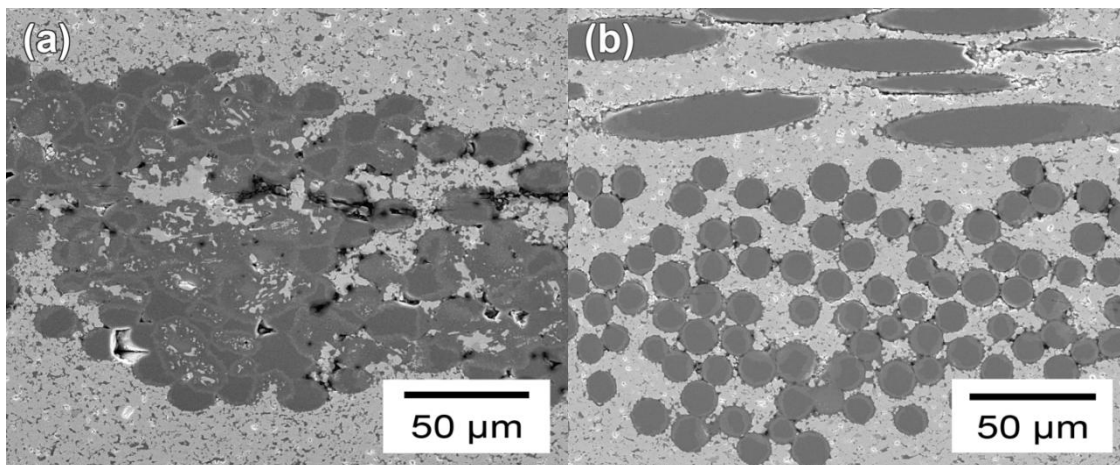
Fig. 2. ZrB$_2$-20vol% ZrSi$_2$ matrix (Z20S-A) with (a) CG-Nicalon and (b) Sylramic iBN fibers incorporated and hot-pressed at 1600°C. A significant amount of degradation was observed in CG-Nicalon fibers.
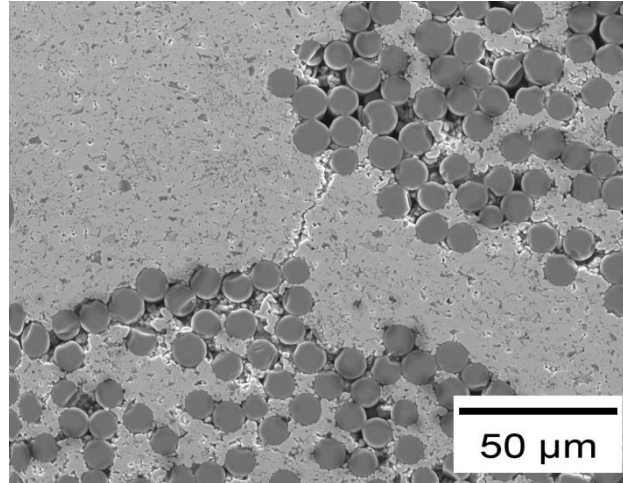
Fig. 3. Representative microstructure of Z10S-Syl$_{0°/90°}$ composite showing microcracking.
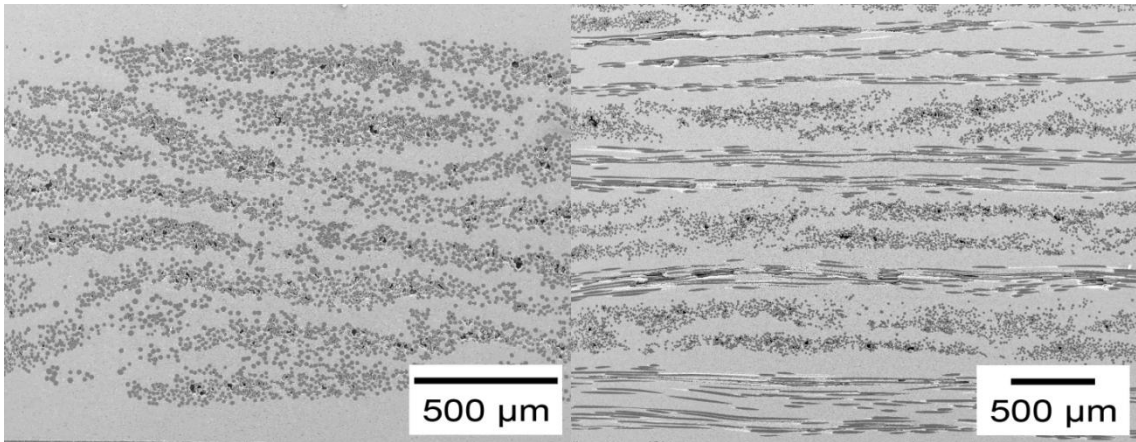
Fig. 4. Representative microstructure of Z10S-Hi(BN)$_{0°}$ and Z10S-Hi(BN)$_{0°/90°}$ composites showing improved fiber loading and good slurry penetration.
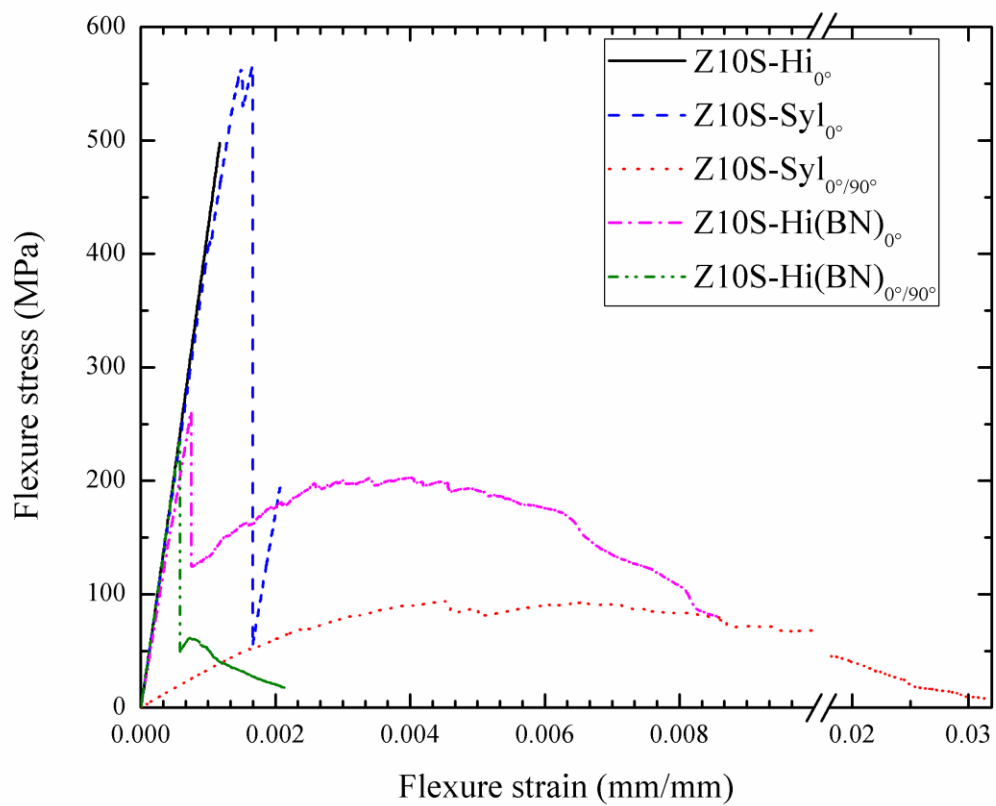
Fig. 5. Representative stress-strain curves for selected composite compositions utilizing Z10S matrix.

SECTION

3.   SUMMARY AND CONCLUSIONS

3.1   SUMMARY OF RESULTS

The densification, microstructure, and mechanical properties of zirconium diboride-zirconium disilicide ceramics were studied. Two studies were presented in the form of manuscripts for technical journal submission. The first paper summarizes the densification, microstructural evolution, and mechanical properties of ZrB_2 containing 5, 7.5, 10, and 20 vol% $ZrSi_2$. The second paper focuses on investigation of mechanical behavior of ZrB_2-$ZrSi_2$ ceramics reinforced with different grades of commercially available continuous SiC fiber. While the first paper is concerned with investigating the feasibility of processing a ZrB_2-based ceramic at temperatures below 1600°C, the second paper demonstrates the compatibility of the ZrB_2-$ZrSi_2$ matrix with a number of continuous SiC fiber types. In this section, the conclusions for both papers are summarized, along with overall conclusions for the thesis.

3.1.1   Paper I: Densification, Microstructure, and Properties of Hot-Pressed ZrB_2-$ZrSi_2$ Ceramics. ZrB_2 ceramics containing 5, 7.5, 10, and 20 vol% $ZrSi_2$ were hot pressed to near theoretical density and analyzed. The densification behavior, microstructure, and mechanical properties were determined to be a function of nominal $ZrSi_2$ content. Relative densities were greater than 96% for ZrB_2 containing greater than 7.5 vol% $ZrSi_2$ after hot pressing at 1400°C or 1600°C. XRD analysis revealed the presence of oxide impurities in the starting $ZrSi_2$ powder. Phase analysis, based on addition of elemental Si, estimated the formation of 4.7 to 12.8 vol% liquid in ZrB_2-$ZrSi_2$ ceramics at 1400°C. Further analysis after high temperature treatment of the starting

"ZrSi$_2$" powder revealed that additional ZrSi$_2$ is formed at 1400°C. Densification is achieved by reaction of surface oxides on starting powders, ductility of ZrSi$_2$ at elevated temperature, as well as Si wetting of ZrB$_2$ to lubricate and aid in the rearrangement of grains during hot pressing. Elastic modulus values for the ZrB$_2$-ZrSi$_2$ ceramics ranged from 440 GPa to 490 GPa, where the only markedly reduced modulus was for ZrB$_2$ containing 20 vol% ZrSi$_2$. ZrB$_2$ containing 7.5 vol% ZrSi$_2$ was found to have the best combination of increased densification at 1600°C and below, along with high strength at 750 MPa. Increased ZrSi$_2$ content yielded slightly increased densification at 1400°C or 1600°C, but was accompanied by decreased hardness, elastic modulus, and flexure strength.

3.1.2 Paper II: ZrB$_2$-ZrSi$_2$ Matrix Composites Reinforced with Continuous SiC Fiber.

ZrB$_2$-ZrSi$_2$ matrix composites reinforced with different grades of SiC fiber were fabricated and tested. Microstructural features and mechanical behavior were evaluated. While 20 vol% ZrSi$_2$ provided a sufficiently dense matrix phase when hot pressed at 1600°C, significant thermal degradation of CG-Nicalon and Hi-Nicalon fibers were observed. A composite consisting of a matrix with 90 vol% ZrB$_2$ and 10 vol% ZrSi$_2$, while incorporating 15 to 20 vol% SiC fiber, achieved a relative density of >96% when hot pressed at 1400°C. The ultimate flexural strength was reduced for composites incorporating continuous SiC fiber, but significantly increased strain to failure (up to 3%). The fibers containing no interfacial coating between the fibers and the matrix displayed the highest relative ultimate flexural strength (~415 MPa for unidirectional Hi-Nicalon and ~500 MPa for unidirectional Sylramic), but evidence of crack deflection, bridging, and branching were not observed to the same degree for composites containing

a 0.2 μm BN coating. This behavior was attributed to strong bonding at the fiber-matrix interface, which inhibited load transfer to the fiber, enhancing the effect of thermal residual stresses, and limiting crack deflection. Composites with a BN interphase coating displayed the most beneficial combination of increased strain to failure, pseudo-ductile failure, and a higher retained strength (i.e. ~260 MPa). Specifically, unidirectional BN coated Hi-Nicalon in a ZrB_2-10 vol% $ZrSi_2$ matrix displayed significant load retention beyond the proportional limit with strains at failure of more than 1%.

3.2   OVERALL CONCLUSIONS

ZrB_2 incorporating a $ZrSi_2$ based additive as a sintering aid allows the ultra-high temperature ceramic to be densified at significantly reduced temperatures ($\leq 1600°C$), which increases its applicability to densification of CMCs that incorporate SiC fibers. As part of this research, it was shown that decreasing the processing temperature of ZrB_2 allows for incorporation of high strength SiC fibers without visible degradation. While 7.5 vol% $ZrSi_2$ in ZrB_2 provides the highest strength (~750 MPa) for a monolithic material, there is inadequate increased sintering for systems that incorporate rigid, fully dense fibers. Therefore, to adequately densify a ZrB_2-$ZrSi_2$ matrix at 1400°C by hot pressing, 10 vol% $ZrSi_2$ additions were needed. Fabrication of ZrB_2-$ZrSi_2$ matrix composites incorporating SiC fibers was demonstrated with varying degrees of success. Incorporation of uncoated Hi-Nicalon and Sylramic iBN fibers yielded the highest relative strengths, but composite global load sharing between the fiber and matrix was significantly reduced. Utilization of an inert interphase coating was necessary to facilitate this behavior. Further, a 0.2 μm thick BN interphase was found to be sufficient for mitigation of the CTE mismatch between the SiC fiber and the ZrB_2-$ZrSi_2$ matrix,

preventing spontaneous microcracking. The significant load retention beyond the proportional limit observed for these composites results in increased reliability and toughness, but at the cost of reduced apparent flexure strength.

Key Technical Questions Addressed By This Research

Several technical questions were presented in the Introduction of this thesis. The body of the thesis, composed of manuscripts for technical journal submission, addresses these questions. The answers to the technical questions are summarized as follows.

1. *How does $ZrSi_2$ affect the densification and mechanical properties of monolithic ZrB_2 with varying processing temperatures?*

   ZrB_2 was densified by hot pressing with addition of $ZrSi_2$. $ZrSi_2$ contents between 7.5 vol% and 20 vol% increased relative density of ZrB_2 when hot pressed at 1400°C or 1600°C. Increasing $ZrSi_2$ content increased the relative density and increased densification rates. Ceramics containing between 7.5 vol% and 20 vol% $ZrSi_2$ achieved >96% relative density by hot pressing at 1400°C or 1600°C for one hour. ZrB_2 containing 20 vol% $ZrSi_2$ yielded the highest relative density (~98%). However, increasing the $ZrSi_2$ content reduced strength, hardness, and elastic modulus. For example, ZrB_2 containing 7.5 vol% $ZrSi_2$ had a strength of ~750 MPa, while a 20 vol% addition reduced strength to ~390 MPa. Hardness was reduced from phase pure ZrB_2 (~22 GPa) and shown to decrease with increasing $ZrSi_2$ addition with values ranging from 15 GPa to 16 GPa for all ZrB_2-$ZrSi_2$ ceramics. The addition of $ZrSi_2$ in small volume fractions (7.5 to 10 vol%) increases the densification of ZrB_2 at 1400°C or 1600°C without significant decrease to flexure strength.

2. *How does continuous SiC fiber reinforcement affect the mechanical properties of ZrB$_2$ based composites?*

Incorporation of continuous SiC fiber decreases apparent peak flexure strength, but increases non-brittle strain to failure. Specifically, Hi-Nicalon SiC fiber additions were shown to decrease the peak flexure strength to ~415 MPa compared to the ZrB$_2$-10 vol% ZrSi$_2$ matrix at ~545 MPa. Further, Sylramic iBN SiC fiber additions, aligned unidirectionally, resulted in a decrease in strength to ~500 MPa. When continuous SiC fiber was well bonded to the matrix the relative reductions to strength could be attributed to the fiber diameter and distribution. The Hi-Nicalon fiber has a diameter of 12-14 µm, while Sylramic iBN is more consistent at ~10 µm. Flexure strength is most likely controlled by the presence of pores resulting from incomplete infiltration of the fiber tows, as dictated by fiber diameter. Therefore, higher strengths are observed for a smaller diameter and narrower distributions of fiber. Composites incorporating BN coated Hi-Nicalon are understandably more complex. Failure is likely still controlled by pores acting as stress risers, but is now enhanced by the presence of an interconnected weaker BN phase on fiber surfaces. High strength and toughness are achievable when incorporating continuous SiC fiber, but residual porosity and fibers that are well bonded, or not adequately dispersed, reduce the apparent peak flexure strength.

3. *What is the effect of different commercially available SiC fiber types, as well as interface coatings, on mechanical performance?*

Several commercially available fibers were able to be incorporated into an ultra-high temperature ZrB$_2$ matrix with varying degrees of success. Incorporation of

CG-Nicalon was incompatible in a ZrB_2-$ZrSi_2$ matrix hot pressed at 1400°C or 1600°C, which led to significant fiber degradation. This is not unexpected due to the high relative oxygen content (~12 wt%) of CG-Nicalon, and its observed reduced stability and mechanical performance above 1000°C, as shown by other studies. ZrB_2-$ZrSi_2$ matrix composites were also fabricated with either Hi-Nicalon or Sylramic iBN fibers in both unidirectional and bidirectional architectures. Apparent flexure strength and failure behavior was dependent on fiber type and architecture. Unidirectional composites using all fiber types displayed higher strengths (~260 MPa to ~500 MPa) compared to bidirectional composites (~80 MPa to ~260 MPa). Unidirectional Hi-Nicalon composites containing 0.2 μm thick BN interphases displayed the greatest strain to failure (~1%) while maintaining higher strength (~260 MPa). Additionally, these composites exhibited the highest work of fracture at 3.5 kJ/m^2. In contrast, Sylramic iBN fiber containing composites were comparatively brittle, and a bidirectional architecture yielded a significantly reduced strength (~80 MPa). This was attributed to an insufficient in-situ BN interphase thickness (< 50 nm) in these composites. Further, interdiffusion of the fiber and matrix was shown to be enhanced, leading to decreased fiber pullout. The thinner coating also limited accommodation of thermal misfit stresses, enhancing tensile stresses in the ZrB_2-$ZrSi_2$ matrix surrounding fibers and ultimately led to microcracking. It is clear that reliable ultra-high temperature composites must contain high strength, high temperature stable fibers, but also a sufficiently thick, weak inert interphase coating to allow for composite toughening mechanisms.

The research presented in this thesis is a systematic study in developing a process to incorporate high strength SiC fibers into a ZrB_2-based matrix. The work presented can be separated into two parts which detail the necessary processing challenges, testing, and characterization. First, the densification of ZrB_2 at temperatures $\leq 1600°C$ was accomplished by utilizing $ZrSi_2$ and its effect on mechanical properties was determined. The results suggest a trade-off between $ZrSi_2$ minimization to retain mechanical performance, while maintaining sufficient amounts to promote densification. Second, incorporation of various SiC fibers is made possible in a ZrB_2-$ZrSi_2$ matrix. Incorporation of $ZrSi_2$ into ZrB_2 ensures that densification temperatures are sufficiently low and do not cause significant degradation in SiC fibers. Additionally, while a ZrB_2-based matrix is not ideal for SiC fiber reinforcement, the mechanical performance lends to improved composite behavior and graceful failure.

4. RECOMMENDATIONS FOR FUTURE WORK

The goal of the research presented in this thesis was to investigate the effects of $ZrSi_2$ addition on the densification and mechanical properties of ZrB_2, as well as ZrB_2 with a continuous SiC fiber reinforcement. Microstructural evolution and mechanical behavior were characterized. During the course of this research, a number of key questions were identified that can be addressed in future research.

1. The effect of phase pure $ZrSi_2$ on the densification and mechanical properties of ZrB_2 should be investigated. The work presented in this thesis unintentionally included a large volume fraction of Si, as well as ZrO_2 and $ZrSiO_4$. These additives can be either studied in depth, or removed completely, to isolate their effect. The addition of these extraneous phases also influences the densification behavior in SiC fiber reinforced composites. The effect of phase pure $ZrSi_2$ on the densification of ZrB_2 with a SiC fiber reinforcing phase could be explored, as well as its influence on mechanical properties. Necessarily, an analysis of the resulting interaction of the matrix and fiber is essential in such a study.

2. The properties of ZrB_2-$ZrSi_2$ matrix reinforced with higher temperature fibers could be explored. In this study, CG-Nicalon, Hi-Nicalon, and Sylramic iBN fibers were used to reinforce ZrB_2-$ZrSi_2$ ceramics, but higher grade fibers exist. For example, Hi-Nicalon Type S fibers have lower oxygen content and have been shown to maintain high strength and creep resistance to higher temperatures compared to CG-Nicalon and Hi-Nicalon. The strength, modulus, and fracture behavior at room and elevated temperatures could be explored.

3. The role of interfacial coating thickness, as well as different SiC fiber coatings, could be explored for the ZrB_2-$ZrSi_2$ matrix composites. Increasing coating thickness ultimately reduces fiber flexibility but improves mechanical performance in final composites. A singular, thin BN coating was applied in this study, but multilayer coatings offer a number of advantages. A multilayer coating will improve environmental protection of ceramic fibers, as well as assisting in fiber-matrix debond during failure, both of which improve high temperature mechanical properties. Multilayered coatings of BN and Si_3N_4 have shown promise recently. An investigation of the interaction between coating and fiber will need to be conducted, as well as the interaction of coating and matrix. The matrix density, the condition of the coating after processing (i.e. spallation, chipping, abrasion), and possible fiber degradation would need to be explored.

REFERENCES

[1]W. G. Fahrenholtz, G. E. Hilmas, I. G. Talmy, and J. A. Zaykoski, "Refractory Diborides of Zirconium and Hafnium," *J. Am. Ceram. Soc.,* **90**[5] 1347-64 (2007).

[2]R. A. Cutler, "Engineering Properties of Borides," pp. 787-803 In *Ceramics and Glasses, Engineered Materials Handbook,* **Vol. 4**, Edited by S. J. Schneider. ASM International, Materials Park, OH, 1992.

[3]B. Stucker, W. Bradley, P. T. Eubank, S. Norasetthekul, and B. Bozkurt, "Zirconium Diboride/Copper Edm Electrodes from Selective Laser Sintering," in *Solid Freeform Fabr. Symp.*, pp. 257-65 1997.

[4]J. Sung, D. M. Goedde, G. S. Girolami, and J. R. Abelson, "Remote-Plasma Chemical Vapor Deposition of Conformal ZrB_2 Films at Low Temperature: A Promising Diffusion Barrier for Ultralarge Scale Integrated Electronics," *J. Appl. Phys.,* **91**[6] 3904-11 (2002).

[5]S. Norasetthekul, P. T. Eubank, W. L. Bradley, B. Bozkurt, and B. Stucker, "Use of Zirconium Diboride-Copper as an Electrode in Plasma Applications," *J. of Mater. Sci.,* **34**[6] 1261-70 (1999).

[6]S. K. Mishra, S. Das, S. K. Das, and P. Ramachandrarao, "Sintering Studies on Ultrafine ZrB_2 Powder Produced by a Self-Propagating High-Temperature Synthesis Process," *J. Mater. Res.,* **15** 2499-504 (2000).

[7]Y. Murata, "Cutting Tool Tips and Ceramics Containing Hafnium Nitride and Zirconium Diboride," U. S. Patent, 3487594, 1970.

[8]P. Vajeeston, P. Ravindran, C. Ravi, and R. Asokamani, "Electronic Structure, Bonding, and Ground-State Properties of AlB_2-Type Transition-Metal Diborides," *Phys. Rev. B.,* **63**[4] 045115 (2001).

[9]J. W. Zimmermann, G. E. Hilmas, W. G. Fahrenholtz, R. B. Dinwiddie, W. D. Porter, and H. Wang, "Thermophysical Properties of ZrB_2 and ZrB_2–SiC Ceramics," *J. Am. Ceram. Soc.,* **91**[5] 1405-11 (2008).

[10]M. Rahman, C. C. Wang, W. Chen, S. A. Akbar, and C. Mroz, "Electrical Resistivity of Titanium Diboride and Zirconium Diboride," *J. Am. Ceram. Soc.,* **78**[5] 1380-2 (1995).

[11]R. P. Tye and E. V. Clougherty, "The Thermal and Electrical Conductivities of Some Electrically Conducting Compounds," in *Proceedings of the Fifth Symposium on Thermophysical Properties*, Dynatech R/D Co., Cambridge, Mass., Newton, MA, pp. 396-401 1970.

[12]A. L. Chamberlain, W. G. Fahrenholtz, G. E. Hilmas, and D. T. Ellerby, "High-Strength Zirconium Diboride-Based Ceramics," *J. Am. Ceram. Soc.,* **87**[6] 1170-2 (2004).

[13]H. Kinoshita, S. Otani, S. Kamiyama, H. Amano, I. Akasaki, J. Suda, and H. Matsunami, "Zirconium Diboride (0001) as an Electrically Conductive Lattice-Matched Substrate for Gallium Nitride," *Jpn. J. Appl. Phys.,* **40** L1280-L2 (2001).

[14]J. W. Zimmermann, G. E. Hilmas, and W. G. Fahrenholtz, "Thermal Shock Resistance of ZrB_2 and ZrB_2–30% SiC," *Mater. Chem. Phys.,* **112**[1] 140-5 (2008).

[15]F. Lamouroux, S. Bertrand, R. Pailler, R. Naslain, and M. Cataldi, "Oxidation-Resistant Carbon-Fiber-Reinforced Ceramic-Matrix Composites," *Compos. Sci. Technol.,* **59**[7] 1073-85 (1999).

[16]K. Nakano, A. Kamiya, Y. Nishino, T. Imura, and T.-W. Chou, "Fabrication and Characterization of Three-Dimensional Carbon Fiber Reinforced Silicon Carbide and Silicon Nitride Composites," *J. Am. Ceram. Soc.,* **78**[10] 2811-4 (1995).

[17]Y. Zhu, Z. Huang, S. Dong, M. Yuan, and D. Jiang, "Manufacturing 2D Carbon-Fiber-Reinforced SiC Matrix Composites by Slurry Infiltration and PIP Process," *Ceram. Int.,* **34**[5] 1201-5 (2008).

[18]S. Zhu, M. Mizuno, Y. Nagano, J. Cao, Y. Kagawa, and H. Kaya, "Creep and Fatigue Behavior in an Enhanced SiC/SiC Composite at High Temperature," *J. Am. Ceram. Soc.,* **81**[9] 2269-77 (1998).

[19]G. Morscher, P. Pirouz, and A. H. Heuer, "Temperature Dependence of Interfacial Shear Strength in SiC-Fiber-Reinforced Reaction-Bonded Silicon Nitride," *J. Am. Ceram. Soc.,* **73**[3] 713-20 (1990).

[20]W.-Z. Zhang, Y. Zeng, L. Gbologah, X. Xiong, and B.-Y. Huang, "Preparation and Oxidation Property of ZrB_2-$MoSi_2$/SiC Coating on Carbon/Carbon Composites," *T. Nonferr. Metal Soc.,* **21**[7] 1538-44 (2011).

[21]S. Guo and Y. Kagawa, "Tensile Fracture Behavior of Continuous SiC Fiber-Reinforced SiC Matrix Composites at Elevated Temperatures and Correlation to in Situ Constituent Properties," *J. Eur. Ceram. Soc.,* **22**[13] 2349-56 (2002).

[22]D. Singh, J. P. Singh, and M. J. Wheeler, "Mechanical Behavior of SiC(F)/SiC Composites and Correlation to in Situ Fiber Strength at Room and Elevated Temperatures," *J. Am. Ceram. Soc.,* **79**[3] 591-6 (1996).

[23]J. J. Brennan, "Interfacial Characterization of a Slurry-Cast Melt-Infiltrated SiC/SiC Ceramic-Matrix Composite," *Acta Mater.,* **48**[18–19] 4619-28 (2000).

[24]J. A. DiCarlo, H. M. Yun, and J. B. Hurst, "Fracture Mechanisms for SiC Fibers and SiC/SiC Composites under Stress-Rupture Conditions at High Temperatures," *Applied Mathematics and Computation,* **152**[2] 473-81 (2004).

[25]T. Mah, M. G. Mendiratta, A. P. Katz, R. Ruh, and K. S. Mazdiyasni, "Room-Temperature Mechanical Behavior of Fiber-Reinforced Ceramic-Matrix Composites," *J. Am. Ceram. Soc.,* **68**[1] C-27-C-30 (1985).

[26]F. E. Heredia, S. M. Spearing, A. G. Evans, P. Mosher, and W. A. Curtin, "Mechanical Properties of Continuous-Fiber-Reinforced Carbon Matrix Composites and Relationships to Constituent Properties," *J. Am. Ceram. Soc.,* **75**[11] 3017-25 (1992).

[27]S. Tang, J. Deng, W. Liu, and K. Yang, "Mechanical and Ablation Properties of 2D-Carbon/Carbon Composites Pre-Infiltrated with a SiC Filler," *Carbon,* **44**[14] 2877-82 (2006).

[28]D. Cho and B. Il Yoon, "Microstructural Interpretation of the Effect of Various Matrices on the Ablation Properties of Carbon-Fiber-Reinforced Composites," *Compos. Sci. Technol.,* **61**[2] 271-80 (2001).

[29]J. Yin, X. Xiong, H. Zhang, and B. Huang, "Microstructure and Ablation Performances of Dual-Matrix Carbon/Carbon Composites," *Carbon,* **44**[9] 1690-4 (2006).

[30]F. E. Heredia, J. C. McNulty, F. W. Zok, and A. G. Evans, "Oxidation Embrittlement Probe for Ceramic-Matrix Composites," *J. Am. Ceram. Soc.,* **78**[8] 2097-100 (1995).

[31]R. E. Tressler, "Recent Developments in Fibers and Interphases for High Temperature Ceramic Matrix Composites," *Composites Part A: Applied Science and Manufacturing,* **30**[4] 429-37 (1999).

[32]R. R. Naslain, "SiC-Matrix Composites: Nonbrittle Ceramics for Thermo-Structural Application," *Int. J. Appl. Ceram. Tec.,* **2**[2] 75-84 (2005).

[33]M. M. Opeka, I. G. Talmy, and J. A. Zaykoski, "Oxidation-Based Materials Selection for 2000°C + Hypersonic Aerosurfaces: Theoretical Considerations and Historical Experience," *J. of Mater. Sci.,* **39**[19] 5887-904 (2004).

[34]F. Monteverde and L. Scatteia, "Resistance to Thermal Shock and to Oxidation of Metal Diborides–SiC Ceramics for Aerospace Application," *J. Am. Ceram. Soc.,* **90**[4] 1130-8 (2007).

[35]D. Sciti, M. Brach, and A. Bellosi, "Oxidation Behavior of a Pressureless Sintered ZrB_2–$MoSi_2$ Ceramic Composite," *J. Mater. Res.,* **20**[4] 922-30 (2005).

[36]D. Sciti, M. Brach, and A. Bellosi, "Long-Term Oxidation Behavior and Mechanical Strength Degradation of a Pressurelessly Sintered ZrB_2–$MoSi_2$ Ceramic," *Scripta Mater.,* **53**[11] 1297-302 (2005).

[37]K. L. Luthra, "Thermochemical Analysis of the Stability of Continuous "SiC" Fibers," *J. Am. Ceram. Soc.,* **69**[10] C-231-C-3 (1986).

[38]T. Mah, N. L. Hecht, D. E. McCullum, J. R. Hoenigman, H. M. Kim, A. P. Katz, and H. A. Lipsitt, "Thermal Stability of SiC Fibres (Nicalon)," *J. of Mater. Sci.,* **19**[4] 1191-201 (1984).

[39]S. M. Johnson, R. D. Brittain, R. H. Lamoreaux, and D. J. Rowcliffe, "Degradation Mechanisms of Silicon Carbide Fibers," *J. Am. Ceram. Soc.,* **71**[3] C-132-C-5 (1988).

[40]T. J. Clark, R. M. Arons, J. B. Stamatoff, and J. Rabe, "Thermal Degradation of Nicalon SiC Fibers," *Proceedings of the 9th Annual Conference on Composites and Advanced Ceramic Materials: Ceramic Engineering and Science Proceedings,* **6**[7-8] 576-88 (1985).

[41]D. J. Pysher, K. C. Goretta, R. S. Hodder, and R. E. Tressler, "Strengths of Ceramic Fibers at Elevated Temperatures," *J. Am. Ceram. Soc.,* **72**[2] 284-8 (1989).

[42]S. C. Zhang, G. E. Hilmas, and W. G. Fahrenholtz, "Pressureless Densification of Zirconium Diboride with Boron Carbide Additions," *J. Am. Ceram. Soc.,* **89**[5] 1544-50 (2006).

[43]W. G. Fahrenholtz, G. E. Hilmas, S. C. Zhang, and S. Zhu, "Pressureless Sintering of Zirconium Diboride: Particle Size and Additive Effects," *J. Am. Ceram. Soc.,* **91**[5] 1398-404 (2008).

[44]M. J. Thompson, W. G. Fahrenholtz, and G. E. Hilmas, "Elevated Temperature Thermal Properties of ZrB_2 with Carbon Additions," *J. Am. Ceram. Soc.,* **95**[3] 1077-85 (2012).

[45]J. Watts, G. Hilmas, and W. G. Fahrenholtz, "Mechanical Characterization of ZrB_2–SiC Composites with Varying SiC Particle Sizes," *J. Am. Ceram. Soc.,* **94**[12] 4410-8 (2011).

[46]L. Silvestroni and D. Sciti, "Oxidation of ZrB_2 Ceramics Containing SiC as Particles, Whiskers, or Short Fibers," *J. Am. Ceram. Soc.,* **94**[9] 2796-9 (2011).

[47]F. Monteverde and A. Bellosi, "Effect of the Addition of Silicon Nitride on Sintering Behaviour and Microstructure of Zirconium Diboride," *Scripta Mater.,* **46**[3] 223-8 (2002).

[48]F. Monteverde, S. Guicciardi, and A. Bellosi, "Advances in Microstructure and Mechanical Properties of Zirconium Diboride Based Ceramics," *Mater. Sci. Eng., A,* **346**[1–2] 310-9 (2003).

[49]L. Silvestroni, D. Sciti, J. Kling, S. Lauterbach, and H.-J. Kleebe, "Sintering Mechanisms of Zirconium and Hafnium Carbides Doped with $MoSi_2$," *J. Am. Ceram. Soc.,* **92**[7] 1574-9 (2009).

[50]S.-Q. Guo, Y. Kagawa, T. Nishimura, and H. Tanaka, "Pressureless Sintering and Physical Properties of ZrB_2-Based Composites with $ZrSi_2$ Additive," *Scripta Mater.,* **58**[7] 579-82 (2008).

[51] O. N. Grigoriev, B. A. Galanov, V. A. Kotenko, S. M. Ivanov, A. V. Koroteev, and N. P. Brodnikovsky, "Mechanical Properties of ZrB_2-SiC($ZrSi_2$) Ceramics," *J. Eur. Ceram. Soc.,* **30**[11] 2173-81 (2010).

[52] S.-Q. Guo, Y. Kagawa, and T. Nishimura, "Mechanical Behavior of Two-Step Hot-Pressed ZrB_2-Based Composites with $ZrSi_2$," *J. Eur. Ceram. Soc.,* **29**[4] 787-94 (2009).

[53] L. Silvestroni, D. Sciti, C. Melandri, and S. Guicciardi, "Toughened ZrB_2-Based Ceramics through SiC Whisker or SiC Chopped Fiber Additions," *J. Eur. Ceram. Soc.,* **30**[11] 2155-64 (2010).

[54] K. Upadhya, J.-M. Yang, and W. P. Hoffman, "Materials for Ultrahigh Temperature Structural Applications," *Am. Ceram. Soc. Bull.,* **58**[12] 51-6 (1997).

[55] A. L. Chamberlain, W. G. Fahrenholtz, and G. E. Hilmas, "Low-Temperature Densification of Zirconium Diboride Ceramics by Reactive Hot Pressing," *J. Am. Ceram. Soc.,* **89**[12] 3638-45 (2006).

[56] Z. Lü, D. Jiang, J. Zhang, and Q. Lin, "Processing and Properties of ZrB_2–SiC Composites Obtained by Aqueous Tape Casting and Hot Pressing," *Ceram. Int.,* **37**[1] 293-301 (2011).

[57] V. Medri, P. Pinasco, A. Sanson, E. Roncari, S. Guicciardi, and A. Bellosi, "ZrB_2-Based Laminates Produced by Tape Casting," *Int. J. Appl. Ceram. Tec.* 349-57 (2011).

[58] S. L. Natividad, V. R. Marotto, L. S. Walker, D. Pham, W. Pinc, and E. L. Corral, "Tape Casting Thin, Continuous, Homogenous, and Flexible Tapes of ZrB_2," *J. Am. Ceram. Soc.* 2749-53 (2011).

[59] A. L. Chamberlain, W. G. Fahrenholtz, and G. E. Hilmas, "Pressureless Sintering of Zirconium Diboride," *J. Am. Ceram. Soc.,* **89**[2] 450-6 (2006).

[60] L. Silvestroni and D. Sciti, "Effects of $MoSi_2$ Additions on the Properties of Hf– and Zr–B_2 Composites Produced by Pressureless Sintering," *Scripta Mater.,* **57**[2] 165-8 (2007).

[61] M. N. Rahaman, "Ceramic Processing," Taylor & Francis Group, LLC, Boca Raton, FL, 2007.

[62] G. Baret, R. Madar, and C. Bernard, "Silica-Based Oxide Systems," *J. Electrochem. Soc.,* **138**[9] 2830-5 (1991).

[63] R. Telle, L. S. Sigl, and K. Takagi, "Boride-Based Hard Materials," pp. 802-945 In *Handbook of Ceramic Hard Materials*, Edited by R. Riedel. Wiley-VCH, Weinheim, 2000.

[64] S. Guo, T. Nishimura, and Y. Kagawa, "Low-Temperature Hot Pressing of ZrB_2-Based Ceramics with $ZrSi_2$ Additives," *Int. J. Appl. Ceram. Tec.,* **8**[6] 1425-35 (2011).

[65]D. Sciti, S. Guicciardi, A. Bellosi, and G. Pezzotti, "Properties of a Pressureless-Sintered ZrB2–MoSi2 Ceramic Composite," *J. Am. Ceram. Soc.,* **89**[7] 2320-2 (2006).

[66]D. Sciti, L. Silvestroni, G. Celotti, C. Melandri, and S. Guicciardi, "Sintering and Mechanical Properties of ZrB_2–$TaSi_2$ and HfB_2–$TaSi_2$ Ceramic Composites," *J. Am. Ceram. Soc.,* **91**[10] 3285-91 (2008).

[67]J. Wachtman, "Mechanical Properties of Ceramics," John Wiley & Sons, Inc., New York, 1996.

[68]P. S. Steif and A. Trojnacki, "Bend Strength Versus Tensile Strength of Fiber-Reinforced Ceramics," *J. Am. Ceram. Soc.,* **77**[1] 221-9 (1994).

[69]ASTM International (ASTM), "Standard Test Method for Flexural Strength of Advanced Ceramics at Ambient Temperature," ASTM Standard C1161-02c, West Conshohocken, PA, 2008.

[70]A. Krell, "A New Look at the Influences of Load, Grain Size and Grain Boundaries on the Room Temperature Hardness of Ceramics," *Int. J. Refract. Met. Hard Mater.,* **16**[4–6] 331-5 (1998).

[71]R. W. Rice, C. C. Wu, and F. Borchelt, "Hardness-Grain-Size Relations in Ceramics," *J. Am. Ceram. Soc.,* **77**[10] 2539-53 (1994).

[72]S. C. Zhang, G. E. Hilmas, and W. G. Fahrenholtz, "Pressureless Sintering of ZrB_2–SiC Ceramics," *J. Am. Ceram. Soc.,* **91**[1] 26-32 (2008).

[73]X. J. Ning and P. Pirouz, "The Microstructure of SCS-6 SiC Fiber," *J. Mater. Res.,* **6**[10] 2234-48 (1991).

[74]R. T. Bhatt and D. R. Hull, "Microstructural and Strength Stability of Cvd SiC Fibers in Argon Environments," pp. 1832-44 In *Proceedings of the 15th Annual Conference on Composites and Advanced Ceramic Materials: Ceramic Engineering and Science Proceedings*. John Wiley & Sons, Inc., 2008.

[75]S. G. Warrier, D. B. Gundel, B. S. Majumdar, and D. B. Miracle, "Interface Effects on the Micromechanical Response of a Transversely Loaded Single Fiber SCS-6/Ti-6Al-4V Composite," *Metallurgical and Materials Transactions A,* **27**[7] 2035-43 (1996).

[76]S. Yajima, K. Okamura, J. Hayashi, and M. Omori, "Development of a Silicon Carbide Fiber with High Tensile Strength," *Nature,* **261** 683-5 (1976).

[77]S. Yajima, K. Okamura, J. Hayashi, and M. Omori, "Synthesis of Continuous Sic Fibers with High Tensile Strength," *J. Am. Ceram. Soc.,* **59**[7-8] 324-7 (1976).

[78]M. Takeda, A. Urano, J.-i. Sakamoto, and Y. Imai, "Microstructure and Oxidative Degradation Behavior of Silicon Carbide Fiber Hi-Nicalon Type S," *J. Nucl. Mater.,* **258–263, Part 2**[0] 1594-9 (1998).

[79]J. A. DiCarlo, "Creep Limitations of Current Polycrystalline Ceramic Fibers," *Compos. Sci. Technol.,* **51**[2] 213-22 (1994).

[80]J. Lipowitz, J. A. Rabe, A. Zangvil, and Y. Xu, "Structure and Properties of Sylramic Silicon Carbide Fiber - a Polycrystalline, Stoichiometric B-SiC Composition," *Ceram. Eng. Sci. Proc.,* **18**[3 A] 147-57 (1997).

[81]X.-J. Ning, P. Pirouz, and S. C. Farmer, "Microchemical Analysis of the SCS-6 Silicon Carbide Fiber," *J. Am. Ceram. Soc.,* **76**[8] 2033-41 (1993).

[82]P. R. Smith, M. L. Gambone, D. S. Williams, and D. I. Garner, "Heat Treatment Effects on SiC Fiber," *J. of Mater. Sci.,* **33**[24] 5855-72 (1998).

[83]R. Naslain, "Design, Preparation and Properties of Non-Oxide Cmcs for Application in Engines and Nuclear Reactors: An Overview," *Compos. Sci. Technol.,* **64**[2] 155-70 (2004).

[84]S. M. Dong, G. Chollon, C. Labrugère, M. Lahaye, A. Guette, J. L. Bruneel, M. Couzi, R. Naslain, and D. L. Jiang, "Characterization of Nearly Stoichiometric SiC Ceramic Fibres," *J. of Mater. Sci.,* **36**[10] 2371-81 (2001).

[85]Y. Katoh, L. L. Snead, T. Nozawa, S. Kondo, and J. T. Busby, "Thermophysical and Mechanical Properties of Near-Stoichiometric Fiber CVI SiC/SiC Composites after Neutron Irradiation at Elevated Temperatures," *J. Nucl. Mater.,* **403**[1–3] 48-61 (2010).

[86]B. Cantor, F. Dunne, and I. Stone, "Metal and Ceramic Matrix Composites," IOP Publishing, London, 2004.

[87]B. Clauß, "Fibers for Ceramic Matrix Composites," pp. 1-20 In *Ceramic Matrix Composites*. Wiley-VCH Verlag GmbH & Co. KGaA, 2008.

[88]K. Kumagawa, H. Yamaoka, M. Shibuya, and T. Yamamura, "Fabrication and Mechanical Properties of New Improved Si-M-C-(O) Tyranno Fiber," *Ceram. Eng. Sci. Proc.,* **19**[3] 65-72 (1998).

[89]S. Dong, Y. Katoh, and A. Kohyama, "Preparation of SiC/SiC Composites by Hot Pressing, Using Tyranno-Sa Fiber as Reinforcement," *J. Am. Ceram. Soc.,* **86**[1] 26-32 (2003).

[90]Y. Katoh, T. Nozawa, and L. L. Snead, "Mechanical Properties of Thin Pyrolitic Carbon Interphase SiC–Matrix Composites Reinforced with Near-Stoichiometric SiC Fibers," *J. Am. Ceram. Soc.,* **88**[11] 3088-95 (2005).

[91]A. G. Evans, F. W. Zok, and J. Davis, "The Role of Interfaces in Fiber-Reinforced Brittle Matrix Composites," *Compos. Sci. Technol.,* **42**[1–3] 3-24 (1991).

[92]L. S. Sigl and A. G. Evans, "Effects of Residual Stress and Frictional Sliding on Cracking and Pull-out in Brittle Matrix Composites," *Mech. Mater.,* **8**[1] 1-12 (1989).

[93]D. B. Marshall, "Analysis of Fiber Debonding and Sliding Experiments in Brittle Matrix Composites," *Acta Metallurgica et Materialia,* **40**[3] 427-41 (1992).

[94]T. A. Parthasarathy, D. B. Marshall, and R. J. Kerans, "Analysis of the Effect of Interfacial Roughness on Fiber Debonding and Sliding in Brittle Matrix Composites," *Acta Metallurgica et Materialia,* **42**[11] 3773-84 (1994).

[95]D. B. Marshall and A. G. Evans, "Failure Mechanisms in Ceramic-Fiber/Ceramic-Matrix Composites," *J. Am. Ceram. Soc.,* **68**[5] 225-31 (1985).

[96]M. D. Thouless, "Frictional Sliding and Pull-out of a Fibre," *Scripta Metallurgica et Materialia,* **27**[9] 1211-4 (1992).

[97]F. Rebillat, J. Lamon, R. Naslain, E. Lara-Curzio, M. K. Ferber, and T. M. Besmann, "Properties of Multilayered Interphases in SiC/SiC Chemical-Vapor-Infiltrated Composites with "Weak" and "Strong" Interfaces," *J. Am. Ceram. Soc.,* **81**[9] 2315-26 (1998).

[98]R. J. Kerans, "Viability of Oxide Fiber Coatings in Ceramic Composites for Accommodation of Misfit Stresses," *J. Am. Ceram. Soc.,* **79**[6] 1664-8 (1996).

[99]K. Shimoda, J.-S. Park, T. Hinoki, and A. Kohyama, "Influence of Pyrolytic Carbon Interface Thickness on Microstructure and Mechanical Properties of SiC/SiC Composites by Nite Process," *Compos. Sci. Technol.,* **68**[1] 98-105 (2008).

[100]G. S. Corman and K. L. Luthra, "Silicon-Doped Boron Nitride Coated Fibers in Silicon Melt Infiltrated Composites," U. S. Patent, 5952100, 1999.

[101]K. L. Luthra, "Oxidation-Resistant Fiber Coatings for Non-Oxide Ceramic Composites," *J. Am. Ceram. Soc.,* **80**[12] 3253-7 (1997).

[102]R. N. Singh and S. K. Reddy, "Influence of Residual Stresses, Interface Roughness, and Fiber Coatings on Interfacial Properties in Ceramic Composites," *J. Am. Ceram. Soc.,* **79**[1] 137-47 (1996).

[103]J. H. Miller, P. K. Liaw, and J. D. Landes, "Influence of Fiber Coating Thickness on Fracture Behavior of Continuous Woven Nicalon® Fabric-Reinforced Silicon-Carbide Matrix Ceramic Composites," *Mater. Sci. Eng., A,* **317**[1–2] 49-58 (2001).

[104]S. Prouhet, G. Camus, C. Labrugere, A. Guette, and E. Martin, "Mechanical Characterization of Si–C(O) Fiber/SiC (CVI) Matrix Composites with a BN–Interphase," *J. Am. Ceram. Soc.,* **77**[3] 649-56 (1994).

[105]J. Takahashi, K. Kemmochi, J. Watanabe, H. Fukuda, and R. Hayashi, "Development of Ultra-High Temperature Testing Equipment and Some Mechanical and Thermal Properties of Advanced Carbon/Carbon Composites," *Adv. Compos. Mater,* **5**[1] 73-86 (1995).

[106]N. S. Jacobson and D. M. Curry, "Oxidation Microstructure Studies of Reinforced Carbon/Carbon," *Carbon,* **44**[7] 1142-50 (2006).

[107]L. U. J. T. Ogbuji and E. J. Opila, "A Comparison of the Oxidation Kinetics of SiC and Si_3N_4," *J. Electrochem. Soc.,* **148**[2] B79-B85 (1995).

[108]D. W. McKee, "Oxidation Behavior of Matrix-Inhibited Carbon/Carbon Composites," *Carbon,* **26**[5] 659-64 (1988).

[109]T. Hinoki, E. Lara-Curzio, and L. L. Snead, "Mechanical Properties of High Purity SiC Fiber-Reinforced CVI-SiC Matrix Composites," *Fusion Sci. Technol.,* **44** 211-8 (2003).

[110]L. Filipuzzi, G. Camus, R. Naslain, and J. Thebault, "Oxidation Mechanisms and Kinetics of 1D-SiC/C/SiC Composite Materials: I, an Experimental Approach," *J. Am. Ceram. Soc.,* **77**[2] 459-66 (1994).

[111]S. G. Lee, J. Fourcade, R. Latta, and A. A. Solomon, "Polymer Impregnation and Pyrolysis Process Development for Improving Thermal Conductivity of Sicp/SiC-PIP Matrix Fabrication," *Fusion Eng. Des.,* **83**[5-6] 713-9 (2008).

[112]W. Kowbel, C. A. Bruce, K. L. Tsou, K. Patel, J. C. Withers, and G. E. Youngblood, "High Thermal Conductivity SiC/SiC Composites for Fusion Applications," *J. Nucl. Mater.,* **283–287, Part 1**[0] 570-3 (2000).

[113]H. Araki, H. Suzuki, W. Yang, S. Sato, and T. Noda, "Effect of High Temperature Heat Treatment in Vacuum on Microstructure and Bending Properties of SiC_f/SiC Composites Prepared by CVI," *J. Nucl. Mater.,* **258–263, Part 2**[0] 1540-5 (1998).

[114]R. T. Bhatt, J. B. Hurst, and J. Z. Gyekenyesi, "Silicon Effects on Properties of Melt Infiltrated SiC/SiC Composites," pp. 331-8 In *24th Annual Conference on Composites, Advanced Ceramics, Materials, and Structures: A: Ceramic Engineering and Science Proceedings*. John Wiley & Sons, Inc., 2008.

[115]J. A. DiCarlo, H. M. Yun, G. N. Morscher, and R. T. Bhatt, "SiC/SiC Composites for 1200°C and Above," pp. 77-98 In *Handbook of Ceramic Composites*, Edited by N. Bansal. Springer US, 2005.

[116]W. L. Vaughn and H. G. Maahs, "Active-to-Passive Transition in the Oxidation of Silicon Carbide and Silicon Nitride in Air," *J. Am. Ceram. Soc.,* **73**[6] 1540-3 (1990).

[117]A. Rezaie, W. G. Fahrenholtz, and G. E. Hilmas, "Effect of Hot Pressing Time and Temperature on the Microstructure and Mechanical Properties of ZrB_2–SiC," *J. of Mater. Sci.,* **42**[8] 2735-44 (2007).

[118]S. Tang, J. Deng, S. Wang, and W. Liu, "Fabrication and Characterization of an Ultra-High-Temperature Carbon Fiber-Reinforced ZrB_2–SiC Matrix Composite," *J. Am. Ceram. Soc.,* **90**[10] 3320-2 (2007).

[119]F. Yang, X. Zhang, J. Han, and S. Du, "Characterization of Hot-Pressed Short Carbon Fiber Reinforced ZrB2–SiC Ultra-High Temperature Ceramic Composites," *J. Alloys Compd.,* **472**[1–2] 395-9 (2009).

[120]C. Yue, W. Liu, L. Zhang, T. Zhang, and Y. Chen, "Fracture Toughness and Toughening Mechanisms in a (ZrB_2–SiC) Composite Reinforced with Boron Nitride Nanotubes and Boron Nitride Nanoplatelets," *Scripta Mater.,* **68**[8] 579-82 (2013).

[121]S. Guicciardi, L. Silvestroni, M. Nygren, and D. Sciti, "Microstructure and Toughening Mechanisms in Spark Plasma-Sintered ZrB_2 Ceramics Reinforced by SiC Whiskers or SiC-Chopped Fibers," *J. Am. Ceram. Soc.,* **93**[8] 2384-91 (2010).

[122]D. Sciti, S. Guicciardi, and L. Silvestroni, "SiC Chopped Fibers Reinforced ZrB_2: Effect of the Sintering Aid," *Scripta Mater.,* **64**[8] 769-72 (2011).

[123]D. Sciti, L. Silvestroni, G. Saccone, and D. Alfano, "Effect of Different Sintering Aids on Thermo–Mechanical Properties and Oxidation of SiC Fibers – Reinforced ZrB_2 Composites," *Mater. Chem. Phys.,* **137**[3] 834-42 (2013).

[124]X. Zhang, L. Xu, S. Du, J. Han, P. Hu, and W. Han, "Fabrication and Mechanical Properties of ZrB_2–SiC_w Ceramic Matrix Composite," *Mater. Lett.,* **62**[6–7] 1058-60 (2008).

[125]J. Ramírez-Rico, M. A. Bautista, J. Martínez-Fernández, and M. Singh, "Compressive Strength Degradation in ZrB2-Based Ultra-High Temperature Ceramic Composites," *J. Eur. Ceram. Soc.,* **31**[7] 1345-52 (2011).

[126]J. M. Fernandez,"Ultra High Temperature Ceramics for Aerospace Use," Technical Documentary Report Grant 07-3087, Directorate for Information Operations and Reports, EOARD, Arlington, VA, 2008.

[127]K. Stuffle, W. Lougher, and S. Chanat, "Preparation and Characterization of Continuous Fiber Reinforced Zirconium Diboride Matrix Composites for a Leading Edge Material," *International SAMPE Technical Conference*[24] T935-T49 (1992).

[128]K. Stuffle and J. Bull, "Continuous Fiber Reinforced Composites for Heat Shield Applications," in *Conference on Processing, Fabrication, and Applications of Advanced Composites*, ASM International, Long Beach, CA, pp. 1993.

VITA

Benjamin John Bowin Lai was born on July 24th, 1987 in San Jose, CA. In August of 2006 Benjamin started his undergraduate degree as a chemical engineer at the University of Missouri - Rolla (now Missouri University of Science and Technology). After many trials, Benjamin decided to join the Ceramic Engineering Department. During his undergraduate years, Benjamin joined the student groups Keramos and Material Advantage. Near the end of these formative years, he was given the opportunity to be an undergraduate research assistant in the UHTC group at Missouri S&T. Benjamin received his B.S. degree in Ceramic Engineering from Missouri S&T in December 2010. This propelled Benjamin into the exciting world of graduate research where he began his Master's work the following year in January, 2011.

Benjamin began his graduate work as a Masters student working on SiC fiber reinforced ultra-high temperature composites. During this time, Benjamin assisted with the Ceramic Processing Lab – Characterization of Materials laboratory. His work led to three conference presentations, and will be accompanied by two publications. After the completion of his Masters requirements, Benjamin will continue his career as a materials engineer with Rolls-Royce Corporation in Indianapolis, IN.